Unsteady Ice Processes in Complex River Systems

by

Jennifer Leah Nafziger

A thesis submitted in partial fulfillment of the requirements for the degree of

Doctor of Philosophy

in

Water Resources Engineering

Department of Civil and Environmental Engineering

University of Alberta

Abstract

River ice processes are among the most important subjects of study for hydrotechnical engineers in cold regions. This is because extremes of both minimum flow (impacting fish habitat and the concentration and transport of pollutants) and maximum water levels (impacting channel geomorphology and the flooding of human infrastructure) often occur during the ice-affected season. However, there is a dearth of data describing many facets of ice cover formation and evolution because river ice processes are often logistically challenging to measure. Nevertheless, these data are essential for developing conceptual models of river ice processes and the predictive numerical models that are based on them.

This research project has improved our understanding of unsteady (i.e. time-varying) river ice processes in a variety of environments. This includes anchor ice processes in small headwater streams, ice jam release processes in single-channel river reaches, and ice jam evolution processes in multi-channel river systems. The primary variables monitored in these studies were water level and ice condition and each was observed continuously for up to six months. Each environment was studied for multiple seasons, and multiple examples of each process were observed. This resulted in an unprecedentedly complete picture of each process, and allowed for the development of new conceptual models of these river ice processes.

This thesis presents several key new results. This work confirms that for these streams, thermal processes are an important control on anchor ice release, and that a linear heat transfer approach can be used to predict anchor ice release. It presents several

fundamental observations of anchor ice processes, such as variations in ice accumulation morphology, event duration, effect on water level, modes of incorporation into seasonal ice cover, modes of release, and growth rates. This thesis provides one of the most complete pictures of anchor ice processes ever compiled.

This thesis presents the first-ever series of simultaneous observations of the water waves and ice runs that emanate from an ice jam release. It shows how the water waves and ice runs advanced downstream together and then separated due to differing celerities. These observations were taken over a channel distance longer than 10,000 undisturbed flow depths, much longer than can be practically accommodated in laboratory physical models. These data provide important validation data for numerical models of ice run and water wave propagation.

This work also qualitatively and quantitatively describes how ice and water moved through a multi-channel river reach and described the underlying mechanisms of ice jam movement at dividing channel junctions. These descriptions allowed for the development of a new conceptual model that describes how unsteady flow conditions and ice cover momentum are particularly important in multi-channel environments. In addition, this thesis presents a new mode of ice jam release, whereby the release is caused by a water wave that emanates from melting and creeping consolidation of the ice jam itself.

Preface

This thesis is an original work by myself, Jennifer Nafziger under the supervision of Dr. Faye Hicks and Dr. Yuntong She in the Department of Civil and Environmental Engineering at the University of Alberta. Versions of Chapters 2 and 3 have been previously published in, and a version of Chapter 4 has been submitted to, the peer-reviewed journal *Cold Regions Science and Technology*.

A version of Chapter 2 of this thesis was published as "Nafziger, J., She, Y., Hicks, F. Cunjak, R. 2017. Anchor ice formation and release in small regulated and unregulated streams. Cold Regions Science and Technology, 141:66-77." This research formed part of a national research collaboration by the Natural Sciences and Engineering Research Council of Canada's strategic network "HydroNet." Dr. Faye Hicks and Dr. Rick Cunjak were lead researchers for the winter regime part of HydroNet Component 1.3: "Physical Drivers of Productive Capacity of Fish Habitats." I was responsible for helping design the study with my collaborators; I planned the field data collection program, I set up the field instrumentation with help from field assistants and collaborators, I performed the data analysis and interpretation with consultation from my coauthors, and I prepared the manuscript with assistance from my coauthors. Dr. Yuntong She consulted on the data analysis and assisted with manuscript preparation. Dr. Faye Hicks assisted with study design, consulted on the data analysis, and assisted with manuscript preparation. Dr. Richard Cunjak assisted with study design and manuscript preparation.

A version of Chapter 3 of this thesis was published as "Nafziger, J., She, Y., Hicks, F. 2016. Celerities of waves and ice runs from ice jam releases. *Cold Regions Science*

and Technology, 123: 71–80." I designed the study with assistance from my coauthors; I planned the field data collection program, I set up the field instrumentation and performed field observations with help from field assistants, I performed the data analysis and interpretation with consultation from my coauthors, and I prepared the manuscript with assistance from my coauthors. Dr. Yuntong She consulted on the data analysis and assisted with manuscript preparation. Dr. Faye Hicks assisted with study design, consulted on the data analysis, and assisted with manuscript preparation.

A version of Chapter 4 of this thesis was submitted to *Cold Regions Science and Technology* in 2017 as "Nafziger, J., She, Y., Hicks, F. Dynamic river ice processes in a river delta network." I was responsible for designing the study with assistance from my coauthors and research assistants; I planned the field data collection program with help from research assistants, I helped set up the field instrumentation and performed field observations with field and research assistants, I performed the data analysis and interpretation with consultation from my coauthors, and I prepared the manuscript with assistance from my coauthors. Dr. Yuntong She consulted on the data analysis and assisted with manuscript preparation. Dr. Faye Hicks assisted with study design, consulted on the data analysis, and assisted with manuscript preparation.

Dedication

For my husband, Michael Marchen.

Thank you for taking this journey with me.

Acknowledgments

Thank you to my supervisor, Dr. Faye Hicks for her continuous support, encouragement, and enthusiasm. I am grateful for the opportunity to learn from her and to be a part of the community of fantastic students she has nurtured. Thank you for indulging my curiosity, and encouraging the many avenues of inquiry that have made me the researcher I am today. Thank you to my co-supervisor Dr. Yuntong She for her invaluable assistance and her insight into many river ice processes. Thank you to Dr. Richard Cunjak for his encouragement and the opportunity to see rivers from a different perspective.

I would like to thank my thesis review committee: Dr. Brian Morse, Dr. Selma Guigard, and Dr. Mark Loewen for volunteering their valuable time and effort. Your participation on short notice and over the holidays is greatly appreciated.

I have had the pleasure of working in the field with so many great people. Thank you for all the good times and for helping make this research a reality. Thanks to Janelle Banack, Michael Brayall, Stefan Emmer, Chris Krath, Josh Maxwell, Vince McFarlane, David Watson, Nadia Kovachis Watson, and Liming Zhao from the University of Alberta; and to Shawne Kokelj and Meg McCluskie of Indigenous and Northern Affairs Canada; and Aaron Fraser, J. Michelle Lavery, Tommi Linnansaari, Diane Parley, and Paula Thoms of the University New Brunswick. Special thanks to Janelle, Josh, and Stefan for all the memories and hard labour on rivers across this great country!

This research was supported by research grants from the Natural Sciences and

Engineering Research Council of Canada and by scholarships to myself from the Natural Sciences and Engineering Research Council of Canada, The University of Alberta Faculty of Engineering, the University of Alberta Faculty of Graduate Studies and Research, the Government of Alberta, the Canadian Engineering Memorial Foundation, the Canadian Dam Association, and the International Association for Impact Assessment. In-kind research support was provided by the Town of Hay River and by Indigenous and Northern Affairs Canada. Thanks to everyone in Hay River, especially Ross Potter of the Town of Hay River. Thanks to Perry Fedun and the Department of Civil and Environmental Engineering at the University of Alberta for technical and administrative assistance. All this support is gratefully acknowledged.

Thank you to the research communities I have had the pleasure to be a part of: the University of Alberta River Ice Research Group, NSERC HydroNet, the International Polar Year SCARF group, and the Canadian Geophysical Union Committee for River Ice Processes and the Environment (CRIPE). These groups have been inspiring and supportive.

Thanks to my children's grandparents: Linda and Peter Marchen and Betty Nafziger. Your significant help with my children have made this journey possible. Thank you for your love and patience.

Last, but certainly not least, thank you to my husband, Michael Marchen. Thank you for being there for me and for putting up with years of field research, paper edits, and poverty. Thanks for donning waders and helping me out, too. I love you.

Table of Contents

List of Tables

List of Figures

List of Symbols and Acronyms

π	≈ 3.1459
ρ_{ai}	anchor ice density (kg/m^3)
ρ_s	density of solid ice (kg/m^3)
ρ_w	density of water (kg/m^3)
ϕ_{sw}	shortwave radiation (W/m^2)
χ^2	test statistic for Kurskall-Wallis non-parametric statistical hypothesis test
AFDH of T_a	accumulated freezing degree hours calculated using the air temperature (°C•h)
C	strength of the bond between the substrate and the bed (N/m^2)
$C_{dynamic}$, C_{dyn}	the celerity of the theoretical dynamic wave (m/s)
$C_{diffusive}$, C_{diff}	the celerity of the theoretical diffusive wave (m/s)
C_{feat}	the celerity of the observed water level feature (m/s)
D	distance travelled from release point by the water wave or ice run (km)
d_s	substrate diameter (m)
ΔE	heat flux to the water per unit area of the water surface (W/m^2)
F_{Bnet}	net buoyant force on the anchor ice per unit area (N/m^2)
g	acceleration due to gravity (m/s^2)
Gr.	"group"
H	stage (i.e. water level) (cm or m)
Δh	change in stage measured over 15 minutes (cm or m)

ΔH_G	change in stage over anchor ice growth period (cm or m)
ΔH_R	change in stage over anchor ice release period (cm or m)
h_{aw}	calibrated linear heat flux coefficient (dimensionless)
j_{aw}	calibrated linear heat flux coefficient (dimensionless)
L_j	length of the ice jam before release (km)
MMLR	"moving multi-layered rubble"
p	probability value of the statistical hypothesis test (dimensionless)
Q_c	discharge in the channel in which a feature was observed (m^3/s)
Q_d	reported discharge flowing through the dam (m^3/s)
$RF_{\alpha,SF}$	calibrated shortwave reduction factor, accounting for water albedo and shading effects (dimensionless)
Δt_G	length of the anchor ice growth period (hours)
Δt_R	length of the anchor ice release period (hours)
T_a	air temperature (°C)
T_w	water temperature (°C)
THR	"Town of Hay River"
U_0	cross-sectionally-averaged water velocity at the carrier discharge (m/s)
WSC	"Water Survey of Canada"
X_1	station of one end of a reach over which celerity was measured (km)
X_2	station of one end of a reach over which celerity was measured (km)
y_0	cross-sectionally-averaged water depth at the carrier discharge (m)
Z	test statistic for Mann-Whitney-U rank sum non-parametric statistical hypothesis test

Chapter 1. Introduction and Objectives

1.1 Overview and Background

This doctoral thesis, entitled "*Unsteady River Ice Processes in Complex River Systems,*" improves our understanding of unsteady river ice processes in a variety of environments. A complete understanding of river ice processes is important because ice affects many rivers in cold regions for a substantial portion of the year. Extremes of both minimum flow (impacting fish habitat and the concentration and transport of pollutants) and maximum water levels (impacting channel geomorphology and the flooding of human infrastructure) often occur during the ice-affected season. Therefore, river ice processes are among the most important subjects of study for hydrotechnical engineers in cold regions. Scientific knowledge of river ice processes is developing and our ability to model many of these processes has improved in recent years. However, there is a dearth of data describing many facets of ice cover formation and evolution because many river ice processes are logistically challenging to measure. Without these data we cannot even develop conceptual models, much less predictive numerical models.

This thesis is the result of detailed field observations of river ice processes over five winters in two provinces and territories. This research (divided into three components) aims to improve our conceptual models pertaining to three different unsteady (i.e. time-varying) river ice processes that occur in three different river environments, including:

1) anchor ice processes in small headwater streams (Chapter 2),
2) ice jam release processes in single-channel river reaches (Chapter 3), and

3) ice jam evolution processes in multi-channel river systems (Chapter 4).

While the stream environments examined in each component differ, the observation methods were similar. The primary variables monitored in these studies were water levels and ice conditions and each was observed continuously, for up to six months. In each environment, water levels were measured (with intervals ranging from 1 min to 20 min) using self-contained pressure transducers and data-loggers placed in the study rivers and attached to the bed to withstand the expected ice conditions. Ice conditions were monitored, when lighting conditions allowed, using time-lapse cameras mounted on the riverbanks (photo intervals: 1 min to 60 min). In order to supplement the continuously measured variables, in some cases additional measurements were made of air and water temperatures, shortwave radiation, and ice jam profiles. In addition, ice conditions were frequently observed from the air. This thesis is the result of the analysis of almost 400,000 time-lapse and aerial photographs and 147 time-series of measured variables, comprised of more than 7.5 million data points. Each environment was studied for multiple seasons, which provided a very detailed picture of the river ice processes that occurred in each environment, and allowed for the development of new conceptual models of these processes. A background on, and a review of, current state of knowledge of each process is provided in the following section.

1.2 Literature Review

1.2.1 Anchor Ice

Anchor ice is a type of river ice accumulation that forms at the bottom of river beds in turbulent, supercooled water. Examples of anchor ice accumulations are shown

in Figure 1.1. Anchor ice forms both through the adhesion of frazil ice to the stream bed and through thermal growth of adhered ice crystals as they exchange heat with the surrounding supercooled water (Qu and Doering, 2007). When anchor ice is forming, the water surface elevation tends to increase because the anchor ice takes up a portion of the channel area. Unlike most surface ice, the entire accumulation of submerged anchor ice exists at a temperature very close to its melting point. Therefore, anchor ice accumulations are often ephemeral and may release and/or melt easily. Anchor ice releases from the stream bed when thermal factors are favourable and/or when the buoyancy of the accumulation or the drag forces acting on it overcome the adhesion force holding the anchor ice in place. The formation and release of anchor ice is often described as occurring daily during freeze-up. This diurnal process involves the formation of anchor ice during the night and the release of this accumulation the next day, presumably under influence from greater incoming solar radiation and warming air temperatures (Tsang, 1982). However, some sources mention multi-day anchor ice events or anchor ice that did not release during the day (e.g. Tremblay et al., 2014; Stickler and Alfredsen, 2009; Bisaillon and Bergeron, 2009) or that persisted for many weeks (Malenchak, 2011).

Anchor ice may exist in different forms. Stickler and Alfredsen (2009) classified anchor ice as two types. Their Type I anchor ice formed in low turbulent areas, grew in the vertical direction, and had a soft, low-density texture made of small frazil particles (< 0.01m). Their Type II anchor ice formed in higher-turbulent areas and grew in the vertical and lateral directions, filling in the spaces between the stream's gravel bed particles with a higher-density accumulation made of larger (up to ~0.1 m) frazil

particles. Turcotte and Morse (2011) described anchor ice based on the morphology of the accumulation: as "carpets" - relatively uniform coating of the river bed, anchor ice "weirs"- accumulations concentrated across the channel, and "dams" - emergent weirs that form with the addition of ice from spray and the cooling of emergent boulders.

Laboratory studies of anchor ice have focused on small-scale morphology of anchor ice accumulations and the impact of hydraulic parameters (i.e. Froude and Reynolds numbers) on the formation and morphology of anchor ice. Kerr et al. (1997) and Qu and Doering (2007) studied anchor ice evolution on a gravel bed in a cooled laboratory. They found that anchor ice started to accumulate on the upstream side of the gravel particles, the downstream side of the gravel particles, and where the particles touched each other. They found that the growth pattern of these initial accumulations of anchor ice depended on the velocity and Froude number of the water flow. Kerr et al. (2002) found that the release of laboratory anchor ice accumulations initiated at a locally thick area and caused a chain reaction that released the entire accumulation. They also noted that if anchor ice did not release early in its formation, the accumulation flattened and grew at a constant rate. In addition, Doering et al. (2001) found that laboratory anchor ice was more likely to release at Reynold's numbers below ~42,000 (see also the discussion in Doering, 2002). In their laboratory experiment, Tremblay et al. (2013) found that rougher pebbles that were more deeply embedded took longer to be released from melting ice. They also noted that the lithology of the pebbles and paint on the pebbles may play a role in how ice and pebbles separate.

Field studies on anchor ice have ranged from mostly observational (e.g. Tesaker, 1996) to detailed observations of the evolution of anchor ice morphology over the winter

period (Turcotte and Morse, 2011). Other researchers focused on the ability of anchor ice to transport sediment. Sediment loads transported by anchor ice may be larger than those carried by the stream at peak flows, despite the low flows typical at freeze-up (Kempema and Ettema, 2011). Kalke et al. (2017) recently quantified sediment concentrations of a large number of fixed and floating anchor ice samples from three rivers in Alberta, Canada and concluded that the majority of sediment transported by anchor ice in these rivers was gravel-sized.

Several studies have attempted to determine the meteorological factors that impact anchor ice. Most descriptions of anchor ice in the literature emphasize the importance of cold clear nights (i.e. those with large heat losses due to long-wave radiation emission) in the formation of anchor ice, and the importance of sunny days (i.e. those with large shortwave radiation) in the release of anchor ice (e.g. Stickler and Alfredsen, 2009; Kempema and Ettema, 2011). Four studies have aimed to be more quantitative in their approach in assessing the factors impacting anchor ice growth and release. Bisaillon and Bergeron (2009) used a statistical approach with meteorological and hydraulic data to predict the presence or absence of anchor ice, both at the site and sub-site scale. This statistical approach correctly classified the presence or absence of anchor ice for 80.9% of 30 observations, including 16 anchor ice events at the site scale. Turcotte et al. (2013) reported on the growth and decay of anchor ice dams in steep streams and presented a heat budget to predict the formation and decay of anchor ice dams. This heat budget was refined and applied more specifically in Dubé et al. (2015). The heat budget models presented in Turcotte et al. (2013) and Dubé et al. (2015) rely on a large number of parameters, many of which are assumed. Turcotte et al. (2013)

included heat flux from groundwater in their heat budget. Their formulation appears very sensitive to the parameter controlling the groundwater heat flux, which only came into play when ice dams were growing or stable. However, these studies still represent the most detailed effort to date to account for all aspects of the heat budget as it pertains to anchor ice. Further, Tremblay et al. (2014) reported on the meteorological conditions prior to the formation and release of seven diurnal and multi-day anchor ice accumulations and concluded that the large incoming solar radiation on sunny days was not by itself sufficient to release anchor ice and considered air temperature to also be an important factor in anchor ice release.

Numerical models of anchor ice growth and decay have accounted for growth by frazil accretion, growth and decay by thermal exchange between the water and the anchor ice, and decay due to the direct absorption of solar radiation of the anchor ice accumulation (Malenchak et al., 2011). Malenchak et al. (2011) modelled the release of an anchor ice accumulation as a combination of a thermal process whereby the underside of an anchor ice accumulation is thermally eroded by a theoretical near-surface substrate flow or mechanically by the buoyancy of the anchor ice accumulation. However, there remains a dearth of field data to validate these approaches or provide insight into the magnitude of modelled parameters.

Anchor ice impacts several hydraulic, ecological, and economic river processes. Anchor ice may reduce the head at hydropower generating stations, reducing the generating capacity of the station (Girling and Groeneveld, 1999). Anchor ice dams may cause significant reductions in stream discharge, through the storage of water behind the accumulations and in the extraction of water from the flow as it forms ice (Turcotte et al.,

2014). This could may reduce the dilution and assimilation potential of pollution-receiving streams. Further, anchor ice dams may cause flooding when the ice dam height exceeds bankfull height of the stream. This has the potential to cause problems with infrastructure (Turcotte et al., 2013) and affect riparian vegetation (e.g. Lind and Nilsson, 2015). Flooding and scour may also occur when anchor ice releases causes a mid-winter ice run (Tesaker, 1994). The discharge increase due to the release of anchor ice over a large stretch of the Peace River in western Canada was recently suspected of causing "anchor ice waves" that have the potential of destabilizing recently-formed downstream ice covers thereby instigating the formation of a freeze-up ice jam with the potential of flooding human settlements (Jasek et al., 2015). The backwater caused by anchor ice accumulations can change the flow patterns of a stream, drowning riffles, and creating a more quiescent flow that can instigate the formation of a floating ice cover. The formation of anchor ice can therefore cause significant changes in the instream environment with minimal changes in discharge (Stickler et al., 2010). Anchor ice may cause some fish to move to ice-free habitats (Brown, 1999), but may also provide shelter for some species (Roussel et al., 2004). The diurnal nature of some anchor ice formation and releases may create a rapidly-changing environment for aquatic organisms that may stress organisms such as overwintering juvenile and adult salmonids as suggested by Stickler et al. (2010), but may provide feeding opportunities for some fish species because anchor ice releases dislodge invertebrates (Martin et al., 2001).

In summary, anchor ice is an important aspect of rivers in cold regions. However, it is largely an ephemeral phenomenon and often occurs at night. It is therefore difficult to study and the total number of anchor ice events that have been documented in the

historical literature has remained small. The study presented in Chapter 2 of this thesis analyzed 161 anchor ice events over two winters in three streams in north-central New Brunswick, Canada. This allowed for an unprecedentedly complete picture of how and under what conditions anchor ice forms and releases.

1.2.2 Ice Jam Releases and Ice Jam Release Waves

An ice jam is a jumbled accumulation of broken river ice that partially blocks a river channel, raises water levels, and potentially causes flooding. An example of an ice jam as viewed from ground level is shown in Figure 1.2a. An ice jam holds behind it impounded water and ice. It has a "head" at its upstream end and a "toe" at the downstream end where the ice accumulation is thickest (Figure 1.2b). In a static situation (i.e. for a 'stable' ice jam), the driving forces acting on the ice jam in the downstream direction (i.e. the downslope component of ice weight and drag from the water flowing underneath) are balanced by forces keeping the jam in place (i.e. the frictional forces along the banks and against any obstructions, which are transferred to the ice mass by the frictional internal strength of the ice accumulation). However, ice jams are inherently unstable, as incoming flow (and possibly incoming ice) act to increase the destabilizing driving forces. This can trigger a dynamic situation where the ice jam fails. When ice jams fail the impounded ice and water is rapidly released. The sudden release of impounded ice and water from an ice jam can be very dangerous for northern riverside communities. Water level rises in excess of 80 cm per minute (Hutchison and Hicks, 2007) and wave celerities of 10.9 m/s have been reported to result from ice jam releases (Beltaos, 2014). Flooding can result, damaging property and threatening lives.

An ice jam release causes a water wave and moving ice accumulation (called an "ice run") to advance downstream. Jasek and Beltaos (2008) refer to this as a "jave" for ice jam release wave. Jasek (2003) and Beltaos and Burrell (2005) refer to the water wave resulting from an ice jam release as a "dynamic forerunner." Herein, the terms "wave" and "ice run" will be used to distinguish the water and ice phases resulting from an ice jam release. These phases travel downstream at separate celerities resulting in two distinct, but initially overlapping, features. Although the ice run spreads out as it propagates, there is still considerable interaction between ice floes and between the ice floes and the riverbanks. This interaction causes the ice run to move slower than the water wave. As a result, the front of the water wave eventually moves out in front of the downstream edge of the ice run as they travel downstream. Jasek (2003) documented that this occurs once the water wave has propagated a distance of approximately 6 times the original ice jam length.

Documenting wave propagation and attenuation requires measurement of water level as a function of time (i.e. measurement of stage hydrographs) at multiple points along the river channel. Obtaining the full stage hydrograph at a number of locations is important in order to capture both the front and the peak of the wave because they travel at different celerities. This is because the wave attenuates (spreads out) due to friction as it travels downstream. Ice jam release events are difficult to measure owing to the difficulty in predicting the location of an ice jam and the time of release. The dynamic nature of ice runs makes instrumentation difficult, as instruments can be easily damaged or lost in the torrent of ice and water of an ice jam release. Finally, ice runs can be observed from the aircraft in remote regions, but water wave processes are invisible from

the air, making simultaneous observation of water and ice difficult.

Researchers have documented the propagation of water waves resulting from ice jam releases. Kowalczyk and Hicks (2003) documented ice jam release water waves initially travelling at the dynamic wave speed (where acceleration dominates), then eventually slowing to the diffusive wave speed (where friction dominates). However, Hutchison and Hicks (2007) also suggested that if the corresponding ice run stalls, even momentarily, water may be sufficiently impounded to create a new release event and the wave will become dynamic again. Considerably more observations of ice run velocities exist, because these can be readily documented without any specific instrumentation. Available data includes observations by Beltaos et al. (1994) on the Saint John River, Jasek (2003) on the Porcupine and Yukon Rivers, Beltaos and Burrell (2005) on the St. John River, NB, Hutchison and Hicks (2007) and She et al. (2009a) on the Athabasca River, AB, Watson et al. (2009) and Watson (2011) on the Hay River, NWT. However, prior to this study, no data existed describing the relative celerities of the water wave and the ice run and their evolution for the same release event as they advanced downstream.

Based on the numerical analyses of some of these observed events, Hicks et al. (1992) and Blackburn and Hicks (2003) determined that numerical models that include only flow hydrodynamics (i.e. ones in which ice effects are ignored) can reliably predict water wave propagation and attenuation. She and Hicks (2006) showed that, including simplified ice effects in ice jam release models, also results in reliable prediction of water wave propagation and attenuation as well as a better match of the shape of the observed hydrograph as compared to those models with ice effects neglected. They were also able to reproduce the separation of the water wave and the ice run with this model. However,

subsequent tests of their model for events measured on the Hay River, NWT (Watson, 2011) showed that ice run arrival times could not be accurately predicted.

Ice jam releases or similar dam break waves were studied in laboratory flumes by Wong et al. (1985) and Khan et al. (2000). Both studies used polyethylene blocks to simulate ice in their experiments. Wong et al. (1985) concluded that the ice had no effect on propagation of the release wave, while Khan et al. (2000) reported the opposite. Different experimental set ups may account for this discrepancy; Wong et al. (1985) had no ice in the receiving channel; Khan et al. (2000) included rubble ice in the receiving channel, but not in the flume section where water was stored prior to release. In addition, these laboratory channels were very short compared to the typical propagation distances in the field, and it is likely their results are only applicable to wave propagation in the reach immediately downstream of the ice jam release point. In reply to Jasek (2003), Beltaos (2003) suggested that when comparing laboratory studies of ice jam releases to full-scale field cases, the undisturbed (pre-water wave) depth should be used. Physical models of ice jam release waves by Wong et al. (1985) modelled a reach of about 100 flow depths and Khan et al. (2000) covered a reach of less than 1800 undisturbed flow depths. In comparison, ice jam release events in full-scale field cases can propagate over tens of thousands of river depths (e.g. Hicks et al., 1992, She et al., 2009a).

Both the water wave and the ice run are important in the emergency management of breakup but for separate reasons. The water wave provides the volume and height of water that can by itself cause flooding or can instigate the breakup of downstream ice covers, or instigate the release or consolidation of existing downstream ice jams. The ice run can interact with an existing downstream ice jam, adding momentum and volume to

the accumulation that can cause the thickening of the accumulation which, in turn, raises water levels and can cause flooding; or causing the release of the jam, sending a wave and ice run downstream with renewed amplitude and celerity. Being able to predict the arrival time of both the water wave and ice run at a point of interest on the river is important for breakup flood warning operations.

In summary, two phases, a water wave and an ice run, result from the release of an ice jam and they travel at separate celerities. While previous research has measured one phase or the other, there are no observations of how both phases evolves as they advance downstream over extended distances from a common jam release. This is because the dynamic, unpredictable, and remote nature of ice jam releases make them difficult to observe. Physical laboratory models of ice jam releases have been attempted but their usefulness is limited by the geometric constraints of typical laboratory flumes. In the study presented in Chapter 3 of this thesis, both the water wave and ice run components of ice jam release events were observed at several locations along a channel length exceeding 10,000 undisturbed flow depths.

1.2.3 Ice Jam Processes in Multi-channel Systems

Ice jams and ice jam flooding can also occur in multi-channel environments. Deltas, a type of multi-channel environment, are particularly prone to ice jams in cold regions because their low gradients, channel junctions, and islands have the effect of reducing the ice conveyance capacity of the channel. An example of an ice jam which formed in the Hay River delta (and analyzed in this thesis) is shown in Figure 1.3. In response to greater external forces, ice jams may release or may consolidate into a thicker

accumulation. The formation, consolidation, and release of ice jams are inherently unsteady and dynamic processes (Zufelt, 1990). What happens to ice jams in multi-channel systems has not been fully explored, particularly with regard to unsteady ice jam processes. Ice jam processes in multi-channel systems may have implications for northern delta communities and for the ecology of these biological "hotspots."

A few studies have examined the hydraulics of ice jam processes in multi-channel networks that are not deltas. For example, Ettema et al. (1999) and Ettema and Muste (2001) explored ice jam processes at channel junctions in detail using physical models. They focused only on situations where flows come together (e.g. where a tributary meets a channel), and not on the flow-dividing junctions that are the defining feature of deltas. Jasek (1995) investigated the theoretical effect of islands (a type of multi-channel environment) on ice jam thickness. His calculations suggested that the presence of islands in channels may result in thinner ice jams (and therefore reduced flooding) because the forces exerted on an ice jam were supported by a longer ice jam perimeter at the banks.

Several researchers have investigated the hydraulics of spring breakup in cold region deltas in Canada. However, these studies focused on steady-state conditions or did not consider channel junctions in their analysis. Beltaos et al. (2012) presented many measurements of ice jamming in the Mackenzie River delta, Northwest Territories. They suggested that ice jams in deltas may result in a water level profiles that have a different, flatter shape when compared to those observed in single-channel sections of rivers. The authors attributed this difference to the flat gradient of the river or to the fact that the channel discharge may decrease along the ice jam because of the many channels that

divide off the ice jam channel. The authors also provided an assessment of the extent to which an observed ice jam changed how river discharge was partitioned between the delta channels. Blackburn et al. (2015) applied the 1D *River1D* network model to the Mackenzie River delta. In this model, channel junctions are modelled without assuming a constant water level at the junction and thereby taking into account the physical effects at the junctions that are necessary to model dynamic unsteady flow in low-gradient environments. The authors modelled how various hypothetical ice jam scenarios may affect the flow distributions in the Mackenzie delta under steady-state conditions. Zhang et al. (2017) used remotely-sensed data to parametrize a 1D *RIVICE* model of a single channel in the Slave River delta, Northwest Territories, Canada. Their focus was on the use of the remotely-sensed data and did not describe how the channel junctions were handled in the model. Kolerski and Shen (2015) simulated a historical ice jam in the multi-channel St. Clair River Flats delta in Ontario, Canada and Michigan, USA, using the 2D *DynaRICE* numerical model. This model partitioned water flow and ice movements between the delta channels, but few observations of ice movements were available to verify the accuracy of this simulation.

Various 1D, 2D, and 3D hydraulic modelling approaches have been recently applied to the Hay River delta. Brayall and Hicks (2012) used the 2D model *River2D* to simulate historical ice jams in the Hay River delta and generate top of ice profiles and flood levels of several hypothetical flow situations. They found that, for the steady flow cases they modelled, the discharge partition at the dividing junction was similar under ice-covered and open water conditions. De Coste et al. (2017) applied a series of three numerical models to the Hay River delta to develop a procedure that can predict ice

profiles more quickly during emergency operations than can be done using 2D models. They applied the *River1D* network model developed by Blackburn et al. (2015) to determine the discharge partition at the delta junction then used a steady-state approximation to calculate ice jam top of ice profiles. Oveisy and She (2017) used the dynamic ice model *MPIce* coupled to the 3D hydrodynamic model *Delft3D* to simulate a historical ice jam in the Hay River delta. This model simulated ice jam movements at the delta junction under steady inflow conditions, and matched measured top of ice elevations well. The modelled ice movements were not compared to observed ice movements, and the model domain was smaller than the historical ice jam. This suggests that the success of the model in matching top of ice profiles may have been the result of model calibration. However, their study indicates that this approach may be applicable to future modelling efforts at channel junctions. All these efforts were focused on flood forecasting and matching measured top of ice profiles, and did not investigate the ice processes that occurred at the channel junction.

A few studies have examined unsteady ice jam processes in single-channel systems. Zufelt (1990) observed ice jam shoving and thickening using a physical model of simulated floating polyethylene ice pieces. The author observed the consolidation of ice accumulations and noted how ice moved starting from the upstream end of the accumulation and how the cessation of ice movement caused the thickening of the ice accumulation, starting at the downstream end. This observation lead the author to suggest that ice momentum may be important in ice jam consolidation. Accordingly, Zufelt and Ettema (2000) presented a model of ice jam dynamics that included terms for ice momentum. Healy and Hicks (2007) provided an exceptionally complete accounting

of unsteady ice jam dynamics under unsteady flow conditions, including particle tracking and water velocity measurements. They concluded that ice jams that formed under a rapid step-wise increase in discharge had a similar thickness to ice jams formed under steady flow conditions at the higher discharge. The authors suggested that this was because most of the ice consolidation occurred when the discharge was steady. The experimental results of Healy and Hicks (2007) were used by She et al. (2009b) to validate a new constitutive model describing the strength of moving ice accumulations that takes the momentum of the ice into account. This ice dynamics model was incorporated into the University of Alberta's *River1D* model.

To date, the study of ice jam processes has largely focused on either unsteady processes in single-channel systems, or on steady-state processes in multi-channel systems. Those very few studies that have examined ice jams in unsteady, multi-channel systems were numerical studies that did not have sufficient accompanying observations of ice jam processes to evaluate their effectiveness in simulating accurate ice jam movements. Therefore, advances in our understanding of how ice moves through delta junctions have been hampered by a lack of field measurements of these difficult-to-observe processes. The study presented in Chapter 4 of this thesis provides detailed qualitative and quantitative observations of unsteady ice jam dynamics at the main delta junction of the Hay River delta, Northwest Territories. It provides a conceptual model of the fundamental processes that occur in such environments.

1.3 Objectives

The research presented in this thesis advances our understanding of three unsteady

river ice processes: (1) anchor ice processes in small headwater streams, (2) ice jam releases in single channel systems, and (3) ice jam processes in multi-channel systems. Each of these components investigates the effects that unsteady, changing water levels and ice have on each other. Because it is not feasible to study these processes in a laboratory setting, field sites where extraneous complexities are minimized were chosen as the location for field experiments. For each field experiment, the ice processes were documented with comprehensive quantitative and qualitative observations of several events over at least two seasons. These observations informed the development of conceptual models and explanations that describe fundamental, real-world river ice process for which data and explanations had previously been unavailable.

1.4 References

Ashton, G.D. (Ed.), 1986. River and Lake Ice Engineering. Water Resources Publications, Littleton, Co. USA.

Beltaos, S. 2003. Discussion of "Ice jam release surges, ice runs, and breaking fronts: field measurements, physical descriptions, and research needs". Canadian Journal of Civil Engineering, 30(5):949-950.

Beltaos, S. 2014. Hydrodynamic properties of ice-jam release waves in the Mackenzie Delta, Canada. Cold Regions Science and Technology, 103: 91-106.

Beltaos, S., and Burrell, B.C. 2005. Field measurements of ice-jam-release surges. Canadian Journal of Civil Engineering, 32(4): 699-711.

Beltaos, S., Burrell, B. and Ismail, S. 1994. Ice and sedimentation processes in the Saint John River, Canada. Proceedings of the 12th IAHR Symposium on Ice, Trondheim, Norway, pp. 11-21.

Beltaos, S., Carter, T., Rowsell, R., 2012. Measurements and analysis of ice breakup and jamming characteristics in the Mackenzie Delta, Canada. Cold Regions Science and Technology, 82:110-123.

Bisaillon, J.F. and Bergeron, N.E., 2009. Modeling anchor ice presence–absence in gravel bed rivers. Cold Regions Science and Technology, 55(2):195-201.

Blackburn, J., Hicks, F. 2003. Suitability of dynamic modeling for flood forecasting during ice jam release surge events. ASCE Journal of Cold Regions Engineering, 17(1): 18-36.

Blackburn, J., She, Y., Hicks, F., Nafziger, J. 2015. Ice effects on flow distributions in the Mackenzie Delta. CGU HS Committee on River Ice Processes and the Environment 18th Workshop on the Hydraulics of Ice Covered Rivers. Quebec City, Canada. August 18-20

Brayall, M., Hicks, F.E. 2012. Applicability of 2-D modeling for forecasting ice jam flood levels in the Hay River Delta, Canada. Canadian Journal of Civil Engineering, 39(6):701-12.

Brown, R.S. 1999. Fall and early winter movements of cutthroat trout, *Oncorhynchus clarki*, in relation to water temperature and ice conditions in Dutch Creek, Alberta. Environmental Biology of Fishes, 55(4):359-368.

De Coste, M., She, Y., Blackburn, J. 2017. Incorporating the effects of upstream ice jam releases in the prediction of flood levels in the Hay River delta, Canada. Canadian Journal of Civil Engineering, 44(8):643-51.

Doering, J.C., 2002. Closure to "Laboratory study of anchor ice growth" by JC Doering, LE Bekeris, MP Morris, KE Dow, and WC Girling. ASCE Journal of Cold Regions Engineering, 16(2):99-100.

Doering, J.C., Bekeris, L.E., Morris, M.P., Dow, K.E. and Girling, W.C. 2001. Laboratory study of anchor ice growth. ASCE Journal of Cold Regions Engineering,15(1):60-66.

Dubé, M., Turcotte, B., Morse, B. 2015. Steep channel freezeup processes: understanding complexity with statistical and physical models. Canadian Journal of Civil Engineering, 42(9):622-633.

Ettema, R., Muste, M. 2001. Laboratory observations of ice jams in channel confluences. ASCE Journal of Cold Regions Engineering, 15(1):34-58.

Ettema, R., Muste, M. and Kruger, A. 1999. Ice Jams in River Confluences. CRREL Report 99-6, US Army Corps of Engineers, New Hampshire, USA.

Girling, W.C. and Groeneveld, J. 1999. Anchor ice formation below limestone generating station. CGU HS Committee on River Ice Processes and the Environment 10th Workshop on River Ice, Winnipeg, Manitoba.

Healy, D., Hicks, F., 2007. Experimental study of ice jam thickening under dynamic flow conditions. ASCE Journal of Cold Regions Engineering 21 (3), 72–91.

Hicks, F., Steffler, P., & Gerard, R. 1992. Finite element modeling of surge propagation and an application to the Hay River, NWT. Canadian Journal of Civil Engineering, 19(3): 454-462.

Hutchison, T.K., and Hicks, F.E. 2007. Observations of ice jam release waves on the Athabasca River near Fort McMurray, Alberta. Canadian Journal of Civil Engineering, 34(4): 473-484.

Jasek, M. 1995. Ice jam simulations in rivers with islands. CGU HS Committee on River Ice Processes and the Environment 8th Workshop on the Hydraulics of Ice Covered Rivers. Kamloops, Canada.

Jasek, M. 2003. Ice jam release surges, ice runs, and breaking fronts: field measurements, physical descriptions, and research needs. Canadian Journal of Civil Engineering, 30(1): 113-127.

Jasek, M., Beltaos, S. 2008. Chapter 8. Ice-jam release: javes, ice runs and breaking fronts. In River Ice Breakup, Beltaos S (ed.). Water Resources Publications: Highlands Ranch, CO.

Jasek, M., Shen, H.T., Pan, J. and Paslawski, K. 2015. Anchor ice waves and their impact on winter ice cover stability. CGU HS Committee on River Ice Processes and the Environment 18th Workshop on River Ice, Québec City, Québec.

Kalke, H., McFarlane, V., Schneck, C., Loewen, M. 2017. The transport of sediments by released anchor ice. Cold Regions Science and Technology, 143:70-80.

Kempema, E.W. and Ettema, R. 2011. Anchor ice rafting: observations from the Laramie River. River Research and Applications, 27(9):1126-1135.

Kerr, D.J., Shen, H.T. and Daly, S.F. 1997. Anchor ice formation and growth on gravel channel bed. CGU HS Committee on River Ice Processes and the Environment 9th Workshop on River Ice, CGU-HS Committee of River Ice Processes and the Environment, Fredericton, NB, September 24-26.

Kerr, D.J., Shen, H.T. and Daly, S.F. 2002. Evolution and hydraulic resistance of anchor ice on gravel bed. Cold Regions Science and Technology, 35(2):101-114.

Khan, A., Steffler, P., Gerard, R. 2000. Dam-break surges with floating debris. Journal of Hydraulic Engineering, 126(5): 375-379.

Kolerski, T., Shen, H.T. 2015. Possible effects of the 1984 St. Clair River ice jam on bed changes. Canadian Journal of Civil Engineering, 42(9):696-703.

Kowalczyk, T. and Hicks, F. 2003. Observations of dynamic ice jam release on the Athabasca River at Fort McMurray, AB. CGU HS Committee on River Ice Processes and the Environment 12th Workshop on River Ice. Edmonton, June19-20.

Lind, L. and Nilsson, C. 2015. Vegetation patterns in small boreal streams relate to ice and winter floods. Journal of Ecology, 103(2):431-440.

Malenchak, J. 2011. Numerical Modelling of River Ice Processes on the Lower Nelson River. Ph.D. Thesis. Department of Civil Engineering. University of Manitoba, Winnipeg, Manitoba, Canada.

Malenchak, J., Doering, J. and Shen, H.T. 2011. Modeling of anchor ice and aufeis formation at Sundance Rapids. CGU HS Committee on River Ice Processes and the Environment 16th Workshop on River Ice. Winnipeg, Manitoba.

Martin, M.D., Brown, R.S., Barton, D.R. and Power, G. 2001. Abundance of stream invertebrates in winter: seasonal changes and effects of river ice. Canadian Field Naturalist, 115(1):68-74.

Oveisy, A., She, Y. 2017. Modelling Ice Jam Formation in the Hay River Delta during 2009 Breakup. CGU HS Committee on River Ice Processes and the Environment 19th Workshop on the Hydraulics of Ice Covered Rivers. Whitehorse, Canada. July 9-12.

Qu, Y.X. and Doering, J., 2007. Laboratory study of anchor ice evolution around rocks and on gravel beds. Canadian Journal of Civil Engineering, 34(1):46-55.

Roussel, J.M., Cunjak, R.A., Newbury, R., Caissie, D. and Haro, A. 2004. Movements and habitat use by PIT-tagged Atlantic salmon parr in early winter: the influence of anchor ice. Freshwater Biology, 49(8):1026-1035.

She, Y., Hicks, F. 2006. Modeling ice jam release waves with consideration for ice effects. Cold Regions Science and Technology, 45(3): 137-147.

She, Y., Andrishak, R., Hicks, F., Morse, B., Stander, E., Krath, C., Keller, D., Abarca, N., Nolin, S., Nzokou Tanekou, F., Mahabir, C. 2009a. Athabasca River ice jam formation and release events in 2006 and 2007. Cold Regions Science and Technology, 55(2): 249-261.

She, Y., Hicks, F., Steffler, P., and Healy, D. 2009b. Constitutive model for internal resistance of moving ice accumulations and Eulerian implementation for river ice jam formation. Cold Regions Science and Technology, 55(3): 286-294.

Stickler, M. and Alfredsen, K.T. 2009. Anchor ice formation in streams: a field study. Hydrological Processes, 23(16):2307-2315.

Stickler, M., Alfredsen, K.T., Linnansaari, T., Fjeldstad, H.P. 2010. The influence of dynamic ice formation on hydraulic heterogeneity in steep streams. River Research and Applications, 26(9):1187-1197.

Tesaker, E. 1994. Ice formation in steep rivers. Proceedings of the 12th International Symposium on Ice, International Association of Hydraulic Engineering and Research, Trondheim, Norway.

Tesaker, E., 1996. Interaction between ice and water flow in rapids. Proceedings of the 13th International Symposium on Ice, International Association of Hydraulic Engineering and Research, Beijing, China.

Tremblay, P., Lacey, R.J. and Leconte, R. 2013. The impact of grain orientation and pebble surface roughness on the bond strength of simulated anchor ice. Cold Regions Science and Technology, 96:36-44.

Tremblay, P., Leconte, R., Lacey, R.J. and Bergeron, N. 2014. Multi-day anchor ice cycles and bedload transport in a gravel-bed stream. Journal of Hydrology, 519:364-375.

Tsang, G., 1982. Frazil and Anchor Ice: a Monograph. Natural Resources Council Subcommittee on Hydraulics of Ice Covered Rivers, Ontario, Ottawa, Canada.

Turcotte, B. and Morse, B. 2011. Ice processes in a steep river basin. Cold Regions Science and Technology, 67(3):146-156.

Turcotte, B., Morse, B., Dubé, M., Anctil, F. 2013. Quantifying steep channel freezeup processes. Cold Regions Science and Technology, 94:21-36.

Turcotte, B., Morse, B. and Anctil, F. 2014. Cryologic continuum of a steep watershed. Hydrological Processes, 28(3):809-822.

Watson, D. 2011. Observation and modeling of ice jam release events on the Hay River, NWT. M.Sc. thesis, University of Alberta.

Watson, D., Hicks, F. and Andrishak, R. 2009. Analysis of Observed 2008 Ice Jam Release Events on the Hay River, NWT. CGU HS Committee on River Ice Processes and the Environment 15th Workshop on River Ice, St. John's, NL.

Wong, J., Beltaos, S., Krishnappan, B. 1985. Laboratory tests on surges created by ice jam releases. Canadian Journal of Civil Engineering, 12(4): 930-933.

Zhang, F., Mosaffa, M., Chu, T., Lindenschmidt, K.E. 2017. Using remote sensing data to parameterize ice jam modeling for a northern inland delta. Water, 9(5),306.

Zufelt, J.E. 1990. Experimental Observations of Shoving and Thickening: Comparison to Equilibrium Thickness Theory. Proceedings of the 10th IAHR International Symposium on Ice. Espoo, Finland.

Zufelt, J.E., Ettema, R. 2000. Fully coupled model of ice -jam dynamics. ASCE Journal of Cold Regions Engineering, 14(1):24-41.

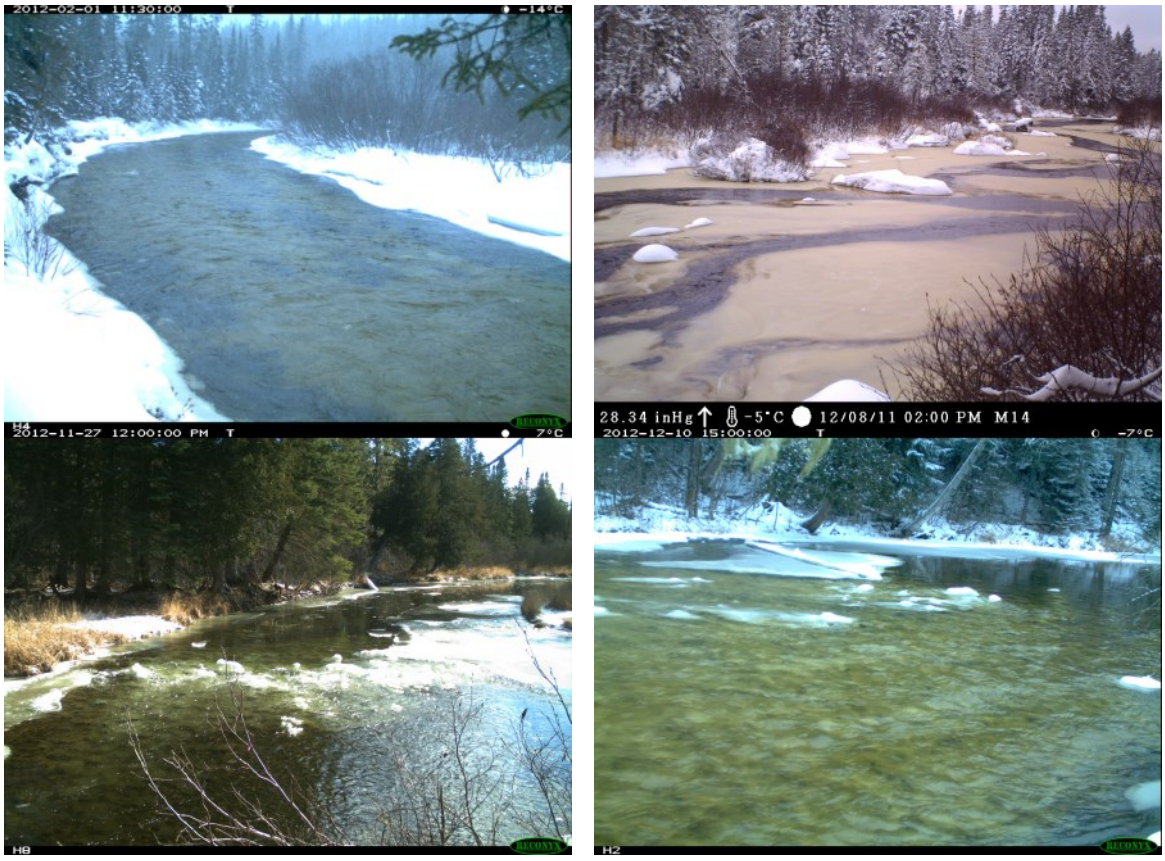

Figure 1.1. Examples of some of the 161 anchor ice accumulations observed on the study streams in north-central New Brunswick and analyzed in this thesis.

a)

b)

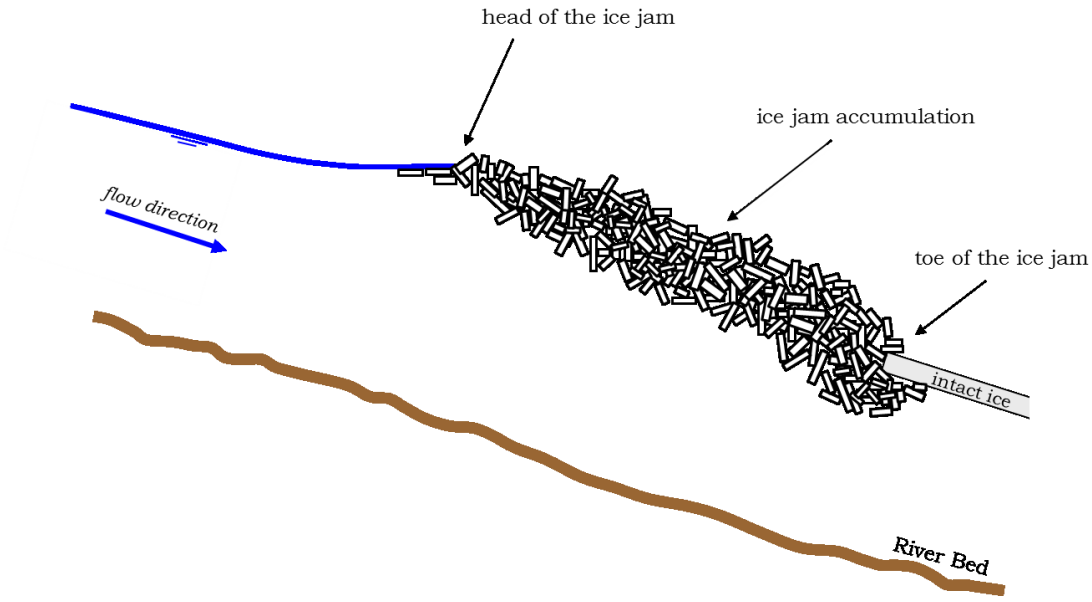

Figure 1.2. a) An ice jam as viewed from ground level and being measured for this research project. b) Typical profile of a stationary river ice jam showing the toe, ice accumulation, and the head of the ice jam (adapted from Ashton, 1986)

.

Figure 1.3. An ice jam in the multi-channel Hay River delta. The flow direction is from bottom left to top right.

Chapter 2. Anchor Ice Formation and Release in Small Regulated and Unregulated Streams

A version of this chapter was published as:

Nafziger, J., She, Y., Hicks, F. Cunjak, R. 2017. Anchor Ice Formation and Release in Small Regulated and Unregulated Streams. Cold Regions Science and Technology, 141:66-77. https://doi.org/10.1016/j.coldregions.2017.05.008

2.1 Abstract

Anchor ice is a type of river ice that occurs on river beds in supercooled, turbulent water. Its formation and release can affect the water level, discharge, bed roughness, and morphology of rivers in cold regions. Despite these important effects, the number of anchor ice events documented in the literature has historically remained small because of the ephemeral nature of anchor ice. The purpose of this study was to determine the hydrometeorological factors that control anchor ice formation, release, and morphology, as well as to determine the impact of hydropower regulation on the anchor ice regime of small streams. In total, 161 anchor ice formation and release events were examined in 2 regulated streams and 1 unregulated stream in north-central New Brunswick, Canada, using hourly or half-hourly ice observations and near-continuously measured environmental variables. The day after formation, anchor ice accumulations either completely released, stayed in place to form multi-day accumulations, or were incorporated into the surface ice cover of the stream. 98% of anchor ice accumulations completely released on days when there was a net heat gain to the water surface and the

air temperature was > -15 °C, indicating a strong thermal control on anchor ice release. The release of one accumulation could not be attributed to either thermal effects or to the 'plucking' of the substrate, suggesting the need for further study of the strength of ice-pebble bonds. Finally, the regulated and unregulated streams had different ice regimes: the regulated stream experienced a greater number of anchor ice events, which occurred with a different seasonal pattern compared to the unregulated streams.

2.2 Introduction

Anchor ice is a type of river ice that forms on river beds in supercooled, turbulent water. Unlike most surface ice, the entire accumulation of submerged anchor ice exists at a temperature very close to the melting point of water. As such, anchor ice accumulations are often ephemeral, and therefore are difficult to study. Consequently, the total number of anchor ice formation and release events documented in the literature has historically remained small. Anchor ice formation can transform streams by increasing the stage, decreasing the discharge (Turcotte et al., 2013), lowering the bed roughness (Kerr et al., 2002), and altering the morphology (Stickler et al., 2010). These transformations can be important for streams regulated for hydropower production; for example, an anchor ice-induced stage increase caused millions of dollars of lost generation potential at Manitoba Hydro's Limestone Generating Station (Malenchak, 2011).

Recent field investigations have enhanced our knowledge of how anchor ice forms and grows. Stickler and Alfredsen (2009) and Turcotte and Morse (2011) described anchor ice based on morphology and density, including: easily released accumulations of

low density; higher-density accumulations that form in the spaces between the bed particles; relatively uniform coatings of the river bed ("carpets"); accumulations concentrated across the channel ("weirs"); and emergent weirs that form with additional ice from water spray and cooling from air-exposed boulders ("dams"). Others (e.g. Tesaker, 1996) observed that anchor ice formation can be the first stage in the formation of a stream's seasonal surface ice cover. Many researchers (e.g. Bisaillon and Bergeron, 2009; Stickler and Alfredsen, 2009) emphasize the importance of cold, clear nights in the formation and growth of anchor ice. Turcotte et al. (2013) and Dubé et al. (2015) employed a heat budget approach for predicting anchor ice formation in small streams; however, the application of this approach is limited by the many parameters that must be assumed, such as the ratio of ice-affected channels in the watershed. Further, the regulation of large rivers for hydropower operations affects their thermal and ice regimes (see Grebe et al., 2013); however, how hydropower operations affect anchor ice in smaller streams has not been documented.

Anchor ice often occurs in a daily cycle; it forms during cooling at night and releases under the warming influence of rising air temperature and increasing shortwave radiation the next day. However, anchor ice accumulations may persist for several days (Tremblay et al., 2014) to many weeks (Malenchak, 2011). Shen (2005) proposed that anchor ice releases either thermally when the ice-substrate bond is weakened by melting, or mechanically when the buoyant thickness of anchor ice is sufficient to 'pluck' (i.e. pull up) the substrate from the bed. Tremblay et al. (2013) investigated the effects of the surface roughness and the orientation of pebbles on the relative strength of the ice-pebble bond, but did not quantify this strength. Jasek (2015) observed "anchor ice waves"

caused by the discharge of stored water following the release of anchor ice. These waves may be accompanied by an increased sediment load transported by free-floating anchor ice (Kempema and Ettema, 2011; Kalke et al., 2016).

This study examined the formation and release 161 anchor ice events over two winters. The anchor ice events were characterized using near-continuously measured environmental variables and hourly or half-hourly ice observations during daylight hours. The objectives of this study were four-fold:

1. Determine which meteorological factors are most important to anchor ice formation;
2. Determine the likely causes of anchor ice release;
3. Determine the factors that lead to different anchor ice morphologies; and
4. Determine the impact of regulation on the anchor ice regime of small streams.

2.3 Study Sites and Field Methods

2.3.1 Site Description

Study sites in three streams in north-central New Brunswick (Figure 2.1) were chosen based on regulation status and comparable morphology. Each stream had a known history of Atlantic salmon spawning activity, which was important for a concurrent study. Table 2.1 summarizes the physical and hydraulic characteristics of these high-gradient (slope > 0.3%), riffle-pool streams that were studied during the winters of 2011-2012 (Year 1) and 2012-2013 (Year 2). One stream, the Gulquac River (N46º56’29.1” W67º4’52.4”), is a natural-flow (unregulated) stream. The other two

streams, the River Dee (N47º4'33.7" W67º1'20.7") and the Serpentine River (N47º10'48.1" W66º50'57.7") are flow-regulated streams each with head pond reservoirs controlled by bottom-draw dams at their origin. Discharge through each dam as reported by NB Power is shown in Figure 2.2.

2.3.2 Instrumentation

Air temperature was measured with a Campbell Scientific 107 temperature sensor (accuracy < 0.9 ºC, data interval: 15 or 30 minutes) installed inside a louvered radiation shield and attached to a Campbell Scientific CR510 datalogger. To accurately capture air temperature in incised stream valleys, the instruments were placed in a sheltered area approximately 3 m above stream elevation at Sites G1 (Year 1) or G2 (Year 2, Figure 2.1). In Year 2, shortwave radiation was also measured with a Kipp and Zonen SPLite pyranometer (data interval: 30 min) attached to a Campbell Scientific CR510 datalogger, located ~2.5 m above ground surface in an open area (Figure 2.1). Both the sensor and datalogger were factory-calibrated prior to deployment. The sensor was manually cleared of snow during and after snowfalls.

Water depth was measured in pools at each study site and downstream of each dam using submersible, self-contained pressure transducers and dataloggers (Schlumberger Diver models 501 and 601, accuracy: 1.0 and 0.5 cmH_2O, and Onset Hobo model U20-001-04, accuracy: 0.3 to 0.6 cmH_2O, measurement intervals: 3, 15, or 20 min). The instruments were installed in silt socks, placed in white perforated PVC casings and weighed down with cinder blocks secured by cables to trees. The elevations of the instruments were surveyed with respect to temporary benchmarks installed at each

site. The pressure data were corrected to eliminate the effects of atmospheric pressure changes using data from a barometric pressure datalogger (Schlumberger Diver model DI500, accuracy: 0.5 cmH2O) installed ~3 m above stream level at Sites S1 (Year 1) or G2 (Year 2). The resulting depths were further corrected for offset errors and differences in elevation between the site and the barometric pressure logger using water depths measured by hand at installation and, where available, at retrieval.

Surface water temperatures were measured using Hobo TidbiTv2 (accuracy: 0.2 ºC) and Vemco Minilog-II-T (accuracy 0.1 ºC) sensors installed in the same PVC casings as the pressure transducers, or in a similar arrangement on a separate cinder block. The water temperature data were corrected using a graphical approach whereby the observed residual supercooling temperature was set to 0 ºC or, where available, through a laboratory comparison of the sensors used in the field to a Seabird model SBE39 temperature sensor (accuracy: 0.002 ºC), as described by Nafziger et al. (2013). This approach has been shown to be effective at minimizing offset errors associated with less accurate instruments.

Ice conditions were photographed at each site every 30 or 60 minutes using tree-mounted time-lapse cameras (various models used: Reconyx PC800, and Reconyx PC85, Moultrie PlotStalker, and Moultrie I-65). None of these cameras was particularly effective in darkness; therefore, ice conditions were typically not documented at night (~17:00-08:00).

2.4 Data Analysis Methods

2.4.1 Detection of Anchor Ice Events

The detection and identification of anchor ice events using photographic observations has limitations. For example, anchor ice is difficult to observe at night without the use of extensive lighting, which was logistically impractical in this remote area. Additionally, anchor ice can be difficult to detect in photographs during daylight if the flow is deep, or if there are waves and/or light reflections on the water surface. Consequently, anchor ice events identified using photographic observations necessarily represent a subset of the total number of anchor ice occurrences.

Anchor ice tends to obstruct the stream flow; therefore, formation and release events are typically associated with a corresponding increase and decrease in local depth. Accordingly, the detection of anchor ice events can be enhanced by examining the stage (i.e. water level) hydrographs in conjunction with photographic observations. However, this requires that other factors that can affect stage (e.g. changing discharge, precipitation, and surface ice development) are not occurring at the same time. Water temperature data can also aid in confirming anchor ice events, which would not be expected at water temperatures > 0 °C.

Anchor ice events were identified based on the available photographic, stage, and water temperature data. They were classified as either *definite* or *indefinite*, based on the type and the quality of the identifying data. Definite anchor ice events were identified based on the presence of a prominent and transient increase in stage, accompanied by at least one concurrent photographic observation of anchor ice. Indefinite anchor ice events were identified where no photos of anchor ice were available but a prominent and transient increase in stage was observed, coupled with supercooled or ~0 °C surface water temperatures, and minimal or no surface ice growth. Indefinite anchor ice events

were also identified in cases where anchor ice was observed in photographs, but for which other factors were also affecting the stage, such as changes in dam discharge or runoff events. The subset of definite anchor ice events was deemed to be representative of all the anchor ice events that occurred in the study streams.

Although both definite and indefinite anchor ice events were used to determine patterns of occurrence and timing, only the definite events were used in the analysis of features of the stage hydrographs, environmental conditions, and the heat flux associated with the anchor ice events. In cases where anchor ice was confirmed to be the only factor affecting the stage, changes in stage were assumed to be directly proportional to changes in the height of anchor ice accumulations, following the approach of Turcotte et al. (2013). This allowed the changes in the measured stage hydrograph to be used as a proxy for the developing height of the anchor ice accumulation. This approach assumes that the hydraulic roughness of the anchor ice is the same as the bed, which could cause some errors in the anchor ice values determined by this method; however, the short distance (<~10 m) between the anchor ice accumulation and the stage measurement location is thought to minimize these errors.

2.4.2 Features of the Stage Hydrographs

The growth and release periods of each definite anchor ice event were determined from the measured stage hydrographs, as shown in Figure 2.3. The start of an anchor ice event was defined as the time prior to the observed increase in stage when a breakpoint in the slope of the stage hydrograph was observed. Similarly, the end of the event was defined as a breakpoint in the slope of the stage hydrograph, after the increase in stage.

The duration of an anchor ice event was defined as the time difference between the start and end of the event. The growth period (Δt_G, Figure 2.3a) was defined as the time period during the anchor ice event before the peak stage; the release period (Δt_R, Figure 2.3a) was the time period after the peak stage. The total changes in stage during those periods were ΔH_G and ΔH_R, respectively. Changes in stage every 15 minutes (Δh) were also documented.

Definite anchor ice events were classified as either *single-day* or *multi-day*. Single-day events released in the first daylight period that occurred after they formed. In contrast, multi-day event persisted throughout the first daylight period that occurred after formation. Consequently, the definitions of the features of multi-day events (Figure 2.3b) were slightly different than those for single-day events. The first growth period of multi-day events was used when describing growth; the last release period of multi-day events was used when describing release.

2.4.3 Anchor Ice Morphology

The morphology of each definite anchor ice accumulation was classified as one of three types (Figure 2.4) based on its appearance in photographic observations:

- *Weir morphology*: consisted of an accumulation of anchor ice that stretched across the channel in a narrow band, usually at the crest of a riffle (Figure 2.4a).
- *Carpet morphology*: consisted of an accumulation of anchor ice that covered the bed of the channel over a significant longitudinal distance, rather than a narrow transverse band (Figure 2.4b).

- *Patchy morphology*: consisted of non-contiguous patches of anchor ice on the stream bed (Figure 2.4c).

2.4.4 Determination of Heat Flux at the Water Surface

The heat flux at the water surface was quantified using a linear heat flux model, which approximates all temperature dependent terms (e.g. convective heat flux, evaporation/condensation, and longwave radiation) as linear functions of temperature. Hicks et al. (1997) found that this approach effectively quantified the heat fluxes relevant to river ice processes. The heat flux was calculated as follows (after Andrishak and Hicks, 2008):

$$\Delta E = \phi_{sw}\left(1 - RF_{\alpha,SF}\right) + h_{aw}(T_a - T_w) - j_{aw} \cdot T_a \qquad (2.1)$$

Where ΔE is the heat flux to the water per unit area of the water surface in W/m^2 (negative values indicate heat loss from the water surface); ϕ_{sw} is the measured shortwave radiation in W/m^2. $RF_{\alpha,SF}$ is a dimensionless calibrated shortwave radiation 'reduction factor' (Table 2.2), which accounts for the effects of both the water surface albedo and the shading effect of the terrain and forest cover, similar to the approach used by Turcotte et al. (2013) in similar terrain. T_a and T_w are the measured air and water temperatures, respectively, in ºC; h_{aw} and j_{aw} are calibrated linear heat flux coefficients between the air and the water. The calibrated parameters (Table 2.2) were determined using data measured from October 25 to November 7, 2012, by matching the first time the water

temperature reaches 0 ºC (example calibration shown in Figure 2.5).

2.4.5 Statistical Analyses

Statistical analyses were performed using the R data analysis language version 3.1.2 (R Core Team, 2014) with the package "coin", version 1.1-2 (Hothorn et al., 2008). Measured or calculated dependent variables were compared across categorical independent variables (e.g. regulation type or ice morphology) using nonparametric alternatives to the independent t-test or analysis of variance (ANOVA) because of the small and uneven sample sizes and non-homogeneous variances between categories. The two-tailed Wilcoxon-Mann-Whitney-U rank sum test was used to compare two categories; and the two-tailed Kruskal-Wallis test was used to compare three categories (Hothorn et al., 2006). Statistically significant differences between categories were concluded to exist when the relevant test yielded $p < 0.05$. The test statistics (Z for Mann-Whitney-U rank sum tests, χ^2 for Kurskal-Wallis tests) and p-values are provided in the text.

2.5 Results and Discussion

2.5.1 Example progressions of anchor ice events

Figure 2.6 shows examples of three consecutive single-day, weir morphology anchor ice events at Site D3, including: the stream stage, H, and anchor ice observations (Figure 2.6a); the measured air temperature, T_a, shortwave radiation ϕ_{sw}; surface water temperature, T_w (Figure 2.6b to 2.6d); and ΔE (Figure 2.6e). The reported discharge at the dam during these events was constant at approximately 0.7 m^3/s. During the growth

periods of these example events, the surface water temperature remained at 0 °C or was supercooled, the air temperature was always < 0 °C, and the shortwave radiation was less than 150 W/m^2. Consequently, the heat flux was almost always negative. The stage increased overnight and by 08:00 each day anchor ice accumulations were visible in the photographs. During each event, the stage peaked between 09:00 and 10:00 and then decreased as the anchor ice started to release in pieces. Anchor ice Event A released more slowly than Events B and C; therefore, its stage hydrograph showed a more rounded shape. During the release periods, clumps of ice were observed floating by the site, indicating the release of anchor ice further upstream. Also, the heat flux increased, becoming positive near the time of the peak stage while the air temperature and shortwave radiation increased. The air temperature stayed < 0 °C during release while the water temperature increased from ~0 °C to approximately +0.4 °C. By 13:00 each day, the stage returned to baseline and anchor ice was no longer visible in the photographs, indicating that the anchor ice events were over.

Multi-day anchor ice events progressed differently than single-day events. Figure 2.7 shows an example progression of two multi-day, carpet-morphology anchor ice events at Site S3 in Year 2. The reported discharge at the dam over these four days had a slight decreasing trend from approximately 5.2 to 5.1 m^3/s. Unlike single-day events, these two events did not completely release on the first day, when the peak heat flux (Figure 2.7e) was +48 W/m^2 (Event D) and +25 W/m^2 (Event E) but the air temperature was very cold (< -15 °C, Figure 2.7b). During these first days, anchor ice pieces were observed to release from the accumulations and small decreases in stage were observed, indicating a partial release of the accumulations. Over the next night the stage increased,

indicating further anchor ice growth and evidenced by the thicker, more opaque accumulations observed the following morning. Event D completely released in the afternoon of February 6 while the peak heat flux and air temperature increased to +48 W/m^2 and -9.4 °C, respectively. This peak heat flux was the same as the previous day, but the air temperature was warmer.

The final release of Event E (Figure 2.7) was more complex than for Event D. The second growth period of Event E (Figure 2.7) started overnight February 7 to 8. The peak of this growth period occurred at 02:50 (February 8), after which the stage decreased slowly at first and then sharply at 05:40. It is unlikely that thermal factors caused these stage decreases because they occurred during a dark period with very cold air temperature (< -25 °C). The slow decrease in stage after 02:50 may be attributable to the flattening of the anchor ice accumulation and the consequent reduction in the roughness of the bed, or to flow abstraction due to ice formation. In contrast, the sudden stage decrease at 05:40 could have been caused by a partial release of the anchor ice due to buoyancy. The final release period for Event E began after the stage peaked at 10:20 (February 8), during which both the peak air temperature (-12.5 °C) and the peak heat flux (+66 W/m^2) were greater than on the previous day.

2.5.2 General Characteristics of the Definite Anchor Ice Events

A total of 161 anchor ice events (68 definite, 93 indefinite) were observed over the two study seasons. In Year 1, 32 definite and 52 indefinite events were observed; in Year 2, 36 definite and 41 indefinite events were observed. Of the definite anchor ice events, carpet morphology was most commonly observed (40 of 68 events: 59%),

followed by weir morphology (22 events: 32%) and patchy morphology (6 events: 9%). There were 19 definite multi-day events (28%) and 49 definite single-day events (72%). The duration of the single-day events ranged from 8 to 31 hrs (average 17.8 hrs), and the duration of the multi-day events ranged from 33 to 100 hrs (average 49.8 hrs).

The growth and release of the anchor ice accumulations determined the shape of the stage hydrograph for each definite anchor ice event. Single-day events had relatively simple shapes with a single growth and a single release period. The most common stage hydrograph shape (35 of 51 definite events: 69%) was a peaked shape (e.g. Events A, B, C in Figure 2.6). In contrast, a more flat-topped stage hydrograph (Figure 2.8a) was observed when anchor ice growth slowed during the day (10 of 51 events: 20%). The stage hydrograph had a two-stepped shape during its release period (Figure 2.8b) when the anchor ice accumulation released in two sections; for example, when an anchor ice weir partially released before the entire accumulation released (3 events: 6%). A two-stepped shape was also observed during the growth period of 3 events (6%).

Some peak-shaped stage hydrographs also had brief (< 2 hrs) secondary peaks in the stage hydrographs, either near their peak (Figure 2.8c) or during their release period (Figure 2.8d). These features were too brief to directly observe their cause. Possible causes include: 1) the superposition of an anchor ice release wave on the stage hydrograph; 2) by actual ice release and re-growth, or 3) when floating pieces of released anchor ice became trapped downstream of an accumulation which blocked the channel and temporarily raised the stage, before being released downstream.

The stage hydrographs associated with the definite multi-day events were

generally more complex than for the single-day events. Most (15 of 17) of the stage hydrographs associated with multi-day accumulations had multiple periods of anchor ice growth and release. In general, each period of anchor ice growth corresponded to an evening/overnight/morning and each period of anchor ice release corresponded to an afternoon (e.g. Event D, Figure 2.7), resulting in one peak for each day the accumulation was in place. However, two anchor ice events (including Event E, Figure 2.7) had a secondary peak on one of the days the accumulation persisted. Two other multi-day anchor ice events had only a single period of growth and release, which lasted for more than one day, resulting in a single-peaked stage hydrograph.

2.5.3 Anchor Ice Formation and Growth

The environmental conditions at the start and during the growth period of each definite anchor ice event demonstrate the importance of cold and dark conditions and negative heat flux for anchor ice initiation and growth. Every event started when the air temperature was < 0 °C, with a maximum air temperature of -3.8 °C. The surface water temperature was 0 °C or supercooled for 66 of 68 (97%) of the definite anchor ice events. The two remaining events had surface water temperatures of +0.16 °C and +0.29 °C and corresponded to patchy anchor ice accumulations that occurred on consecutive days in February of Year 2. Warmer hyporheic discharge may account for the higher water temperatures and patchy morphology of these events. The shortwave radiation at the start of the anchor ice events was always small, with an average value of 4 W/m^2. Finally, heat flux to the water was always negative at the start of the anchor ice events, with a maximum value of -17 W/m^2. The average air temperature during the growth period was always < 0 °C for each event, with a maximum of -4.1 °C. The average calculated heat

flux during the growth period was negative for each of the 68 definite anchor ice events and ranged from -168 W/m^2 to -26 W/m^2.

The maximum stage increase for all definite events ranged from 5.5 cm to 47.2 cm (average 16.9 cm). The rate of stage rise averaged over the growth period ($\Delta H_G / \Delta t_G$) ranged from 0.5 cm/hr to 5.0 cm/hr with an average of 1.1 cm/hr; and 67 of 68 anchor ice events had an average stage rise rate of 2.0 cm/hr or less. The largest stage rise rate measured in any 15 minute period was 23 cm/hr (0.00006 m/s). In a laboratory flume, Kerr et al. (2002) measured an anchor ice growth rate of 0.05 cm/(ºC・hr), expressed in terms of accumulated freezing degree hours of air temperature. This result was compared to the stage rise observed during the growth period of each of the 49 definite single day anchor ice events in Figure 2.9. The laboratory anchor ice growth rate was in the same range as the rate of stage rise of these field-measured anchor ice events, but was lower than 46 of 49 (94%) field-measured events.

The morphology of the anchor ice accumulations was dependent on both site morphology and flow conditions. At most sites, specific areas of the channel always experienced anchor ice with the same morphology. For example, the long riffle at Site S3 always experienced a carpet of anchor ice. However, some sites experienced different anchor ice morphologies depending on the flow and depth conditions. For example, at Site D3, a specific riffle sometimes experienced anchor ice with weir morphology and had carpet-like anchor ice at other times. The anchor ice at this riffle was weir-like when the stream discharge was low (< 4 m^3/s) and the downstream channel was unobstructed by ice. These conditions occurred most often at the beginning and end of the season,

before significant border ice had formed or after it had melted. However, when the stream discharge was high (> 4 m^3/s) or the riffle was in the backwater zone of downstream border ice, the riffle experienced anchor ice events with a carpet-like morphology. Therefore, at this site, flow conditions that allowed for a shallow depth and high relative roughness were important in creating weir-like anchor ice accumulations; and deeper, less turbulent conditions were important in forming carpet-like anchor ice accumulations.

The anchor ice accumulations contributed to the formation of a surface ice cover. This occurred by two different mechanisms, shown in Figure 2.10. The first mechanism occurred when border ice formed in the relatively quiescent backwater zone upstream of a weir-like anchor ice accumulation (Figure 2.10a and 2.10b). In some cases, the border ice narrowed the open channel sufficiently to allow floating frazil to accumulate and form a complete ice cover. The second mechanism was associated with carpet-like anchor ice accumulations. In shallow areas, the anchor ice accumulations grew from the bed to just below the water surface, often in patches (Figure 2.10c). When the stage decreased, possibly due to the release of downstream sections of anchor ice, the anchor ice partially drained and was left exposed to the cold air (Figure 2.10d). In some cases, these shallow areas also trapped floating ice pieces or falling snow, further exposing the accumulations to the cold air. Border ice then grew between the exposed anchor ice patches and formed a surface ice cover.

2.5.4 Anchor Ice Release

Three modes of anchor ice release were observed in the 40 definite events where

this process could be observed in photographs. The air temperature and shortwave radiation conditions during each release period in Year 2 are summarized in Figure 2.11. The first mode of release was through a process of slow melt where the accumulation was observed to get smaller from its margins over several hours. This mode was observed for 6 of the 40 (15%) anchor ice events. In Year 2, it occurred only on days when the peak shortwave radiation during the release period was < 250 W/m^2 and when the peak heat flux to the water during the release period was < 100 W/m^2 (Figure 2.11).

The second mode of release occurred when the accumulation released in pieces. In these cases, pieces of the accumulation were observed to disappear between photographic observations (30 or 60 minute intervals). This was the most common type of release, observed in 27 of 40 (68%) anchor ice events. The size of the pieces that released over 1 hour ranged from small (< 1 m^2) up to the entire accumulation (~150 m^2). In three of these events, anchor ice was observed to release in strips parallel to the flow direction, but releases of random patches were more common. In Year 2, the mode of release occurred over a wide range of meteorological conditions (Figure 2.11): from cold days to warm days (range of peak air temperatures: -12.5 °C of +5.3 °C) and dull to sunny days (range of peak shortwave radiation: 122 W/m^2 to 646 W/m^2).

The third mode of release occurred when the stream stage decreased, exposing suspended anchor ice accumulations which collapsed into the stream. This mode of release occurred when anchor ice of carpet morphology formed in the shallow sections of the stream. The stage decreased, possibly because of the release of a downstream ice accumulation. This exposed the structure of the accumulation, which was observed to be top-heavy: it consisted of a carpet of ice attached to the bed at a few locations, and at

emergent boulders. The top portion of the anchor ice then collapsed into the stream and was carried away by the current. This type of release occurred in 7 of 40 (18%) definite events and may be dependent on site morphology, because it was observed only at shallow sections of Sites G1 and D2.

The environmental conditions during the release period of the definite anchor ice events demonstrate the importance of positive heat flux at the water surface and of shortwave radiation in causing anchor ice releases. A positive heat flux to the water surface was observed at some point in the release period of 35 of 36 (97%) of the definite anchor ice events in Year 2. Only one anchor ice event (here called "Event F", at Site D2 in Year 2) released without a positive heat flux during its release period. The peak heat flux during the final release period of the definite anchor ice events in Year 2 ranged from (~0 W/m^2 to 313 W/m^2). The average air temperatures over the final release periods ranged from -21.3 °C to +4.7 °C and were < 0 °C for 62 of 68 (91%) of the definite events. Therefore for the majority of cases, the only warming contribution to the heat flux at the water surface was from shortwave radiation. However, air temperatures tended to increase during the day, which allowed the shortwave radiation to counteract the cooling effect of the cold air. Only one definite anchor ice event (Event G, Figure 2.11) released without the influence of shortwave radiation; its release period occurred entirely at night on a night when the air temperature climbed to slightly > 0 °C.

Figure 2.11 also shows the meteorological conditions during the multi-day events in Year 2 on the day they did not release. Each of the four multi-day events in Year 2 is represented by 2 points in Figure 2.11; one point represents conditions during its final release period, and the other represents conditions during the previous daylight period

when the accumulation did not release. The diagonal grey line in Figure 2.11 separates conditions that led to a complete release from those that led to the accumulation remaining in place. The value of the peak heat flux to the water surface is shown for each anchor ice event below the grey line. All anchor ice events above the grey line had a positive peak heat flux to the water surface, ranging from ~0 to 313 W/m^2.

The meteorological conditions and the direction of the heat flux together determined whether an accumulation would completely release during the day or whether it would stay in place to form a multi-day accumulation. Figure 2.11 shows that anchor ice accumulations did not completely release during cloudy or dull periods (peak shortwave radiation < 100 W/m^2) unless the air temperature was > 0 °C; nor did they release on sunny days (peak shortwave radiation >200 W/m^2) when the air temperature was < -15 °C. Combining these observations resulted in the diagonal grey line in Figure 2.11. The definite anchor ice events in Year 2 completely released if the heat flux was positive at some point during the event and if the peak air temperature was > -15 °C. Of the four multi-day anchor ice events, two had negative heat flux during the entire day that the accumulation did not release and the other two stayed in place while the heat flux turned positive (with maximum values of +25 and +48 W/m^2). Anchor ice events with a positive peak heat flux only stayed in place when the air temperature was < -15 °C. Therefore, the criteria that a positive heat flux to the water surface would cause a complete release of anchor ice accumulations could be used to predict complete releases on 37 of 40 (93%) of days with a definite anchor ice accumulation. Including the criteria that positive heat flux would only cause the release of the accumulation if air temperatures were > -15 °C would correctly predict the release of anchor ice

accumulations on 39 of 40 (98%) of days for all definite events at all sites in Year 2.

A similar pattern of environmental conditions leading to the formation of multi-day anchor ice events was also observed in Year 1, when shortwave radiation was not measured. Anchor ice accumulations did not release on cloudy days or when the sun angle was very low (as observed in the photographs) and the peak air temperature was < 0 °C. For accumulations to stay in place on sunny days (as observed in photographs), the peak air temperature during daylight hours had to be < -10 °C.

Event F is an exception to the above rules. It was the only accumulation that completely released while the air temperature was cold and when shortwave radiation was low (i.e. it plots below the diagonal grey line in Figure 2.11). It was also the only definite event that completely released while heat was being lost by the water at the water surface (maximum heat flux: -34 W/m^2). The stage fall rate ($\Delta H_R/\Delta t_R$) during the release period of Event F was high (13.4 cm/hr), in the 99th percentile for all definite events. Taken together, this indicates that Event F may not have released because of thermal effects, but because of a physical mechanism such as buoyancy.

To determine if the buoyant release of Event F was probable, the anchor ice thickness needed to pluck the substrate from the bed was calculated using the approach of Malenchak (2011). Equation 2.2 (after Malenchak, 2011) assumes spherical substrate with hexagonal packing where anchor ice fills the space between the top half of the particles:

$$t_{ai} = \frac{\frac{\pi d_s}{3\sqrt{3}}(\rho_s - \rho_w)g + C}{\frac{\rho_{ai}}{\rho_i}(\rho_w - \rho_i)g} - \frac{d_s}{2} + \frac{\pi d_s}{6\sqrt{3}} \qquad (2.2)$$

Where t_{ai} is the anchor ice thickness in m, measured above the top of the substrate; d_s is the substrate diameter in m; ρ_w, ρ_i, ρ_{ai}, *and* ρ_s are the densities of water, solid ice, anchor ice, and the substrate particles in kg/m^3, respectively; and C is the strength of the bond between the substrate and the bed in N/m^2. A limiting case can be constructed whereby Equation 2.2 generates the smallest anchor ice thickness required to pluck the substrate by assuming that the anchor ice density is equal to that of solid ice (917 kg/m^2) and C = 0 N/m^2. If d_s = 0.1 m (similar to the size of the substrate on riffles at these sites), ρ_s = 2600 kg/m^3, this limiting case results in an anchor ice thickness required to pluck the substrate of 1.15 m. However, the maximum water level change during Event F was 0.16 m, indicating that the anchor ice was not thick enough to pluck the substrate in the manner described by Equation 2.2.

There are other possible mechanisms of buoyant anchor ice release. The anchor ice may release when its buoyancy overcomes the strength of the bond between the ice and the particles, rather than by overcoming the weight of the substrate. This may be more common in cases where the substrate diameter is large. Alternatively, a combination of mechanisms may occur; the buoyant force of a single anchor ice mass may pull apart the anchor ice-substrate bond at some locations, but pluck the substrate at other locations. This would result in a mass of released anchor ice with occasional pieces of substrate in it, similar to what was observed by Kempema and Ettema (2011). Other possibilities for the mechanism of release include the influence of anchor ice release

waves originating from upstream releases and hydraulic dislodgment, as observed by Jasek et al. (2015).

Regarding Event F, sufficient data were not available to verify its exact mechanism of release. However, if it did release when buoyant forces overcame the anchor ice-substrate bond, an estimate of this bond strength can be obtained by Equation 2.3 (after Malenchak, 2011):

$$F_{B_{net}} = (t_{ai} + \frac{d_s}{2} - \frac{\pi d_s}{6\sqrt{3}}) \frac{\rho_{ai}}{\rho_i} (\rho_w - \rho_i) g \qquad (2.3)$$

Where F_{Bnet} is the net buoyant force on the anchor ice per unit area in N/m^2, which would be equal to the anchor ice-substrate bond strength at release. For an anchor ice thickness at release of 0.15 cm with a sediment size of 0.1 m, F_{Bnet} ranges from 45 N/m^2 to 138 N/m^2 for corresponding anchor ice densities ranging from 300 to 917 kg/m^3. This represents possible brackets of the strength of the ice-substrate bond at this location.

There were several notable features of the stage hydrographs during the release periods. The average stage fall rates during the final release periods ($\Delta H_R/\Delta t_R$) ranged from 0.5 cm/hr to 14.0 cm/hr, which was significantly larger ($p \approx 2 \times 10^{-14}$, Z=7.647) than the average stage rise rates. This is expected if hydrodynamic or buoyancy factors dislodged a large amount of anchor ice at one time, a faster process than the deposition and thermal processes dominating the growth of anchor ice. There was a statistically significant difference (p=0.006, χ^2=10.08) in average stage fall rates between the different ice release modes: piece-wise releases resulted in a wide range (1.1 to 11.8 cm/hr) while stage fall rates for the drain and collapse mode ranged from 1.2 cm/hr to 3.8 cm/hr and

the range for slow melt release mode was 0.5 cm/hr to 1.7 cm/hr. There were no statistically significant (p=0.699, χ^2=0.7153) differences in average stage fall rates between events with different ice morphologies. The largest stage fall rate measured over any 15 minute period during the definite events was 0.71 cm/hr (0.0002 m/s), three times larger than the largest stage rise rate observed.

Finally, surface water temperatures typically increased during the release period of the anchor ice events, and this increase tended to continue for up to two hours after the ice had completely released. Of the 68 definite anchor ice events, 29 (43%) had an increase in surface water temperature near the end of the event of 0.1 ºC or more and 12 of 68 events (18%) had an increase of 0.5 ºC or more. This temperature increase may be because once a proportion of the anchor ice had melted, released, and was transported downstream, heat gained by the water was then used to increase the water temperature, rather than melt the ice.

2.5.5 Effects of Regulation on Anchor Ice Regime

In the regulated streams, the ice regime was different closer to the dam than further downstream. The study sites directly downstream of the dams (i.e. Sites D1, S1) had no anchor ice events and the number of anchor ice events increased with increasing distance from the dam (Figure 2.12). In contrast, the unregulated stream experienced an approximately equal number of anchor ice events at each site, showing no stream-wise trend. Additionally, in the regulated streams, the number of days with a surface ice cover (>25% channel area) also increased with distance downstream; whereas the unregulated stream showed no stream-wise trend (Figure 2.12).

Based on these observations, a regulated river downstream of a bottom-draw dam may be conceptually divided into three sections. The first section is located immediately downstream of a dam, where no anchor or surface ice forms, and the surface water temperature remains > 0 °C. In the second section, downstream of the first, relatively more anchor ice events occur than would occur on a similar reach of an unregulated stream. In this reach, the water temperature frequently changes from ~ 0 °C to > 0 °C depending on the hydrometeorological conditions. The third section is a reach where all the excess heat from the reservoir has been dissipated and the ice regime of the regulated stream approaches that of an unregulated stream. The relative lengths of these conceptual reaches would be a function of the heat dissipation capacity of the stream as governed by channel morphology, flow conditions, and meteorological conditions.

Figure 2.12 compares anchor ice and surface ice formation for each study site within the context of the three-reach conceptual model described above. Sites S1 and D1 were located in the first conceptual reach and experienced neither surface ice nor anchor ice formation. The remainder of the sites in the regulated streams fall within the second conceptual reach, where anchor ice is the dominant ice formation process. Site D3 in Year 1 experienced a similar number of anchor ice events, but relatively more days with surface ice cover than the other regulated sites. In fact, anchor ice and surface ice were observed at the same time at the same cross-section at Site D3. This site may therefore fall near the boundary between the second and third conceptual reaches, where the ice processes of regulated streams begin to approximate those of unregulated streams. In Figure 2.13, the first reach would plot only at the origin, and the exact boundary between the second and third conceptual reaches may be indistinct, but would be expected to have

a positive slope, similar to how it is shown on Figure 2.13. This is because natural streams that experience both surface ice and anchor ice would be expected to experience more days with surface ice than anchor ice.

The seasonal pattern of anchor ice formation was also different between the regulated and unregulated streams. Anchor ice events (definite and indefinite) in the regulated streams occurred throughout the winter, in every month from November to March. No anchor ice events occurred in the regulated streams in April. In contrast, in the unregulated sites no definite or indefinite anchor ice events occurred in January and February; they occurred only in the "shoulder" seasons (i.e. before the formation, or after the breakup of a surface ice cover). In both years the earliest and the latest anchor ice events occurred in the unregulated Gulquac River, including events in April in both years.

The seasonal differences in anchor ice formation between regulated and unregulated streams were reflected in the characteristics of the anchor ice events. This may be attributed to the fact that air temperatures were colder during the main part of the winter season when many anchor ice events occurred on the regulated streams. For example, the rate of stage rise during the growth period ($\Delta H_G / \Delta t_G$) on the regulated streams (average 1.2 cm/hr) was significantly (p=0.030, χ^2=4.688) higher than on the unregulated stream (average 0.9 cm/hr). In addition, in the regulated streams 18 of 57 (32%) definite anchor ice events were multi-day events. In contrast, there were no definite multi-day events in the unregulated stream; instead, a surface ice cover formed whenever anchor ice persisted for more than one day.

2.6 Summary and Conclusions

The formation and release of 161 anchor ice events were observed in three regulated and unregulated study streams over two winters in north-central New Brunswick, Canada. Sixty-eight of these events were confirmed by photographic observations and distinct water level signatures, including 36 with sufficient accompanying data to apply a linear heat flux model. Events were characterized based on the environmental conditions during the formation and release periods, features of the stage hydrographs, event duration, accumulation morphology, and mode of release.

Anchor ice formed when the heat flux to the water surface was negative, and the water was supercooled. Anchor ice morphology was classified as either: patchy, weir-like, or carpet-like. The same ice morphology tended to occur at the same location, indicating that site morphology was an important control on anchor ice morphology. However, when flow conditions changed, some locations experienced different anchor ice morphology, indicating that flow conditions are also an important factor determining anchor ice morphology.

The day after their formation, anchor ice accumulations either completely released, stayed in place to form multi-day accumulations, or were incorporated into the surface ice cover of the stream. Anchor ice contributed to the development of a surface ice cover by two mechanisms through border ice growth upstream of an anchor ice accumulation or through the growth of border ice between air-exposed anchor ice patches. Both multi-day and single-day anchor ice events were observed, but single-day events were more common, representing 72% of events. In the study sites, thermal factors heavily

influenced anchor ice release. Anchor ice completely released on 93% of days with a positive heat flux at the surface. Furthermore, when a positive heat flux was coupled with air temperatures > -15 °C, the release rate increased to 98%. Despite the importance of thermal factors in anchor ice release, one anchor ice accumulation released on a day with a negative peak heat flux and cold air temperatures. The release of this atypical event was not likely due to anchor ice buoyancy overcoming the weight of the particle and the bed-substrate bond and therefore demonstrates the need for further investigation into the magnitude of the strength of anchor ice-substrate bonding and other anchor ice release mechanisms such as hydraulic dislodgement and anchor ice waves.

The regulated and unregulated streams experienced different ice regimes. The unregulated stream experienced anchor ice only in the shoulder seasons, before and after the existence of a surface ice cover. In contrast, the regulated streams experienced anchor ice throughout the winter months and had a surface ice cover for a shorter period of time. The regulated streams, on average, experienced more anchor ice events, and the number of events increased with downstream distance from the dam. A conceptual model was proposed linking the occurrence of anchor and surface ice with regulation type and distance downstream, which may be useful for those conceptually determining the effect regulation has on a stream.

2.7 Acknowledgements

This project was funded as part of the Natural Science and Engineering Research Council's HydroNet strategic network grant and through NSERC Discovery grants; this support is gratefully acknowledged. The authors would also like to thank Aaron Fraser,

Paula Thoms, and J. Michelle Lavery of the University of New Brunswick; Janelle Banack and Stefan Emmer of the University of Alberta; and Alyre Marquis of the Serpentine Lodge for their assistance in the field. The authors would also like to thank NB Power for their support of HydroNet and provision of the discharge data. The suggestions of three anonymous reviewers also improved this article, thank you.

2.8 References

Andrishak, R. and Hicks, F. 2008. Simulating the effects of climate change on the ice regime of the Peace River. Canadian Journal of Civil Engineering, 35(5):461-472.

Bisaillon, J.F. and Bergeron, N.E. 2009. Modeling anchor ice presence–absence in gravel bed rivers. Cold Regions Science and Technology, 55(2):195-201.

Dubé, M., Turcotte, B., Morse, B. 2015. Steep channel freezeup processes: understanding complexity with statistical and physical models. Canadian Journal of Civil Engineering, 42(9):622-633.

Gebre, S., Alfredsen, K., Lia, L., Stickler, M., Tesaker, E. 2013. Review of ice effects on hydropower systems. Journal of Cold Regions Engineering. 27(4):196-222.

Hicks, F., Cui, W., Andres, D. 1997. Modelling thermal breakup on the Mackenzie River at the outlet of Great Slave Lake, NWT. Canadian Journal of Civil Engineering, 24(4):570-85.

Hothorn, T., Hornik, K., van de Wiel, M.A., Zeileis, A. 2006. A lego system for

conditional inference. The American Statistician, 60(3):257-263.

Hothorn, T., Hornik, K., van de Wiel, M.A., Zeileis, A. 2008. Implementing a class of permutation tests: the coin package. Journal of Statistical Software, 28(8):1-23.

Jasek, M., Shen, H.T., Pan, J. and Paslawski, K. 2015. Anchor ice waves and their impact on winter ice cover stability. Proceedings of the 18th Workshop on River Ice, CGU-HS Committee of River Ice Processes and the Environment, Québec City, Québec.

Kalke, H., Schneck, C., McFarlane, V., Loewen, M., Jasek, M. 2016. Rafting of sediment by anchor ice releases. In Proceedings of the 23rd International Symposium on Ice, International Association of Hydraulic Engineering and Research, Ann Arbor, Michigan.

Kempema, E.W. and Ettema, R. 2011. Anchor ice rafting: observations from the Laramie River. River Research and Applications, 27(9):1126-1135.

Kerr, D.J., Shen, H.T., Daly, S.F. 2002. Evolution and hydraulic resistance of anchor ice on gravel bed. Cold Regions Science and Technology, 35(2):101-114.

Malenchak, J. 2011. Numerical Modelling of River Ice Processes on the Lower Nelson River. Ph.D. Thesis. Department of Civil Engineering. University of Manitoba, Winnipeg, Manitoba, Canada.

Nafziger, J., Hicks, F., Thoms, P., McFarlane, V., Banack, J., Cunjak, R.A. 2013. Measuring supercooling prevalence on small regulated and unregulated streams in

New Brunswick and Newfoundland, Canada. Proceedings of the 17th Workshop on River Ice, CGU-HS Committee of River Ice Processes and the Environment, Edmonton, Alberta.

R Core Team. 2014. R: A language and environment for statistical computing. R Foundation for Statistical Computing, Vienna, Austria. URL: http://www.R-project.org.

Shen, H.T. 2005. CRISSP1D Programmer's Manual. CEATI Report No. T012700-0401. Department of Civil and Environmental Engineering, Clarkson University, Potsdam, New York.

Stickler, M. and Alfredsen, K.T. 2009. Anchor ice formation in streams: a field study. Hydrological Processes, 23(16):2307-2315.

Stickler, M., Alfredsen, K.T., Linnansaari, T., Fjeldstad, H.P. 2010. The influence of dynamic ice formation on hydraulic heterogeneity in steep streams. River Research and Applications, 26(9):1187-1197.

Tesaker, E. 1996. Interaction between ice and water flow in rapids. Proceedings of the 13th International Symposium on Ice, International Association of Hydraulic Engineering and Research, Beijing, China.

Tremblay, P., Lacey, R.J., Leconte, R. 2013. The impact of grain orientation and pebble surface roughness on the bond strength of simulated anchor ice. Cold Regions Science and Technology, 96:36-44.

Tremblay, P., Leconte, R., Lacey, R.J., Bergeron, N. 2014. Multi-day anchor ice cycles and bedload transport in a gravel-bed stream. Journal of Hydrology, 519:364-375.

Turcotte, B. and Morse, B. 2011. Ice processes in a steep river basin. Cold Regions Science and Technology, 67(3):146-156.

Turcotte, B., Morse, B., Dubé, M., Anctil, F. 2013. Quantifying steep channel freezeup processes. Cold Regions Science and Technology, 94:21-36.

Table 2.1 Hydraulic characteristics of the study streams.

River	Regulation	Slope[a]	Width, m[b]	Depth, m[b]	Dam discharge, m^3/s[c]
River Dee	regulated	0.62 %	10 to 12	0.1 to 0.3, riffle 0.3 to 0.6 pool	0.6 to 13.4 m^3/s
Serpentine River	regulated	0.36%	10 to 16	0.1 to 0.5, riffle 0.3 to 0.7, pool	0.3 to 5.8 m^3/s
Gulquac River	unregulated	1.1%	10 to 17	0.1 to 0.3, riffle 0.4 to 0.7, pool	-

[a] measured over study reach

[b] measured at study sites at fall low flow levels

[c] range over study period: November 1 to April 30, 2011-2012 and 2012-2013

Table 2.2 Heat flux calibration parameters for each site.

Site	$RF_{\alpha,SF}$	h_{aw}	j_{aw}
D1	-	-	-
D2	0.5	12.5	2
D3	0.5	12.5	2
S1	-	-	-
S2	0.5	9	4
S3	0.5	10.3	3.5
G1	0.4	11	3.5
G2	0.6	10.6	3.5
G3	0.5	12.5	3

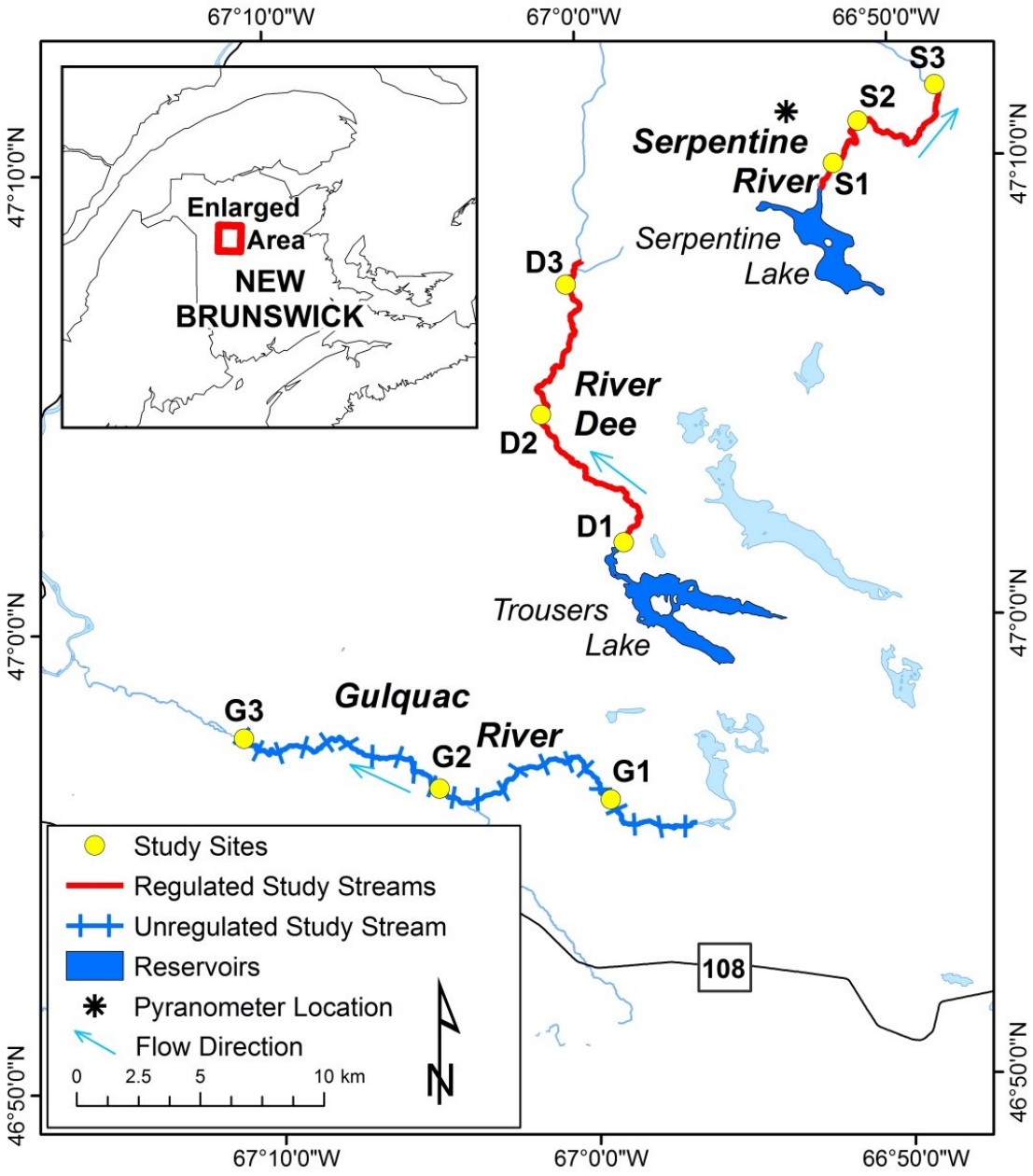

Figure 2.1. Location of the study sites and study streams in New Brunswick, Canada.

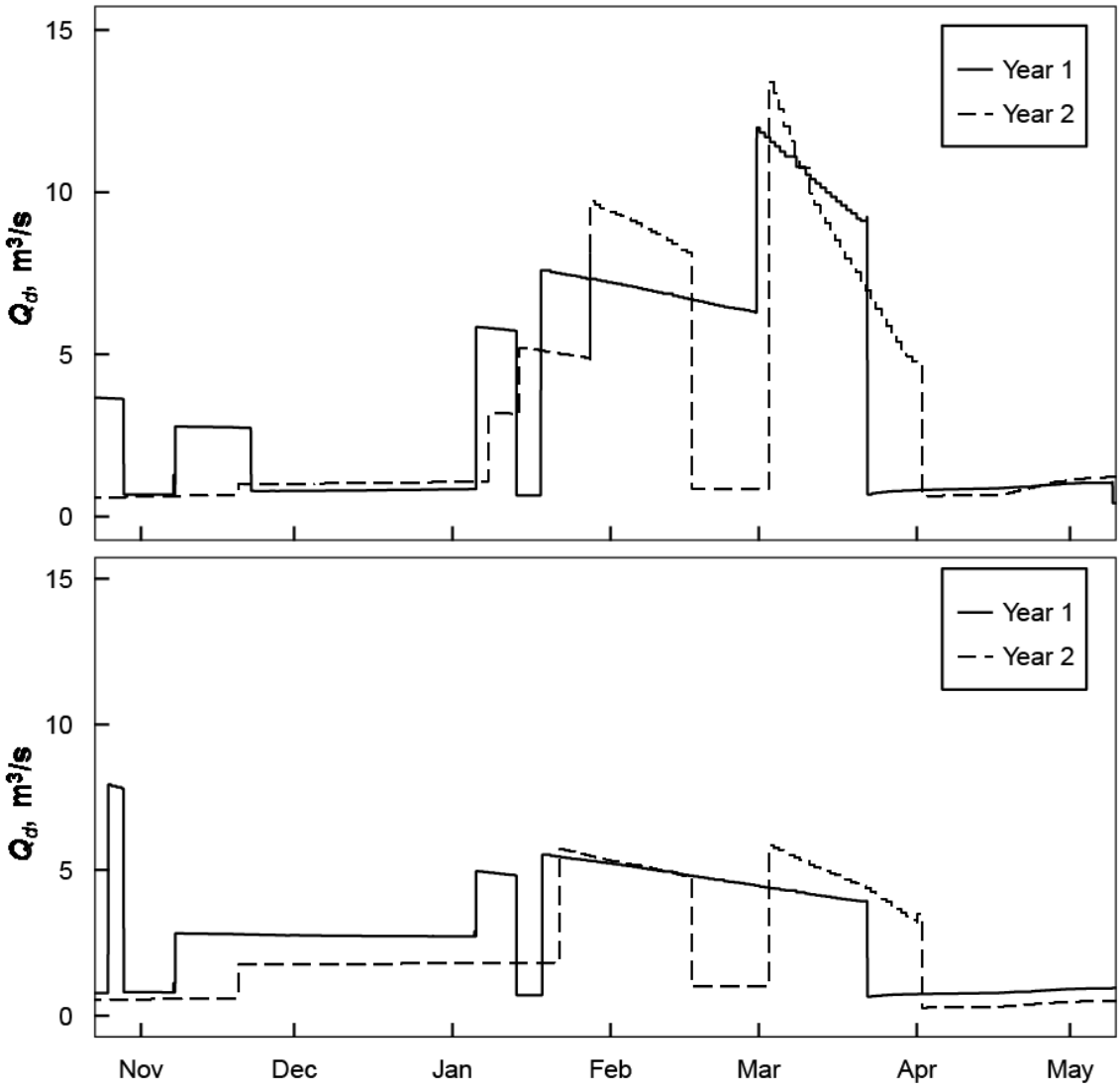

Figure 2.2. Discharge through the dams (Q_d) on the regulated streams: a) River Dee and b) Serpentine River. Discharge data was provided by NB Power.

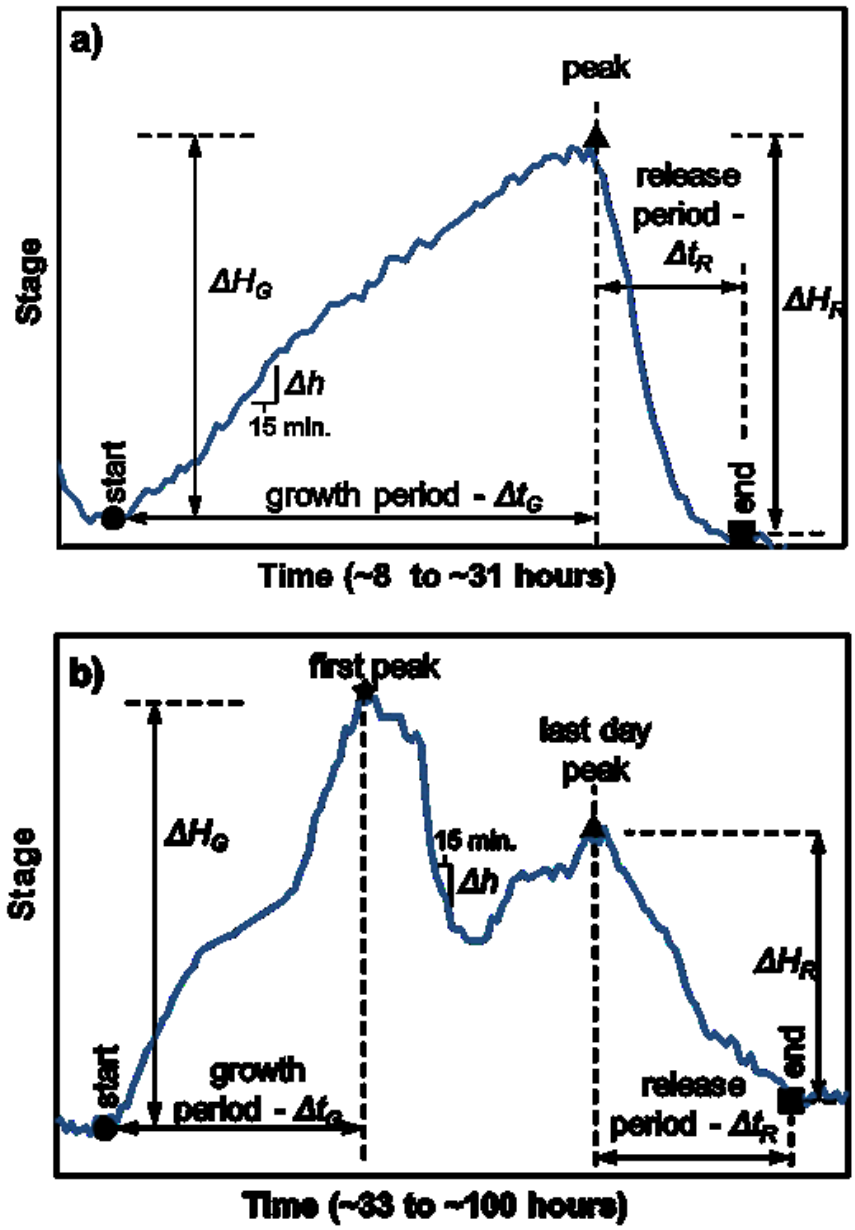

Figure 2.3. Definitions of various measures of the features of the water level hydrographs of a) a single-day event, and b) a multi-day, multi-peak event; Δh was defined for every 15 minute interval of all events.

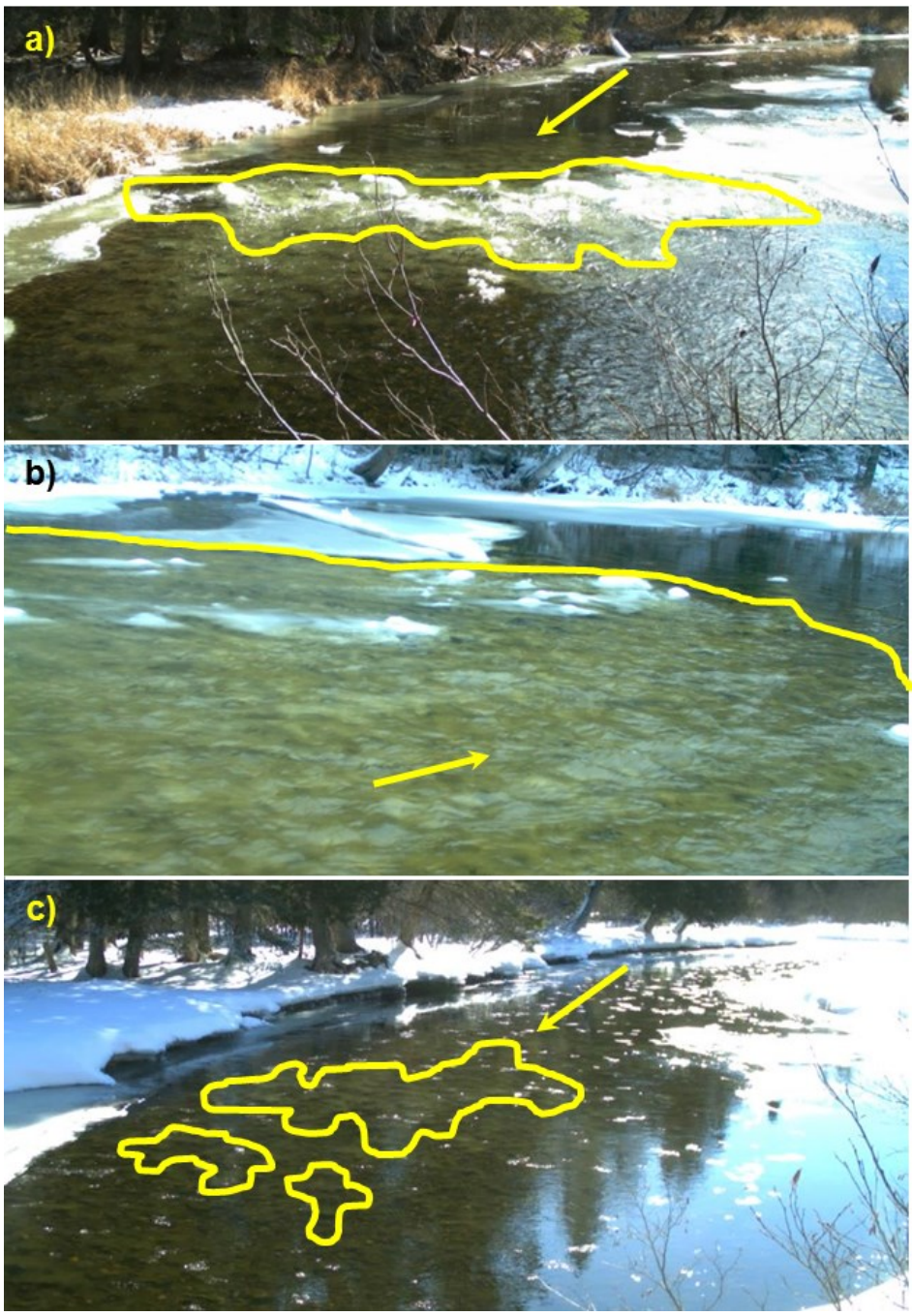

Figure 2.4. Examples of different anchor ice morphologies observed on the New Brunswick study streams: a) weir-like at Site D3, b) carpet-like at Site G3, c) small accumulation at site D3. Anchor ice accumulations are outlined, arrows indicate flow direction.

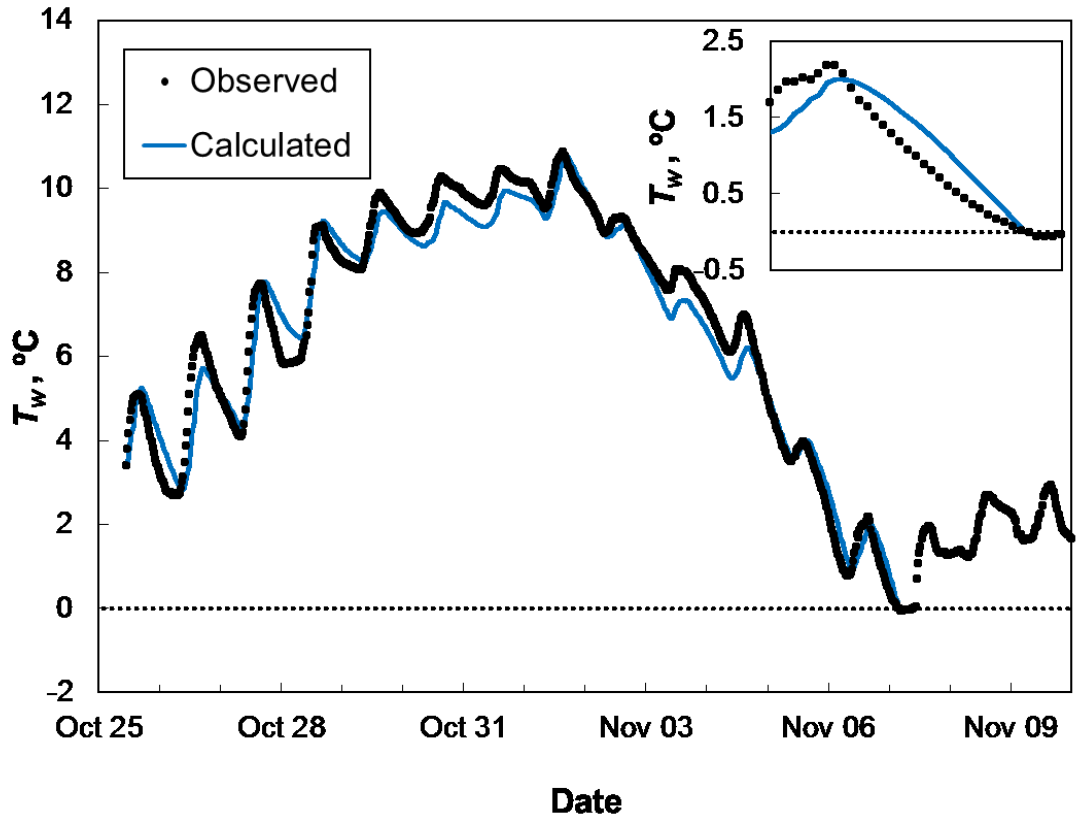

Figure 2.5. Example of heat flux calibration at Site G1. Inset graph is enlarged around the time when the water temperature first reached 0 ºC.

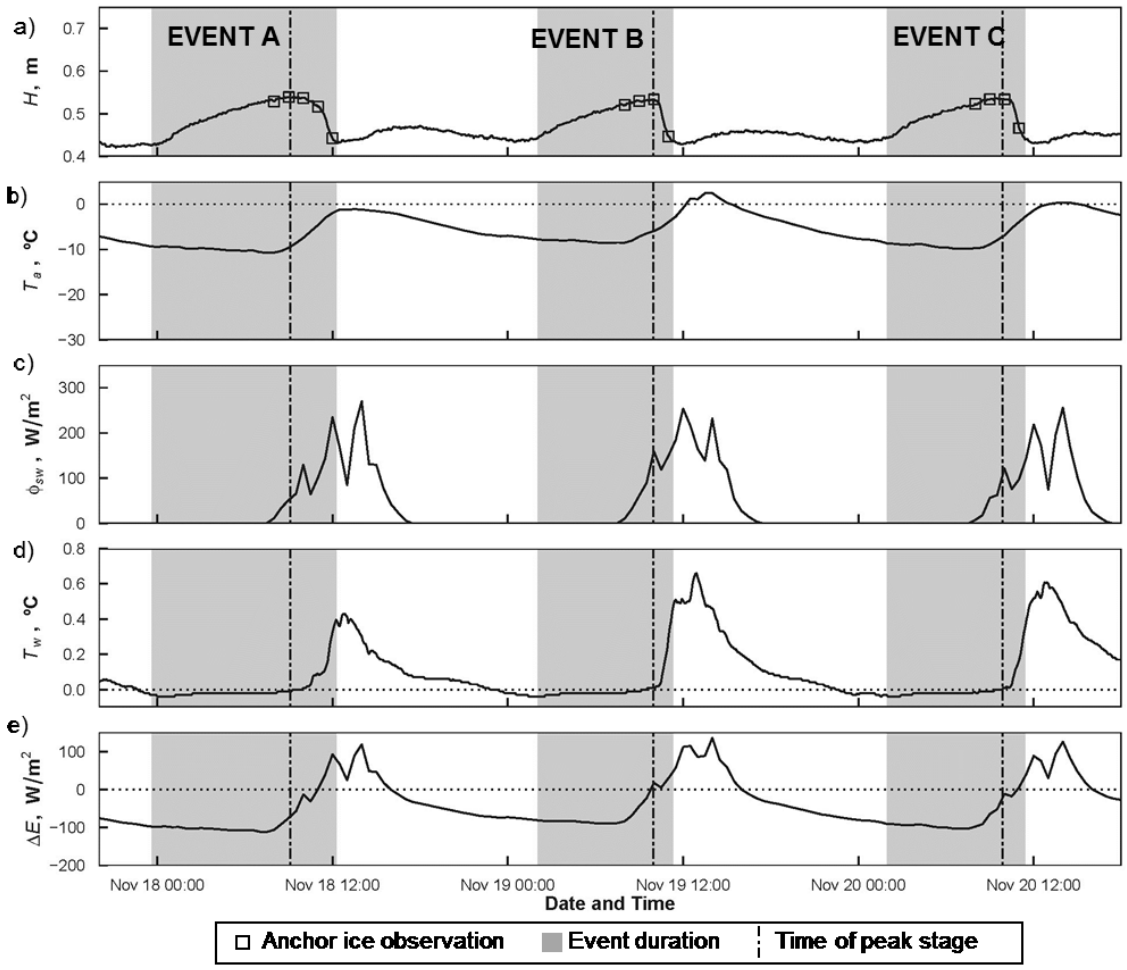

Figure 2.6. Summary of three single-day anchor ice events on the River Dee at Site D3 in November 2012 including: a) H = stage, and times of anchor ice photographic observations; b) T_a = air temperature; c) ϕ_{sw} = shortwave radiation; d) T_w = surface water temperature; e) ΔE = calculated heat flux to the water surface.

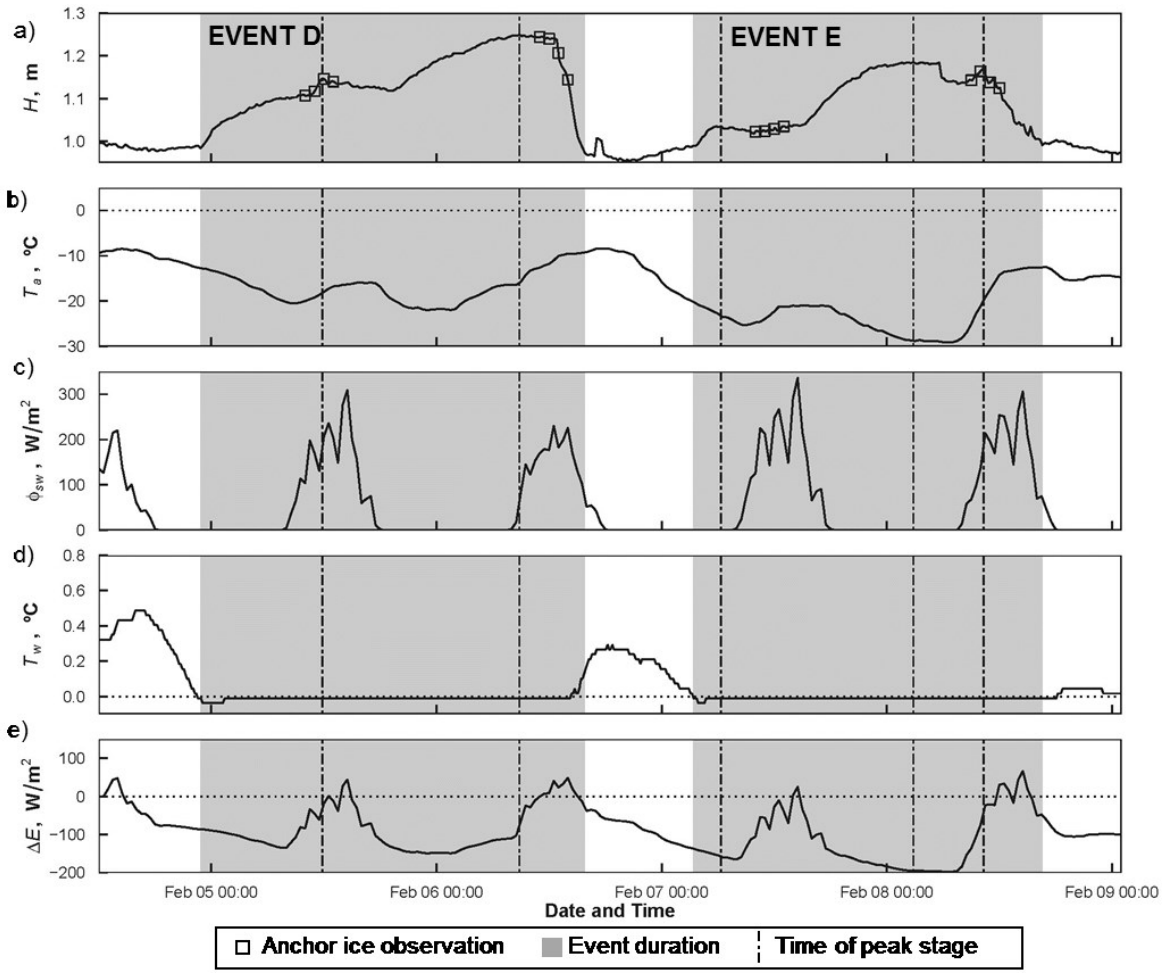

Figure 2.7. Summary of two multi-day anchor ice events on the Serpentine River at Site S3 in February 2013, including: a) H = stage, and times of anchor ice photographic observations; b) T_a = air temperature; c) ϕ_{sw} = shortwave radiation; d) T_w = surface water temperature; e) ΔE = calculated heat flux to the water surface.

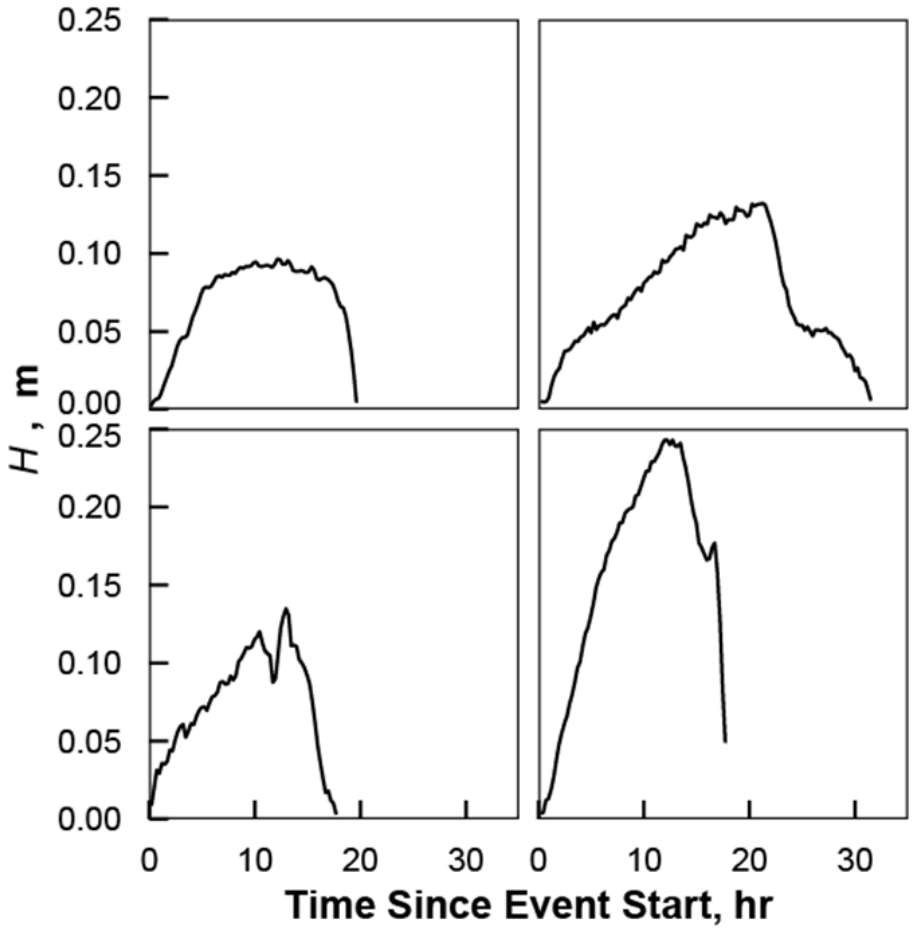

Figure 2.8. Examples of the observed different shapes of the stage hydrographs associated with anchor ice formation and release, additional examples are in Figures 2.6 and 2.7.

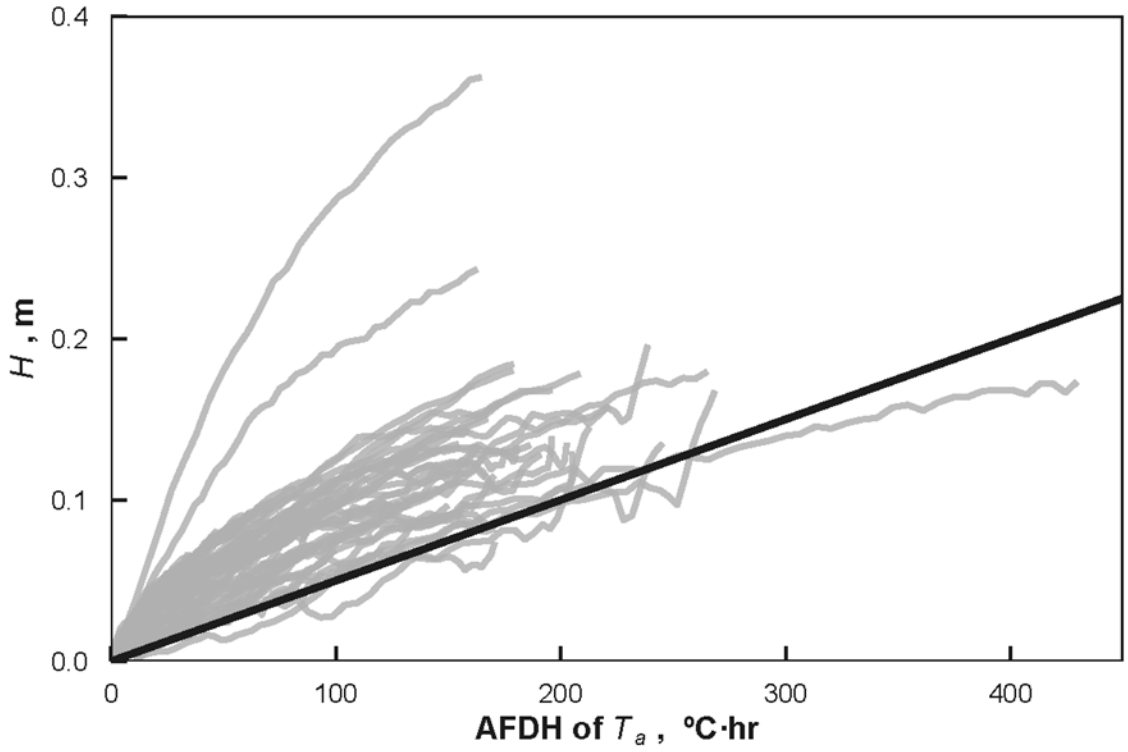

Figure 2.9. Accumulated freezing degree hours of air temperature (AFDH of T_a) versus stage for the growth period of each of the 49 definite single anchor ice events. The dark line represents the anchor ice growth rate observed in a laboratory flume by Kerr et al. (2002) of 0.05 cm/(ºC・hr).

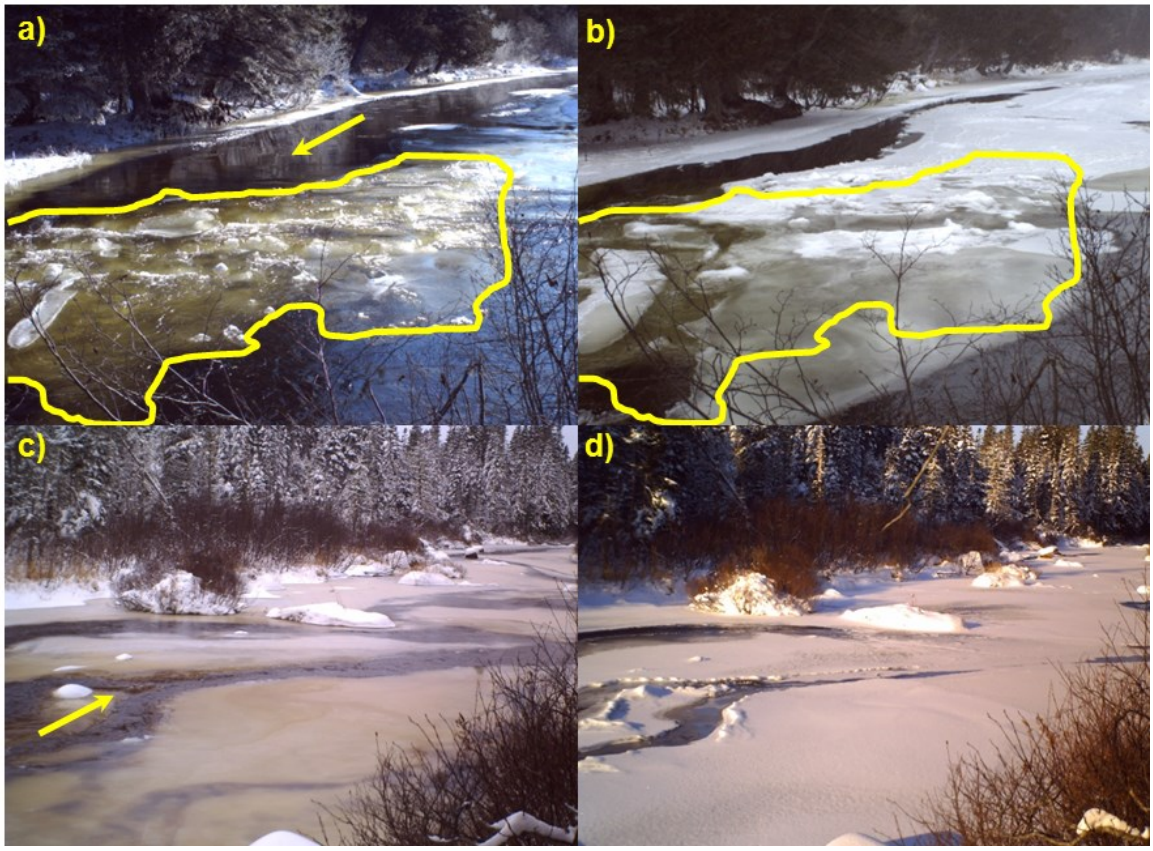

Figure 2.10. Different mechanisms by which anchor ice accumulations contributed to the formation of a surface ice cover: a) before and b) after surface ice formation upstream of an anchor ice weir at Site D3 (location of original anchor ice accumulation outlined); c) before and d) after surface ice formed between anchor ice patches at Site G1. Arrows indicate flow direction.

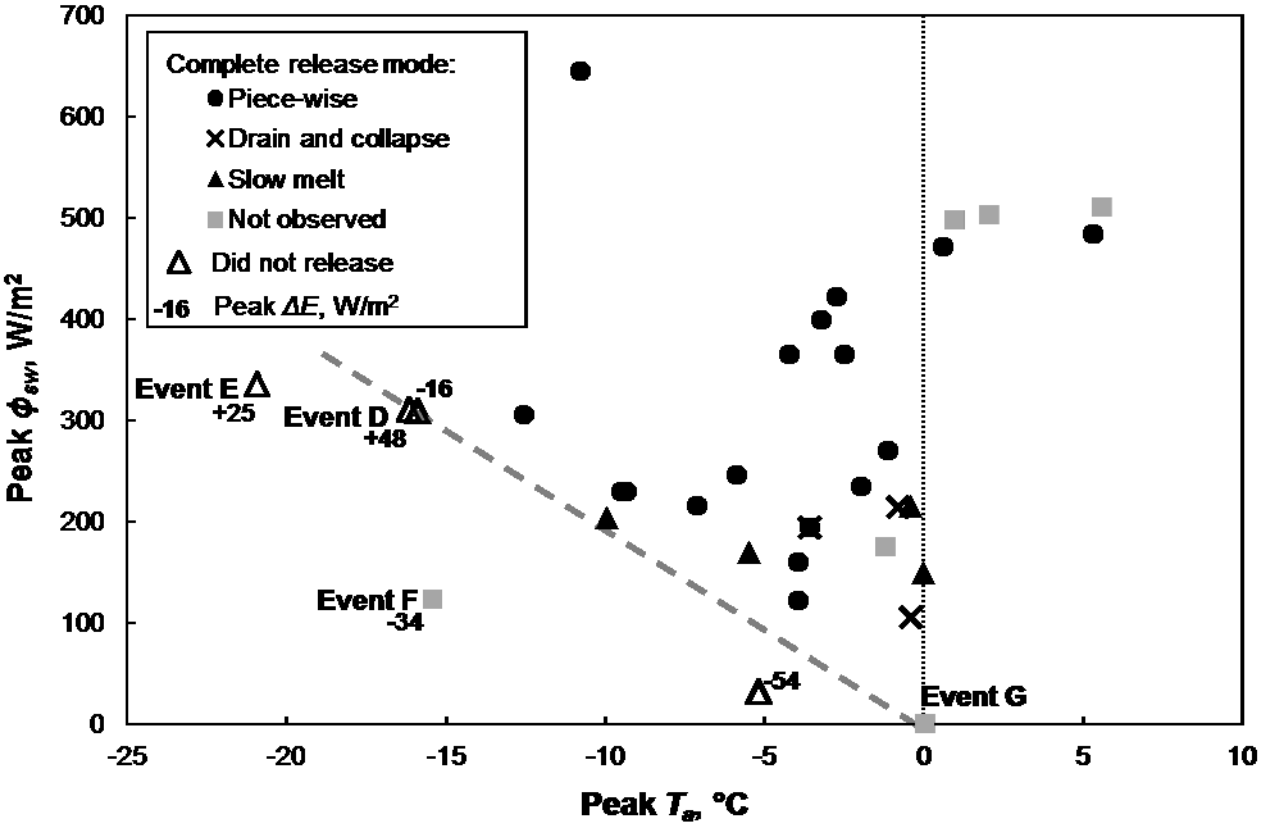

Figure 2.11. Meteorological conditions (ϕ_{sw} = shortwave radiation, T_a = air temperature) leading to the release of each definite anchor ice event in Year 2 and the observed release mode, separated by whether the accumulation released. The peak ΔE is labeled for events below the grey line, all events above the grey line had a positive peak ΔE, ranging from ~0 to 313 W/m^2.

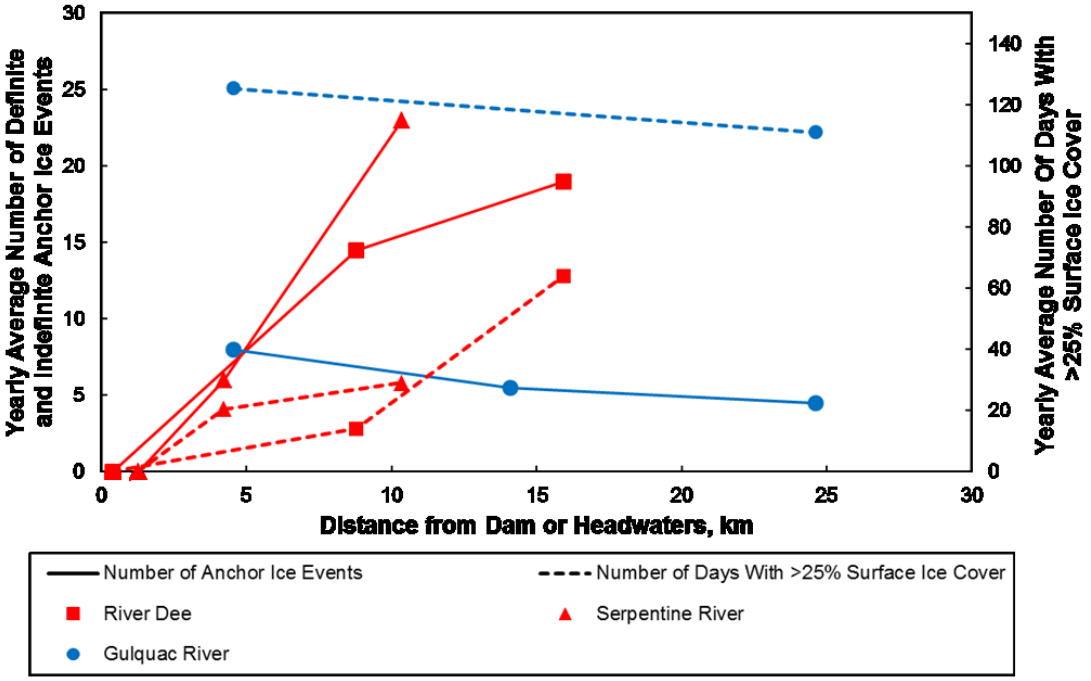

Figure 2.12. Number of definite and indefinite events and number of days with a surface ice cover (>25% of channel area) versus distance from headwaters (Gulquac River) or the dam (River Dee and Serpentine Rivers) for each study site averaged over the two study years. Temporal extent of surface ice at site G2 in Year 1 is not known because of a camera failure.

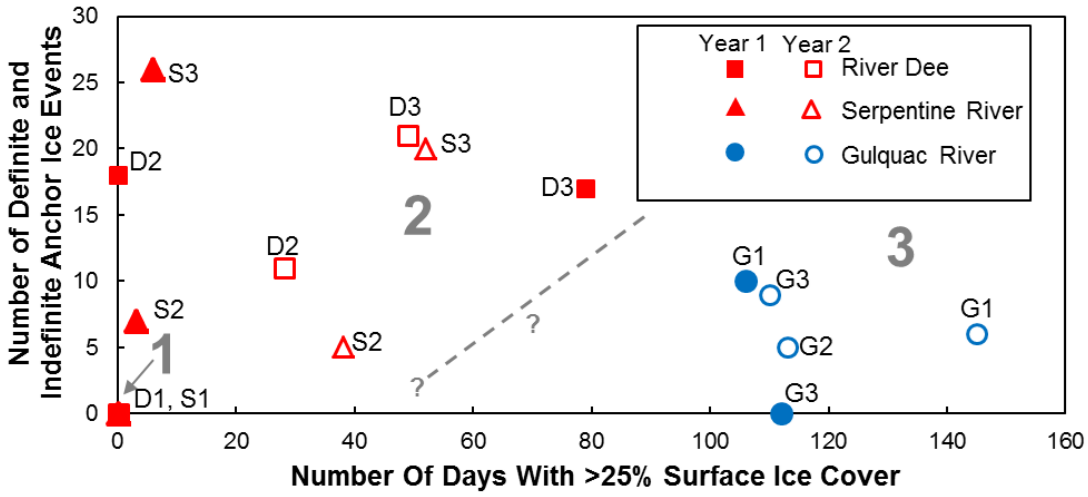

Figure 2.13. Number of definite and indefinite anchor ice events versus number of days with a surface ice cover (>25% of channel area) for each study site (labelled) in both years. Grey numerals refer to the conceptual reaches referred to in the text; the grey diagonal line is a possible divide between Reaches 2 and 3. Temporal extent of surface ice at site G2 in Year 1 is not known because of a camera failure.

Chapter 3. Celerities of Waves and Ice Runs from Ice Jam Releases

A version of this chapter was published as:

Nafziger, J., She, Y., Hicks, F. 2016. Celerities of waves and ice runs from ice jam releases. *Cold Regions Science and Technology*, 123:71-80. https://doi.org/10.1016/j.coldregions.2015.11.014

3.1 Abstract

The release of a river ice jam can lead to rapidly rising water levels and a fast-moving torrent of water and ice that can threaten riverside communities. Two phases are released when an ice jam fails: a water wave and a moving ice accumulation (called an "ice run"). The propagation of the water component of an ice jam release wave is relatively well understood. However, a dearth of simultaneous observations of both the water and ice components of an ice jam release has hampered the development of tools to predict of the effects of these releases. This paper presents a field experiment on the Hay River in the Northwest Territories where both water level and ice condition were observed simultaneously at several locations over a distance of more than ten thousand flow depths. This research shows that the water wave and the ice run travel at different celerities resulting in two distinct, but initially overlapping, features. The celerity of the leading edge of the water wave was found to be higher than the ice components, making the water wave move out in front of the ice after 4 to 8 ice jam lengths of travel.

3.2 Introduction

The sudden release of impounded ice and water from an ice jam can be very dangerous for northern riverside communities. Rises in water level exceeding 0.8 m/min and wave celerities of 10.9 m/s resulting from ice jam releases have been measured (Hutchison and Hicks, 2007; Beltaos, 2014). The flooding that results can damage property and threaten lives. Two phases are released when an ice jam fails: a water wave and a moving ice accumulation (called an "ice run"). The water wave is characterized by faster water velocities at the peak and front of the wave, and slower water velocities at the tail of the wave. The ability to predict both the magnitude and the arrival time of ice jam releases is important for the emergency management of breakup floods.

To correctly forecast the consequences of an ice jam release event in terms of its flooding potential, it is essential to be able to predict the celerity and shape of the water wave as well as the celerity and size of the ice run. The water wave provides the volume and height of water that can itself cause flooding; it can also instigate breakup of downstream ice covers or bring about the release or consolidation of existing downstream ice jams. The ice run can likewise interact with an existing ice jam: it may add momentum and volume to the ice accumulation, causing thickening of the ice jam, raising water levels and causing flooding. Ice runs can also cause the release of an ice jam, sending a water wave and ice run downstream with renewed amplitude and celerity. Furthermore, whenever the local ice velocity is slower than the surface water velocity, the ice run has the potential to attenuate the water wave's peak and/or impede its velocity. It has been hypothesized that this is why ice jam release models that neglect ice-water interactions tend to underestimate water levels in the falling limb of stage hydrographs (e.g. Blackburn and Hicks, 2003). Further, She and Hicks (2006) found that the addition

of side friction for a limited time after release may improve the prediction of the falling limb.

Currently available ice jam release models have proven quite effective at predicting the arrival time and size of the water wave (e.g. Liu and Shen, 2004, She and Hicks, 2006). However, correctly predicting the propagation speed of the concurrent ice run movements has been more elusive. This is, in part, due to the scarcity of field observations with which to validate numerical models aimed at predicting ice jam release and the propagation of the water wave and ice run. In particular, there have been numerous field studies of ice jam release events (e.g. Jasek 2003, Beltaos and Burrell 2005, Hutchison and Hicks 2007, She et al. 2009a) but none present simultaneous data detailing the sizes and relative velocities of both the water waves and their associated ice runs and how these change with distance travelled. Some laboratory studies of ice jam release or wave-ice interactions have also been conducted (e.g. Wong et al. 1985, Khan et al. 2000). However, laboratory flumes do not capture the attenuation of the water wave and ice run that occur in a natural river because the distances travelled in a river, D, are thousands to tens of thousands times the undisturbed flow depth, y_0, and cannot be accommodated at laboratory scales.

The purpose of this study was to take the first step in addressing this knowledge gap by simultaneously documenting the celerities of both water waves and associated ice runs as they propagate downstream. This was achieved by establishing a field experiment on the Hay River where both the water wave and ice run components of ice jam release events were observed at several locations over a channel length exceeding 10,000 undisturbed flow depths.

3.3 Study Reach and Methods

Figures 3.1 and 3.2 illustrate the Hay River and the reach instrumented for this study. The Hay River drains 51,700 km^2 and flows into Great Slave Lake in the Northwest Territories. The Town of Hay River and the K'atl'odeeche First Nation are located where the Hay River flows into Great Slave Lake. These settlements have often experienced severe flooding caused by ice jams.

The study reach is situated just upstream of Alexandra Falls. In this reach, the Hay River meanders through alluvial plains and contains occasional islands. This reach was chosen because of its consistent slope, relatively simple geometry, and the fact that ice jams normally form and release at consistent locations during spring breakup. In addition, Alexandra Falls opens sufficiently early in the breakup period to enable discharge estimation using an open water rating curve. Discharge estimates were also available at the Water Survey of Canada (WSC) station 07OB008 located at km 945.6, upstream of the study reach. The average channel width in the study reach is 114 m (min: 70 m, max: 210 m) with an average slope of 0.0002. Ice conditions and water levels were observed at six stations in 2011 and seven stations in 2013. The subreaches between the stations are numbered Reach 1 to 6. Each observation station is identified with a river kilometer number referenced to the origin of the Hay River (modified from Hicks et al., 1992).

The observation station at km 1032.0 (2.2 km upstream of Alexandra Falls) was operated as a near-real-time communicating station by the Town of Hay River Emergency Measures Organization as part of their spring flood monitoring operations.

Water levels were measured at 5 minute intervals with an Omni Controls Inc. DCU-1104 ultrasonic sensor suspended over the river on a cantilever boom (estimated accuracy +/- 0.1 m, due to wind movement in the boom). Ice conditions were observed during daylight hours with a Campbell Scientific CC640 digital camera at 5 to 15 minute intervals. A geodetic benchmark was not established here; therefore, the water levels at this station are reported in terms of stage.

The remaining stations were installed by the University of Alberta's River Ice Research Group at river km 1012.2, 1004.1, 997.4, 993.4, 986.8 (2013 only), and 980.0. Each station consisted of a self-contained submersible pressure transducer and datalogger (Schlumberger Diver models 501 and 601, accuracy: 1.0 and 0.5 cmH_2O, measurement interval: 1 and 2 min.) and a tree-mounted game camera (various models used: Reconyx PC800, Moultrie PlotStalker, and Moultrie I-65; photo interval: 5 min., 10 min., or 1 hr.). Because remote lighting was not installed, ice condition data was typically not available at night (~23:00-04:30). The pressure transducers' clocks were synchronized and the instruments were installed in silt socks and fixed inside perforated heavy steel cases, which were driven flush with the river bed before the onset of breakup. The case elevations were measured with respect to control points established with a GPS static survey and processed with Natural Resources Canada's precise point positioning tool (vertical 95% error: 0.074 to 0.185 m). The pressure data was corrected to eliminate the effects of atmospheric pressure changes using data from a barometric pressure datalogger (Schlumberger Diver model DI500, accuracy: 0.5 cmH_2O) located along the river within 15.5 km of the observation stations. The cameras were retrieved directly after breakup. The pressure transducers were retrieved in late June to early September, after remnant

shear walls had melted and high water levels had subsided, when the riverbed was again accessible

Ice conditions were also observed from fixed-wing aircraft, allowing for periodic documentation of ice conditions between ground-based observation stations, as well as upstream and downstream of the study reach from the Alberta-Northwest Territories border to Great Slave Lake (km 942 to 1114). Observational flights were typically conducted daily during breakup, weather and equipment permitting, and more often if ice was moving. The ice jams and ice runs described in this paper were observed from the air at the following times: the afternoons of May 5 and 6, 2011, and the morning and evening on May 11, 2013.

The oblique photographs taken by the cameras at each observation station were used to observe ice condition (presence of intact ice, ice jams, floating ice debris, or open water) and to estimate the surface concentration of floating ice debris. This approach for estimating surface ice concentration is susceptible to an error of approximately 10%, based on comparison with estimated surface ice concentrations observed from aircraft. However, it is believed to be accurate enough to delineate important features of individual ice runs such as the start and end of the ice run and the identification of the peak concentration. A similar approach has been employed by other researchers (e.g. Jasek, 2003).

To identify the ice runs, it was necessary to devise a consistent means of distinguishing ice runs from "background ice"—that is, the remnant ice from along the river banks that was refloated by the passing wave and/or ice associated with the tail end

of an ice run. The fronts and backs of the ice runs were taken to be the points at each end where the surface ice concentration was 20%. Alternative approaches for delineating the start and end of an ice run include using the 100% surface ice concentration or using the peak concentration. The 100% concentration was not employed in this study to delineate the start and end of the ice runs because not all ice runs had a peak concentration of 100% at each observation station. The peak concentration was not used because for many ice runs (i.e. Ice Runs I, II, III, Figure 3.4) the peak concentration was typically observed in three or fewer photographs, thus making it unrepresentative of the entire ice run. Therefore, for consistency, the 20% surface ice concentration was chosen to delineate the ice runs, as it was large enough separate the ice runs from background ice but small enough to capture those ice runs with the lowest concentrations.

The celerities of water wave and ice run features were calculated from the time a specific feature took to travel between observation stations. The error in the calculated celerity of ice run features is due to the interval between subsequent observation photos and the error in estimating the surface ice concentration. The latter source of error is a function of the steepness of the ice concentration versus time graph. For the 2011 observations, an error of ± 0.1 to 0.5 m/s was due to the photo interval and an average error of ± 1.4 m/s was due to errors in estimating the surface ice concentration. For the 2013 observations, an error of 0.1 to 0.2 m/s was due to the photo interval and an average error of 0.3 m/s was due to the error in estimating the surface ice concentration. The relatively large error for the 2011 observations is due to the more gradual slope of the concentration versus time graph at km 1012.2.

For comparison purposes, the celerities of theoretical dynamic and diffusive

waves were approximated using a steady-state analysis and 'carrier discharges' (i.e. the discharges unaffected by the ice jam releases), following the approach suggested by Beltaos and Burrell (2005). The carrier discharges (280 m^3/s in 2011 and 340 m^3/s in 2013) were estimated from rating curves at km 1032.0 and 945.6 (WSC station 07OB008). The diffusive wave celerity ($C_{diffusive}$) was calculated using Equation 3.1 (after Henderson, 1966); the dynamic wave celerity ($C_{dynamic}$) was calculated using Equation 3.2 (Henderson, 1966):

$$C_{diffusive} = \frac{5}{3}U_0 \tag{3.1}$$

$$C_{dynamic} = U_0 + \sqrt{gy_0} \tag{3.2}$$

Where U_0 and y_0 are the respective reach-averaged velocity and depth of the undisturbed flow at the carrier discharge, and g is the gravitational acceleration. Note that the form of Equation 3.1 used here is derived using Manning's equation resulting in the coefficient of 5/3, whereas Henderson (1966) derived Equation 3.1 using Chezy's equation, resulting in a coefficient of 3/2. The values of U_0 and y_0 resulting from the steady-state approximation are found in Table 3.2.

These celerities represent approximate values of the theoretical upper and lower bounds of wave celerity that may be observed in the field, and are therefore useful for assessing the relative importance of the dynamic versus diffusive wave components in the observed events. To compare events of different magnitudes, the distance travelled by the water wave and the ice runs, D, was normalized using the length of the original ice jam, L_j, and the undisturbed flow depth, y_0, as the scale. This resulted in two non-

dimensional parameters D/L_j and D/y_0; the former is most useful for comparing between field-scale events, and the latter is most useful for comparing to laboratory-scale analogs. This follows the approaches proposed by Jasek (2003) and Beltaos (2003). The reach-averaged undisturbed flow depths (y_0) were estimated from the steady-state analysis using the carrier discharges.

3.4 Results

The breakups of 2011 and 2013 in the study reach were both dynamic. Several ice jam formation and release events were observed and multiple ice runs occurred in both years, which resulted from a cascade of ice jam release events. A single ice jam release event in 2011 and a cascade of release events in 2013 are analyzed in this paper. These releases resulted in a single wave feature for each year, one ice run (Ice Run A) in 2011, and four ice runs (Ice Runs I to IV) in 2013. Several other ice jams, ice jam releases, and ice runs were observed or inferred, but the number and quality of observations for these events were limited by darkness when ice conditions could not be observed. The ice jams analyzed in this study formed towards the end of the progression of spring breakup; that is, after the ice had deteriorated, cracked, and started to become mobile. Aerial observations were taken and all ice movements were tracked at the observation stations in the days prior to the formation of the ice jams analyzed in this study. Based on these observations, the ice runs described in both years were unimpeded ice runs and the water waves traveled through a channel free of intact ice.

A summary of the ice jams, ice runs, and release events that were analyzed in this paper is presented in Table 3.1. The ice jam extents presented in Table 3.1 are estimated

from aerial observations taken before the jams released. Some ice jams were still lengthening when last observed, so the locations of the heads of the jams were estimated based on the extent of the shear walls observed from the air after the release events. Where these estimates were necessary, they are noted in Table 3.1. Large uncertainty in original ice jam length makes the normalized distance D/L_j inaccurate. Therefore, analyses using D/L_j in this study omit Ice Run I and Ice Run IV. Ice Run I was omitted because the uncertainty in the original length was particularly large due to intermittent remnant shear walls observed from the air; Ice Run IV was omitted because it resulted from three ice jam releases (with three separate toes) making for inconsistency in calculating the distance travelled, which is defined from the toe of the jam. Values of D/y_0 are not reported for Ice Run IV for the same reason.

Figures 3.3 and 3.4 provide a summary of the water level and ice conditions at each station for 2011 and 2013, respectively. Three points on each hydrograph are highlighted to aid in describing the waves' behavior: 1) the wave leading edge: the point where the first water level rise is observed, or where there was a breakpoint in the slope of the water level hydrograph; 2) the "wave front": the point on the steepest part of the hydrograph, where the water level is half-way between the elevation of the leading edge and the peak; and 3) the wave peak: the highest water level elevation measured on the waveform. These features were not recorded where the waveform was not obvious because of the presence of an ice jam (Figure 3.4c and 3.4d). In addition, the leading edge of the 2013 wave at km 1032.0 (Figure 3.4g) was not recorded because of the presence of a smaller rise in water surface in front of the main 2013 wave at approximately 18:00–19:00. The events precipitating this smaller rise were not observed.

Figures 3.3 and 3.4 also show the surface ice concentrations of the observed ice runs, which were marked by a prominent increase in ice surface concentration. Ice Run A had steep sides on the concentration versus time graphs (Figure 3.3), with the exception of the observations at km 1012.2 (Figure 3.3c). This is likely because the larger photo interval at km 1012.2 did not capture the complete shape of the concentration versus time graph. Ice run peak concentrations tended to decrease with distance travelled due to longitudinal dispersion (e.g. Ice Run II: 95% at km 997.4, width=95 m, Figure 3.4d; 50% at km 1004.1, width=110 m, Figure 3.4e). However, peak concentrations of ice runs with concentrations below 100% depended on the channel width at the location they were observed. For example, Ice Run II had a peak concentration of 50% at km 980.0 where the channel was 150 m wide (Figure 3.4a), and a peak concentration of 90% at km 993.4 where the channel was 85 m wide (Figure 3.4c). Finally, Ice Run IV at km 1012.2 had two distinct peaks (Figure 3.4f) because it originated from multiple ice jam releases.

3.5 Analysis and Discussion

3.5.1 Waveform and Wave Celerity

Figure 3.5 shows changes in the height of the wave peaks and the rates of rise of the hydrographs as the waves travelled downstream. The height of the wave peak was defined as the difference in water surface elevation between the wave leading edge and the wave peak. The rate of rise of the hydrograph was taken as the maximum slope of a tangent drawn through the wave at or before the wave front. In 2011 (Figure 3.5a), where a single event was documented, both the height of the wave and the rate of rise of

the hydrograph decreased as the wave travelled downstream. The wave height at km 997.4 is omitted from Figure 3.5a because this observation station was within the ice jam, which raised the water level prior to the arrival of the wave. Therefore, the peak height was representative of what was measured at subsequent stations.

In 2013 (Figure 3.5b), the water wave was observed after the release of Ice Jam 2013C and then again after the release of the Ice Jams 2013D, -E and -F. In this case, the height of the wave and the rate of rise decreased with distance travelled after the release of Ice Jam 2013C. The wave then interacted with the downstream ice jams, causing the peak to be amplified and the hydrograph to be re-steepened. Over Reach 5 the height of the wave and the rate of rise of the hydrograph again decreased. In Reach 6, the wave may have interacted with remnant ice in the channel as both the height of the wave and the rate of rise of the hydrograph increased as the event propagated downstream.

Figures 3.6 and 3.7 are phase diagrams showing the observed times that the wave and ice run feature passed each observation station. In Figure 3.7, Ice Run III is shown as representative of the 2013 ice runs. The celerities of the features are represented by the slopes of the line segments and are summarized in Table 3.2. The ice jam extents and their approximate times of release are also illustrated on these diagrams. Where uncertainty exists with respect to the extents and release time of an ice jam, it is indicated with a question mark. The release of each ice jam is shown at a discrete time with a horizontal line in the phase diagram. Because ice jams do not release instantaneously, the release of the jam would be better represented with a curve or a sloping line; however, information on the rate of release of the ice jams was not available.

The observed celerities of the peaks and leading edges of the water waves shown in Table 3.2 are similar to, but smaller than, the average water wave celerities reported in previous studies. Specifically, the leading edge celerities observed in this study ranged from 2.9 to 5.6 m/s and the celerities of the wave peaks ranged from 1.3 to 4.2 m/s. In comparison, Beltaos (2013) observed celerities of 2.7 to 7.7 m/s, and 1.4 to 6.7 m/s for the leading edge and wave peak celerities, respectively, on the Saint John and Restigouche Rivers in New Brunswick, Canada for waves traveling in open-water conditions. Beltaos (2014) also observed a water wave with a celerity of 10.9 m/s in the Mackenzie River Delta, Northwest Territories, Canada. Hutchison and Hicks (2007) and She et al. (2009a) presented measured and historically-observed celerities of water waves ranging from 0.02 to 8.0 m/s on the Athabasca River in Canada.

As seen in Table 3.2 and Figures 3.6 and 3.7, the leading edges of the waves travelled with larger celerities than the celerities of the waves' fronts or peaks. Whether the wave peak was faster than the wave front depended upon the distance the wave had travelled. Where the celerity was measured over a reach directly downstream of the jam toe (i.e. 2011 Reach 4; 2013 Reach 1, Table 3.2) the celerity of the peak was greater than the celerity of the wave front. The celerity of the peak was less than the celerity of the wave front when measured over reaches further from the jam toe (i.e. Reaches 5 and 6, both years). This means that the celerity of the wave peak decelerates more than the celerities of the wave front and the leading edge of the wave, causing the wave to flatten.

The celerities of the wave features were compared to the celerities of theoretical dynamic and diffusive waves in Figures 3.6 and 3.7. The leading edges of the waves travelled at approximately the dynamic wave celerity for a distance of approximately 1 to

3 jam lengths after release and then slowed. In 2011, the leading edge travelled at the dynamic wave celerity for at least 14.8 km (Figure 3.6: Reach 4 and 5, $D/L_j > 1$, $D/y_0 > 6200$); in 2013 the leading edge travelled at the dynamic wave celerity for at least 8.7 km (Figure 3.7, Reach 1, $D/L_j > 3$, $D/y_0 > 3200$) after the release of Ice Jam 2013C and at least 8.1 km after the releases of Ice Jams 2013D–F (Figure 3.7: Reach 5, D undefined). In 2011, the leading edge of the wave slowed to approximately one-half of the dynamic wave celerity in Reach 6 (Figure 3.6).

The wave peaks travelled at celerities intermediate to the dynamic and diffusive wave speeds. The peak of the 2011 wave travelled at approximately 75% of the dynamic wave velocity for 0.3 ice jam lengths downstream of the large (L_j=13.6 km) Ice Jam A (Figure 3.6: Reach 4, D/L_j=0–0.3, D/y_0=0–1730). The wave peak then slowed to close to the diffusive wave celerity over Reaches 5 and 6 (Figure 3.6: D/L_j=0.3–2.4, D/y_0=1730–13,700). The peak of the 2013 wave travelled at approximately 40% of the dynamic wave celerity downstream of the release of Ice Jam 2013C (L_j=3.0 km) (Figure 3.7: Reach 1, D/L_j=0.6–2.9, D/y_0=800–3649) and close to the diffusive wave celerity in Reach 5. This indicates that the peak travels very fast close to the toe of the ice jam (where $D/L_j < 1$) and that the peak celerity eventually slows to close to the diffusive wave celerity. It may also indicate that larger ice jams cause the release of more dynamic waves.

The wave fronts also travelled at celerities intermediate to the dynamic and diffusive waves, but showed a slightly different pattern than the wave peaks. The front of the 2011 wave travelled at approximately 75% of the dynamic wave velocity for 0.3 ice jam lengths downstream of Ice Jam A (Figure 3.6: Reach 4, D/L_j=0–0.3, D/y_0=0–1730). The front of the 2011 wave then slowed to approximately 40-50% of the dynamic wave

celerity in the subsequent reaches (Figure 3.6: Reaches 4 and 5, D/L_j=0.3–2.4, D/y_0=1730–13,700). The front of the 2013 wave travelled at 40-50% of the dynamic wave celerity in all reaches where it was observed (Figure 3.7). Therefore, the wave peaks and the wave fronts travelled at similar (and large) celerities close to the point of release (where $D/L_j < 1$). Afterwards, the wave peaks slowed more abruptly than the wave fronts, which travelled at a fairly constant celerity (within 0.2 to 0.5 m/s) over a long distance (30 to 50 km).

Each wave feature behaved differently when the wave interacted with and caused the release of Ice Jams 2013D–F. The celerity of the leading edge of the wave increased from 4.9 to 6.4 m/s after interacting with and releasing Ice Jams 2013D–F, while the celerity of the wave front remained almost constant (2.5 versus 2.6 m/s) and the celerity of the peak of the wave decreased from 2.8 to 1.3 m/s. Therefore, interaction with channel ice may have a greater effect on the wave peak and leading edge than on the wave front.

3.5.2 Ice Run Celerity

Figure 3.6 (2011) and Figure 3.7 (2013) are phase diagrams showing the movements of the ice runs in relation to the water wave. Figure 3.7 shows Ice Run III as an example of the movement of the 2013 ice runs because it had the greatest number of observations and is representative of the movements of all ice runs observed in 2013. The celerities of the fronts and backs of the 20% surface ice concentrations of each ice run are summarized in Table 3.2.

Three general observations were made from the ice run celerities, with some

exceptions. First, the celerities of the ice runs (average: 1.5 m/s, Table 3.2) were much slower than the celerities of all parts of the water wave (average: 3.3 m/s, Table 3.2), meaning that the water wave moved ahead of the associated ice run. Second, ice run celerity decreased with distance travelled. The decrease was 0.03 to 0.08 m/s per km of travel. The ice celerity was slightly higher than the diffusive wave celerity close to the point of release and then slowed to below the diffusive wave celerity (Figure 3.6 and 3.7). Third, the fronts of the ice runs travelled with a greater celerity (average: 1.6 m/s, Table 2) than the celerity of the back of the 20% concentration of the ice runs (average: 1.4 m/s, Table 3.2). These latter two observations are the result of the water wave moving ahead of the ice run; when this occurred, the ice run travelled on water with a slower surface velocity, causing the ice run to slow. The ice run slowed regardless of whether the peak surface ice concentration was 100% (e.g. Ice Run III, Reaches 1 to 3, Table 3.2) or less than 100% (e.g. Ice Run II, Reaches 1 to 3, Table 3.2). Similarly, the front of the 20% ice concentration travelled faster than the back of the 20% ice concentration because it was travelling on water located closer to the wave front which had a higher surface velocity.

An exception to the general observations noted above was in Reach 6, where ice run celerities tended to increase (Table 3.2 and Figures 3.6 and 3.7: Ice Run A, Ice Run IV). This increase in celerity may have been due to very short-lived stalling of the ice run on channel constrictions. Reach 6 had six sections where the channel width was below 75 m, contained 2 islands, and was of higher sinuosity (Figure 3.8). Therefore, a brief stall could conceivably occur here. The 2013 wave also had a small increase in wave height and steepness in this reach (Figure 3.5), further evidence of that ice Run IV

may have stalled in Reach 6.

A second exception to the general observations noted above was that the celerity of the back of the 20% concentration tended to increase in Reach 4 and 5 (Table 3.2: Ice Runs II, III, and IV). This increase in celerity occurred after the celerity of the back of the 20% concentration had decreased and occurred at the same time as the celerity of the front of the 20% concentration continued to decrease. This observation could be explained by the longitudinal dispersion of the ice run. Dispersion caused the surface ice concentration of the ice runs to decrease. When the concentration of the back of an ice run decreased to below 20%, the point taken to delineate the ice run moved downstream towards the center of the ice run and thereby artificially increased the apparent celerity of the back of the ice run. This does introduce some error into calculated ice run celerities. However, it is likely that this error only becomes significant when the ice run concentration is low.

3.5.3 Interactions Between Water Waves and Ice Runs

The preceding observations of water wave and ice run celerities highlight what may occur when a water wave or an ice run is impeded by ice in the river channel. In the case of a water wave, the wave may interact with a stationary or a more slowly-moving ice accumulation. As seen in Figure 3.5b, this causes the peak water level to increase and the driving forces behind the wave to rebuild; the wave may then release with increased celerity and a higher peak water level. In the case of an ice run, the ice run may slow or stall completely at a channel constriction (e.g. a tight bend, an island, or narrowing of the channel). Similar to what occurs when a water wave encounters stationary ice, the stalled

ice run may cause a buildup of water behind it, which may almost instantly release. This buildup may be sufficient to cause an increase in celerity of the ice run or the ice run and the associated water wave, if the two were travelling together. This phenomenon was also observed by Hutchison and Hicks (2007).

The difference in celerity between the ice runs and the water waves caused the ice run to lag behind the water wave in a predicable manner. Figure 3.9 shows the difference in arrival time (the lag time) between the front of the water wave and the start of the ice run compared to D/L_j. At all observation locations, the ice run was behind the front of the wave, so the lag times were positive and increased with distance travelled. The coefficient of determination (r^2) of the linear regression of these variables (forced through the origin) was 0.85; and the maximum residual was 54 minutes. Ice Runs I and IV were omitted from Figure 3.9 because of the uncertainty in determining the length of the original ice jams or the distance the features travelled.

Figure 3.10 shows the lag time between the peak of the wave and the start of the 20% concentration of the ice run compared to D/L_j. Ice Runs I and IV were omitted from Figure 3.10 for reasons mentioned above. Ice Runs II and III transitioned from having a negative lag time to a positive lag time with distance travelled. The transition between the ice run travelling on the front of the wave (negative lag time) or the back of the wave (positive lag time) occurred 4 to 8 ice jam lengths from the toe of the jam (D/L_j = 4 to 8). This transition (where lag time = 0), is important because it also represents the distance over which the ice run has the most effect on the shape and propagation of the water wave. These observations agree with those in Jasek (2003) where the peak of the water wave moves ahead of the ice run after D/L_j= 7.5 to 8.1. Ice Run A had a fairly constant

lag time (≈ -50 minutes), possibly owing to the relatively short normalized distance (< 3 D/L_j) over which this ice run was observed.

Jasek (2003) introduced the "moving multi-layered rubble" (MMLR) conceptual model to describe how water waves (therein termed "dynamic forerunners") and ice runs interact and propagate downstream. A few observations in this study differ somewhat from the description of the MMLR. First, observations presented in this paper show that the ice run may travel entirely ahead of the peak water level (e.g. Ice Run III, Figure 3.4a and 4b), or largely behind the peak water level (e.g. Ice Run A, Figure 3.3d; Ice Runs I and II, Figure 3.4b), as opposed to tending to stay with the peak water level. Furthermore, Jasek (2003) also suggested that ice run celerity increases when the surface ice concentration falls below 100%. Observation stations in this study were spaced too far apart to determine if a short-lived increase in ice run celerity occurred when ice run peak concentration fell below 100%. However, the general trend in the observed ice runs was for the ice runs celerity to decrease, even when their peak concentration fell below 100%. This is likely because the ice run and water wave separated, leaving the ice run to travel with more slowly moving water at the trailing end of the wave. Differences in observations between this study and those of Jasek (2003) may be because the events observed in this study are the result of a cascade of ice jam releases. In addition, the ice runs observed in this study are relatively short, and also likely relatively thin, compared to the larger ice runs observed by Jasek (2003).

Finally, observations presented in this study suggest that the presence of an ice run on the trailing end of a wave does not necessarily cause a measureable rise in water level. Stationary ice causes a water level rise due to backwater effect from increased

friction at the larger wetted perimeter; however, the amount of backwater caused by a moving ice accumulation is a function of the difference between the surface water velocity and the ice velocity. In this study, ice runs observed after the peak of the wave had passed did not raise the water level, even if their peak surface ice concentration was 100%. For example, the water levels at km 997.4 (Figure 3.4d) showed the same recession rate before, during, and after each of the Ice Runs I, II, and III passed the observation station. Specifically, while these three ice runs passed km 997.4 (between 17:15 and 23:20, Figure 3.4d) the water level stayed within 4 cm of the overall recession slope. Therefore, even at 100% surface ice concentration, the ice runs may have been travelling close to the surface water velocity, and they were not appreciably slowed by interactions with the banks. However, to get a clearer picture of the effect of the ice on the water level, the water velocity beneath the ice runs as well as the thickness and roughness of the moving ice accumulation would have to be measured.

3.6 Summary and Conclusions

This study provides an analysis of the relative celerities of the water waves and ice runs that result from ice jam releases. Ice jam releases were observed on the Hay River in the Northwest Territories over a reach much longer than any simulated in a laboratory flume. Both the water and ice phases resulting from ice jam releases were observed at 6 to 7 stations as they travelled downstream. This provides very detailed data that could potentially be used to validate numerical models of ice jam release events.

The ice jam releases observed in this study produced water waves whose leading edges travelled close to the dynamic wave celerity for at least 1.1 to 2.9 ice jam lengths.

The peak and the front of the waves travelled at celerities 40% to 75% of the dynamic wave celerity close to the point of release (where $D/L_j < 1$). Further from the point of release, the wave front remained within 40% to 50% of the dynamic wave celerity while the wave peak tended to slow to close to the diffusive wave celerity.

In most cases observed, the wave features travelled faster than the ice run features. This caused the ice runs and the water waves to separate. The ice runs travelled in front of the peak of the water wave for 4 to 8 ice jam lengths. In general, ice run celerity slowed with distanced travelled. However, geomorphological features such as tight bends and islands may have caused an ice run to stall momentarily, allowing driving forces to rebuild. The ice run and water wave may then be released with renewed celerity and amplitude.

3.7 Acknowledgments

This research was funded through grants from the Natural Sciences and Engineering Research Council of Canada; financial and logistical support was also provided by Aboriginal Affairs and Northern Development Canada (AANDC). All of this support is gratefully acknowledged. The authors would also like to thank the Town of Hay River (THR) for their in-kind and logistical support of this study. Special thanks to Fire Chief Ross Potter (THR), as well as to Shawne Kokelj and Meg McCluskie (AANDC) for their logistical and technical support in the field. The authors would also like to thank Joshua Maxwell, Janelle Banack, Liming Zhao, and Stefan Emmer for their assistance in the field. Finally, the efforts of the reviewers, whose comments helped to clarify and improve this paper, are gratefully acknowledged.

3.8 References

Beltaos, S. 2003. Discussion of "Ice jam release surges, ice runs, and breaking fronts: field measurements, physical descriptions, and research needs". Canadian Journal of Civil Engineering, 30(5):949-950.

Beltaos, S. 2013. Hydrodynamic characteristics and effects of river waves caused by ice jam releases. Cold Regions Science and Technology, 85:42-55.

Beltaos, S. 2014. Hydrodynamic properties of ice-jam release waves in the Mackenzie Delta, Canada. Cold Regions Science and Technology, 103: 91-106.

Beltaos, S., Burrell, B. 2005. Field measurements of ice-jam-release surges. Canadian Journal of Civil Engineering, 32(4): 699-711.

Blackburn, J., Hicks, F. 2003. Suitability of dynamic modeling for flood forecasting during ice jam release surge events. Journal of Cold Regions Engineering, 17(1): 18-36.

Henderson, F. 1966. Open Channel Flow. Macmillan Publishing Co., Inc., New York.

Hicks, F., Steffler, P., & Gerard, R. 1992. Finite element modeling of surge propagation and an application to the Hay River, NWT. Canadian Journal of Civil Engineering, 19(3): 454-462.

Hutchison, T. Kowalczyk, and Hicks, F. 2007. Observations of ice jam release waves on the Athabasca River near Fort McMurray, Alberta. Canadian Journal of Civil Engineering, 34(4): 473-484.

Jasek, M. 2003. Ice jam release surges, ice runs, and breaking fronts: field measurements, physical descriptions, and research needs. Canadian Journal of Civil Engineering, 30(1): 113-127.

Liu, L., Shen, H. T. 2004. Dynamics of ice jam release surges. *In* Proceedings of the 17th IAHR Symposium on Ice. June 21-25, 2004. St. Petersburg, Russia.

Khan, A., Steffler, P., Gerard, R. 2000. Dam-break surges with floating debris. Journal of Hydraulic Engineering, 126(5): 375-379.

She, Y., Hicks, F. 2006. Modeling ice jam release waves with consideration for ice effects. Cold Regions Science and Technology, 45(3): 137-147.

She, Y., Andrishak, R., Hicks, F., Morse, B., Stander, E., Krath, C., Keller, D., Abarca, N., Nolin, S., Nzokou Tanekou, F., Mahabir, C. 2009a. Athabasca River ice jam formation and release events in 2006 and 2007. Cold Regions Science and Technology, 55(2): 249-261.

Wong, J., Beltaos, S., Krishnappan, B. 1985. Laboratory tests on surges created by ice jam releases. Canadian Journal of Civil Engineering, 12(4): 930-933.

Table 3.1 Summary of ice jam locations, times of release, and ice runs resulting from ice jam releases on the Hay River.

Study Year	Ice Jam	Toe, river km	Head, river km	Jam Length, L_j, km	Approximate Time of Release	Associated Ice Run
2011	2011A	999.8	986.2 (estimated)	13.6	06/05/2011 09:00	Ice Run A
2013	2013A	962.3	953 (estimated)	9.3	release not observed (last observed intact 11/05/2013 12:07)	Ice Run I
	2013B	972	970.2	1.8	release not observed (last observed intact 11/05/2013 12:09)	Ice Run II
	2013C	978.1	975.1	3.0	11/05/2013 14:22 (estimated)	Ice Run III
	2013D	999.3	995.5 (estimated)	3.8	11/05/2013 16:20	
	2013E	1002.8	1001.5	1.3	11/05/2013 16:30 (estimated)	Ice Run IV
	2013F	1004.3	1003.9	0.4	11/05/2013 16:37	

Table 3.2 Celerities of wave and ice run features resulting from ice jam releases observed over six study reaches on the Hay River.

Feature	Description	Reach 1	Reach2	Reach 3	Reach 4	Reach 5	Reach 6
Reach Characteristics:							
	Upstream station, km	980	986.8	993.4	997.4	1004.1	1012.2
	Downstream station, km	986.8	993.4	997.4	1004.1	1012.2	1032
	Reach length, km	6.8	6.6	4	6.7	8.1	19.8
	Average width, m	124	118	114	109	119	110
Wave celerities:							
2011 Wave	Leading edge, m/s	-	-	-	5.4	5.6	2.9
	Wave front, m/s	-	-	-	3.9	2.7	2.5
	Peak, m/s	-	-	-	4.2	1.6	1.8
2013 Wave	Leading edge, m/s	4.9	-	-	-	6.4	-
	Wave front, m/s	2.5	-	-	-	2.6	3.1
	Peak, m/s	2.8	-	-	-	1.3	2.6
	Back of 20%, m/s	-	-	-	1.2	1.4	-

Table 3.2 is continued on the next page.

Table 3.2. *continued*. Celerities of wave and ice run features resulting from ice jam releases observed over six study reaches on the Hay River.

Feature	Description	Reach 1	Reach2	Reach 3	Reach 4	Reach 5	Reach 6
Ice run celerities:							
Ice Run A	Start of 20%, m/s	-	-	-	-	1.8	1.9
	Back of 20%, m/s	-	-	-	1.1	0.9	2.1
Ice Run I	Start of 20%, m/s	2.0	1.4	1.1	-	-	-
	Back of 20%, m/s	1.5	-	-	-	-	-
Ice Run II	Start of 20%, m/s	2.1	1.5	1.2	1.2	-	-
	Back of 20%, m/s	1.7	1.3	1.1	1.4	-	-
Ice Run III	Start of 20%, m/s	1.9	1.7	1.3	1.1	1.0	-
	Back of 20%, m/s	1.8	1.2	1.2	1.3	1.5	-
Ice Run IV	Start of 20%, m/s	-	-	-	-	1.3	2.7

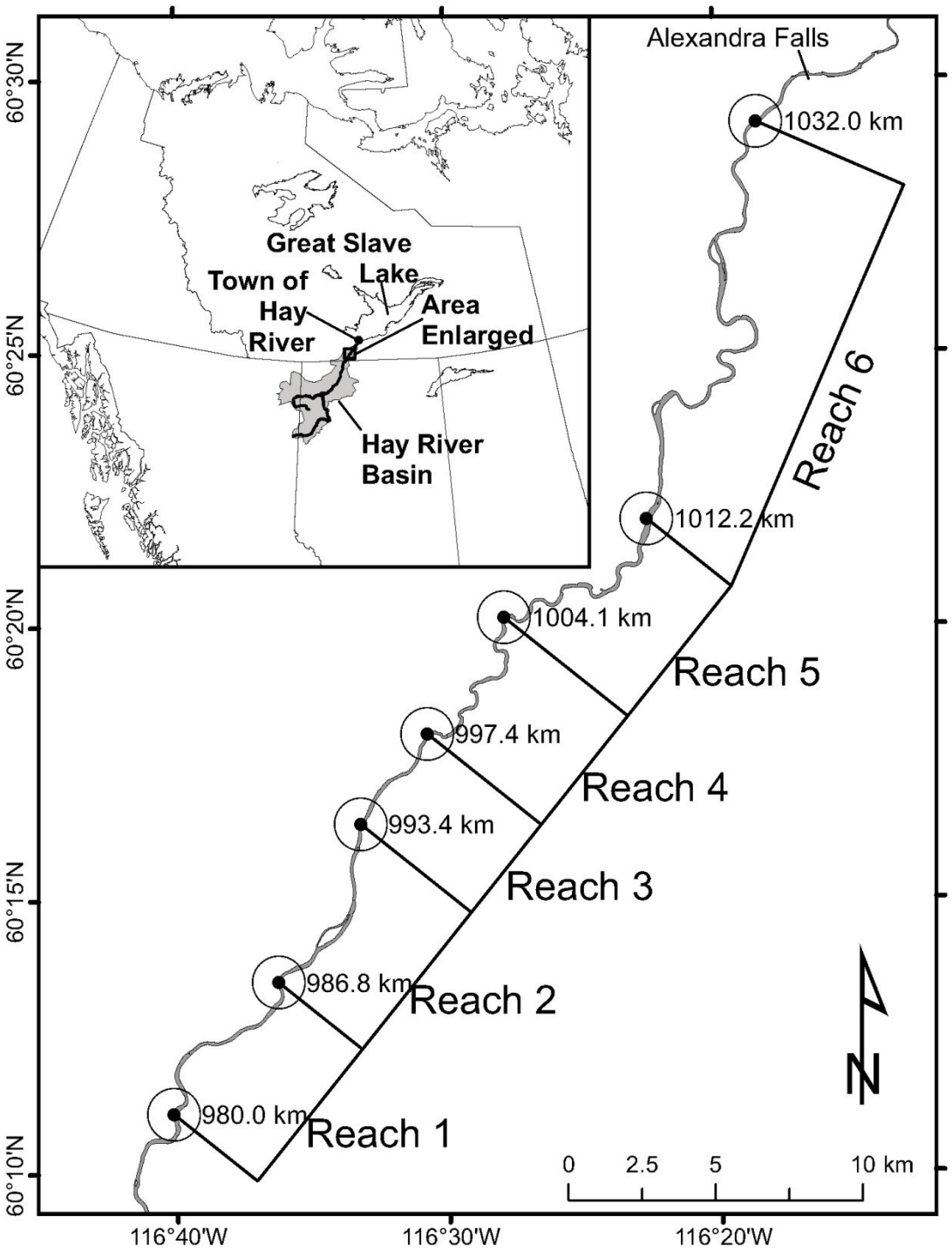

Figure 3.1. Location of the Hay River basin and study reaches.

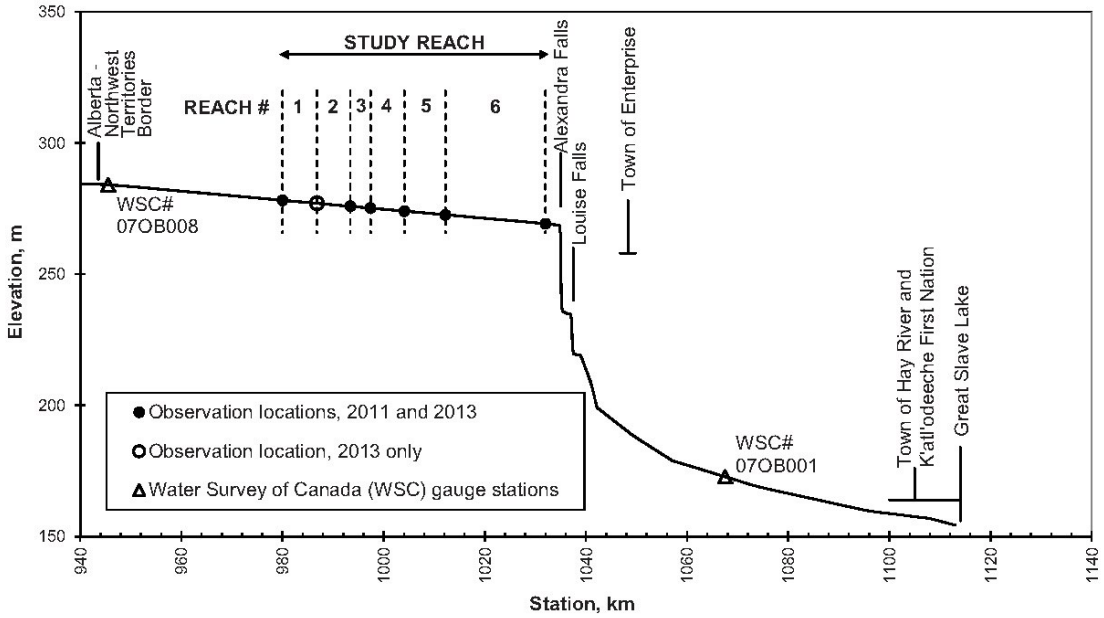

Figure 3.2. Profile plot of the Hay River showing bed profile, study reach, and river features.

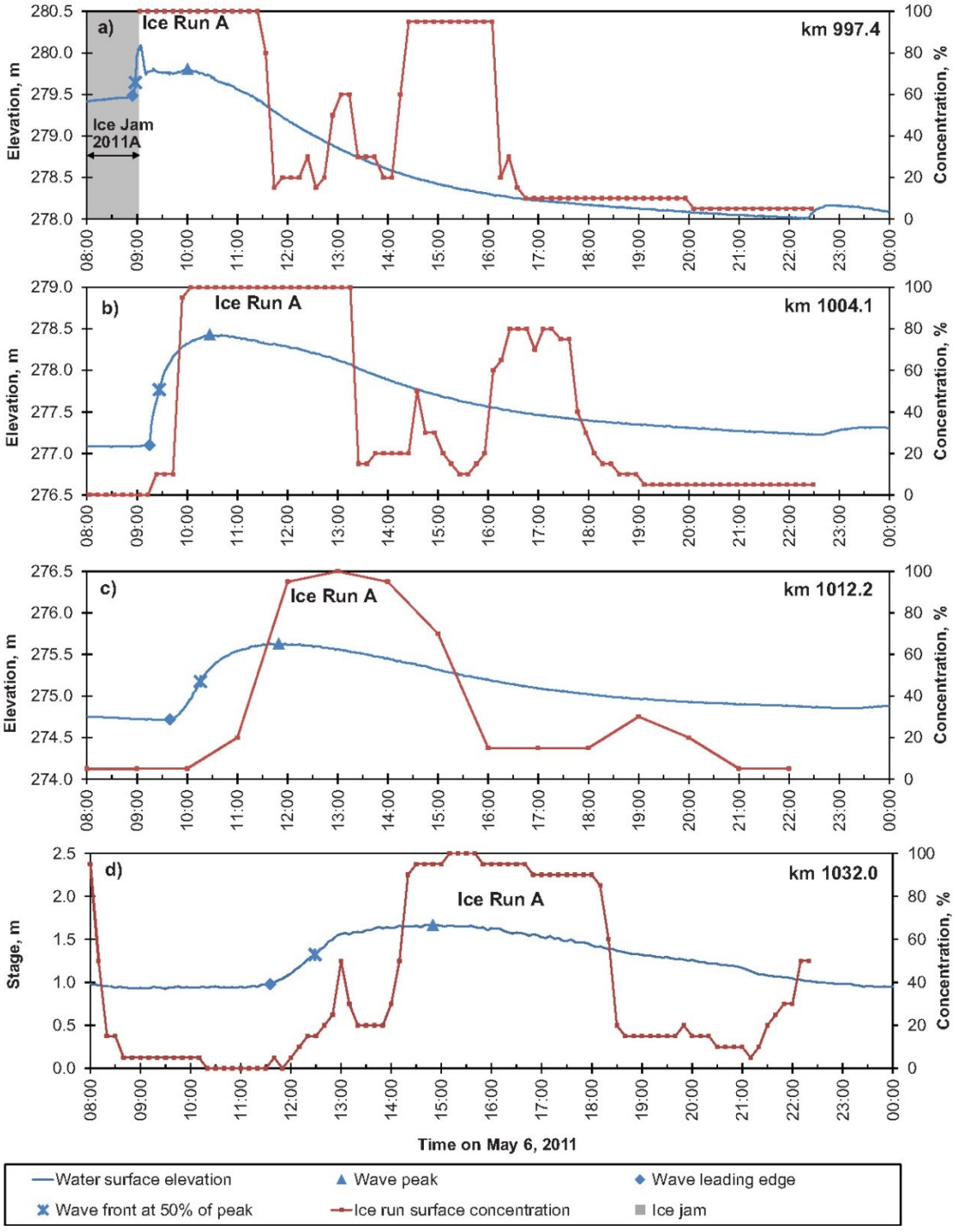

Figure 3.3. Water surface elevation and surface ice concentration observed in 2011 on the Hay River. Each ice concentration data point represents one photographic observation.

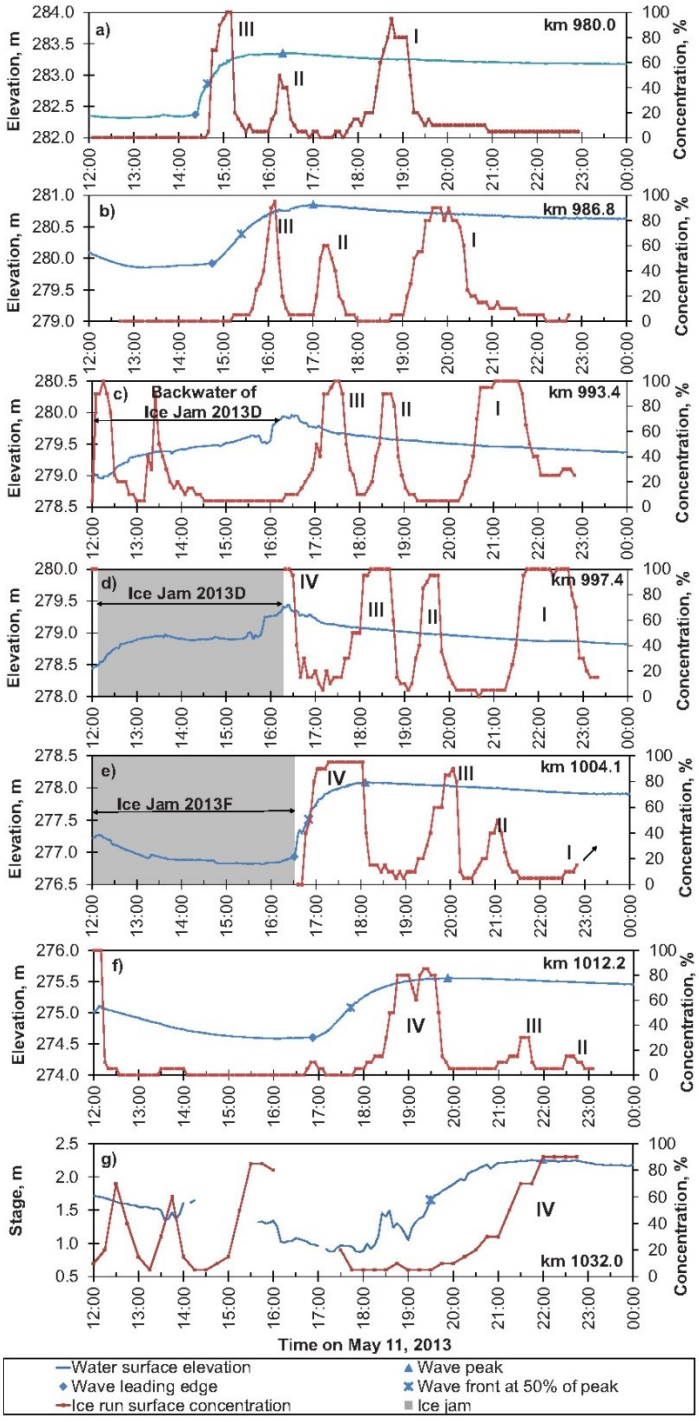

Figure 3.4. Water surface elevation and surface ice concentration observed in 2013 on the Hay River. Individual ice runs are identified with a Roman numeral. Each ice concentration data point represents one photographic observation.

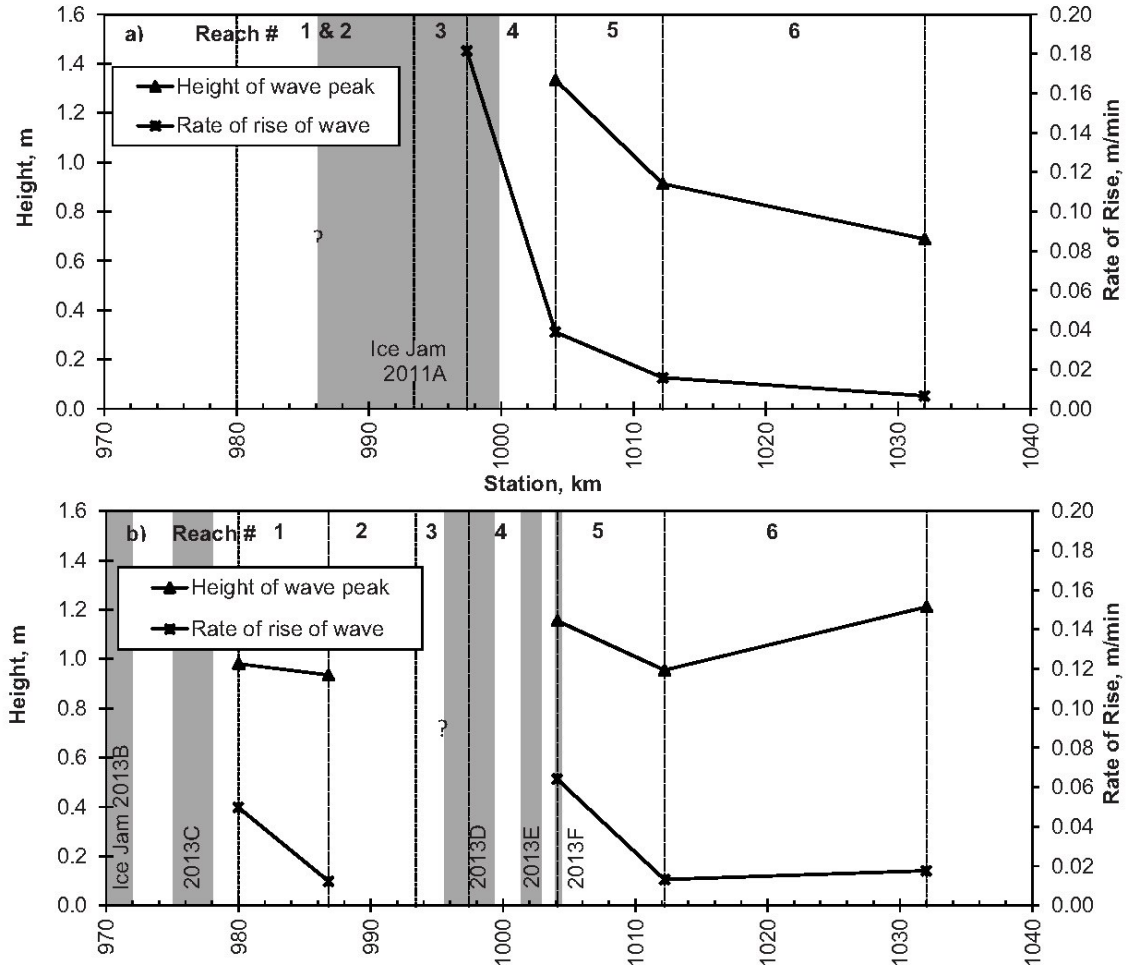

Figure 3.5. Wave height and rate of rise for waves observed in a) 2011 and b) 2013 on the Hay River. Gray bars represent location of ice jams. Question marks indicate uncertainty in upstream extents of the ice jams.

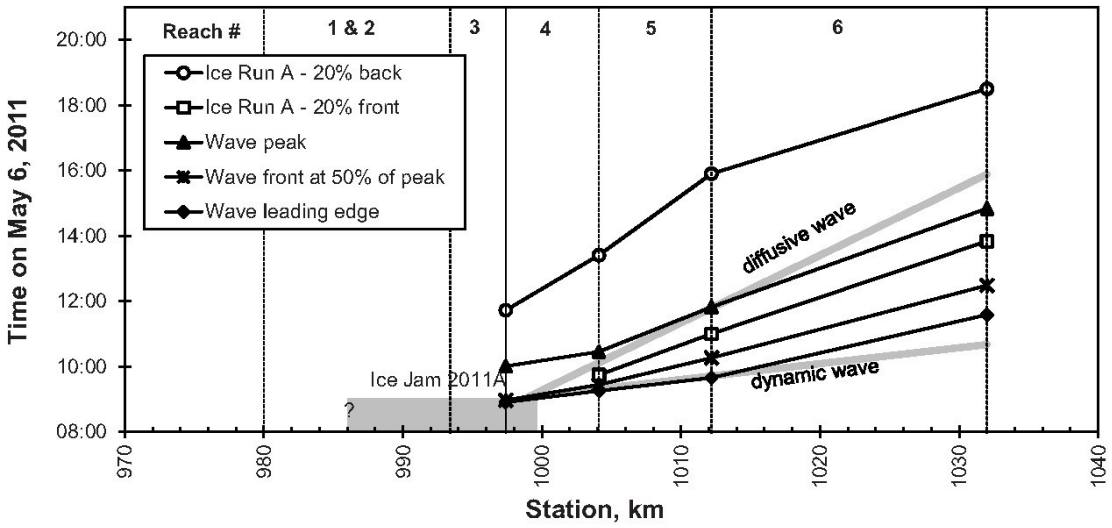

Figure 3.6. Phase diagram of 2011 water wave, ice run, and ice jam features observed on the Hay River. The ice jam extents are shown with a gray box. The question mark indicates uncertainty in the upstream extent of the ice jam.

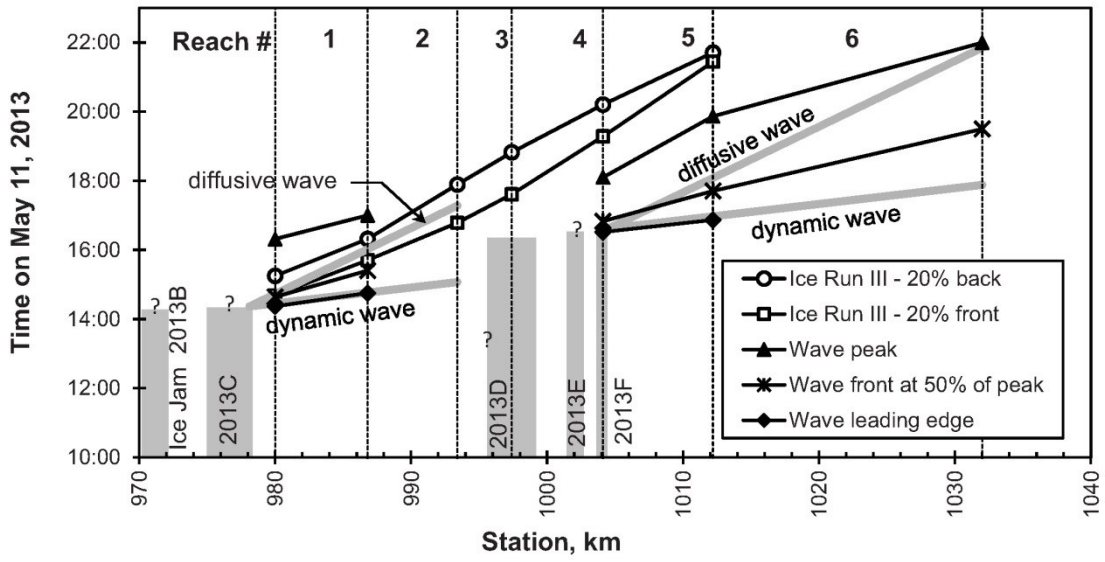

Figure 3.7. Phase diagrams of a) water wave and ice jam features, and b) example ice run (Ice Run III) with wave and ice jam features observed on the Hay River in 2013. Ice jam extents are shown with gray boxes. Question marks indicate uncertainty in the extents or release time of an ice jam.

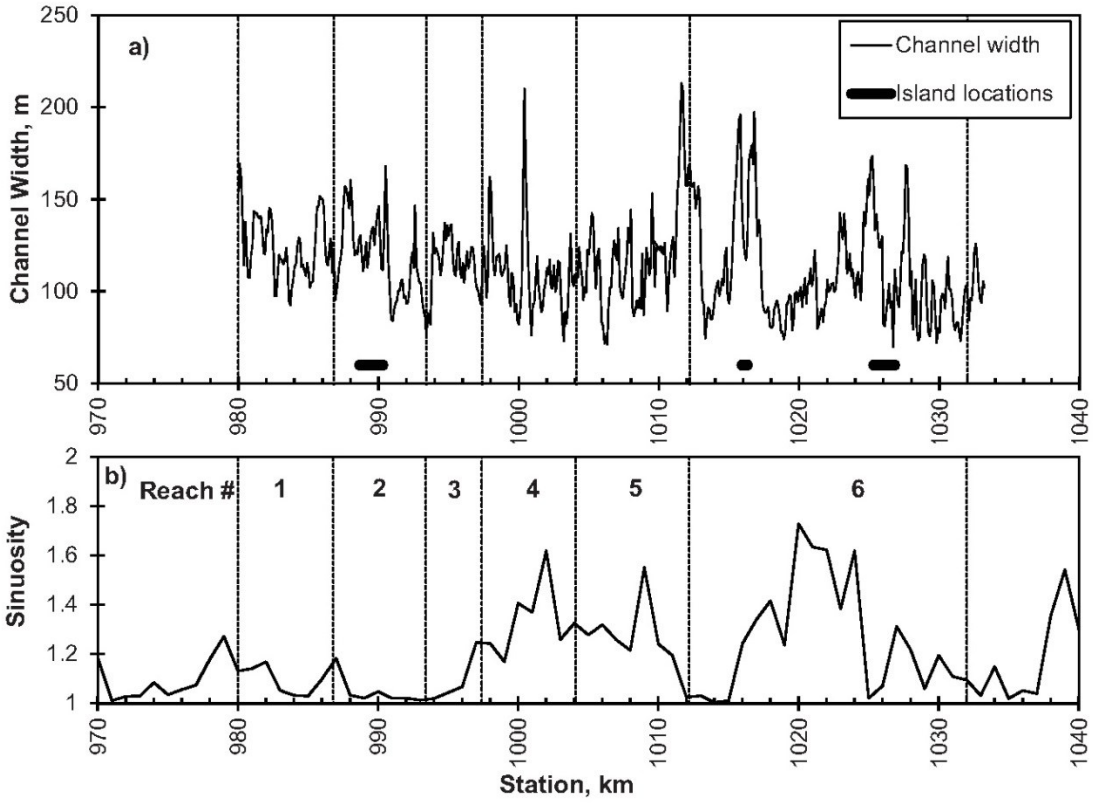

Figure 3.8. Geomorphological characteristics of the study reach on the Hay River including: a) channel width and island locations, and b) channel sinuosity.

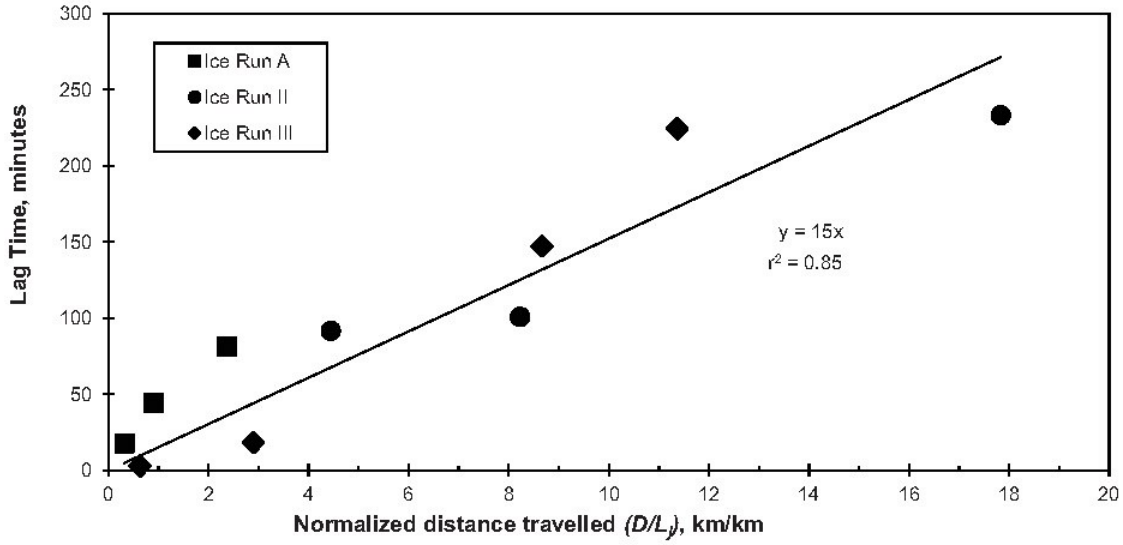

Figure 3.9. Lag time between the fronts of the waves and the starts of 20% ice concentration of the ice runs observed on the Hay River in 2011 and 2013; showing relationship between lag time and normalized distance travelled (D/Lj). Ice Runs I and IV were omitted due to uncertainty in determining the original ice jam length (Lj) or the distanced travelled (D).

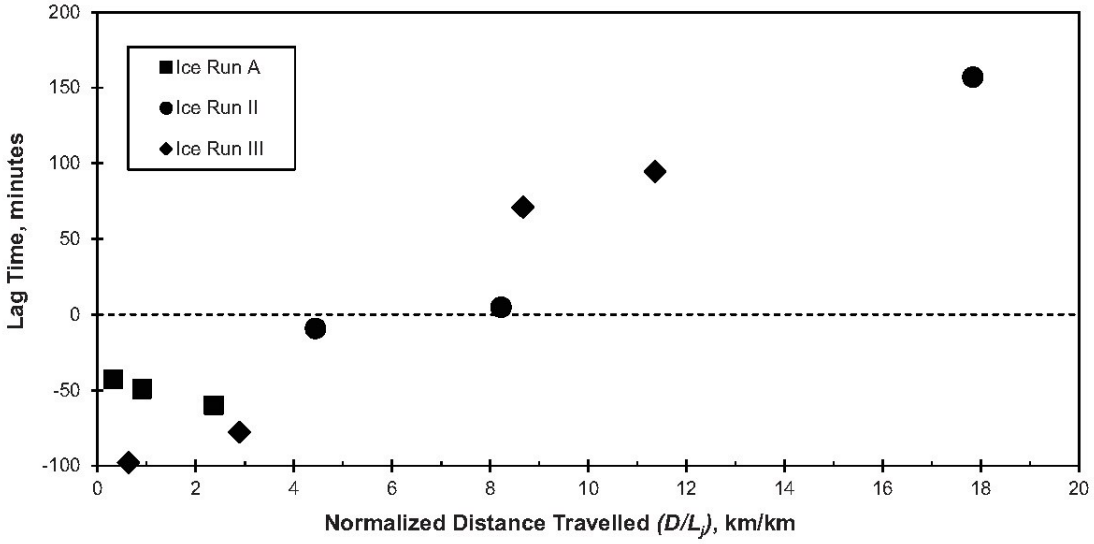

Figure 3.10. Lag time between peaks of the waves and the starts of 20% ice concentration of the ice runs observed on the Hay River in 2011 and 2013; showing that the crossover between when the ice runs travel before the peak of the water wave (negative lag) to behind the peak of the water wave (positive lag) occurs between 4 and 8 ice jam lengths of travel (D/Lj). Ice Runs I and IV were omitted due to uncertainty in determining the original ice jam length (Lj) or the distanced travelled (D).

Chapter 4. Dynamic River Ice Processes in a River Delta Network

A version of this chapter was submitted in to the journal *Cold Regions Science and Technology* in December 2017 as:

Nafziger, J., She, Y., Hicks, F. Dynamic river ice processes in a river delta network.

4.1 Abstract

Deltas and other multi-channel river systems in cold regions are particularly prone to ice jam flooding. The Hay River delta in the Northwest Territories, Canada is a unique full-scale field laboratory for studying such events because of its relatively simple network geometry and easy access throughout. This paper presents detailed analyses of ice formation and consolidation events at the main channel junction of the Hay River delta. Water waves and ice movements were tracked continuously at 22 locations over three breakup seasons. In the six analyzed events, ice jam movements were initiated at the upstream end of the ice jams while the stopping of these movements was initiated at the downstream end. This resulted in ice movements that alternated between the delta channels, due to the unsteady flow conditions at the channel junctions and the momentum of the ice upstream of the junction. This alternating pattern of ice movement had been observed in the Hay River delta for many decades; but until this study, it had remained unexplained. These findings suggest that the prediction of the extent of ice jam consolidation, and thus ice jam flooding, may require consideration of unsteady ice jam dynamics. Finally, a unique cause for ice jam consolidation was observed: a wave

generated by the melting and "creeping consolidation" at the upstream end of an ice jam caused the jam to consolidate and release.

4.2 Introduction

Breakup ice jams are a prominent and important feature of rivers in cold regions. An ice jam is a large, jumbled accumulation of broken river ice that partially blocks a river channel, raises water levels, and potentially causes flooding. The mechanical strength of ice jams is due to frictional forces between the ice pieces in the accumulation. Thus, the strength of the accumulation increases with its thickness. Ice jams consolidate into thicker accumulations when larger external forces are exerted on them. The formation, consolidation, and release of ice jams are inherently unsteady and dynamic processes (Zufelt, 1990). As such, ice jam flooding can occur quickly and without warning, affecting communities located along northern rivers. However, ice jam flooding can also be a benign process: it replenishes water and nutrients to the landscape of cold region deltas, which are "hot spots" of biological activity (e.g. Emmerton et al., 2007). Multi-channel delta environments are particularly prone to ice jams because their low gradients, channel junctions, and islands have the effect of reducing the ice conveyance capacity of the channel.

Past studies have examined the hydraulics of ice jam processes in multi-channel networks. Ettema and Muste (2001) explored ice jam processes at channel junctions using physical models. They focused only on situations where flows come together (e.g. where a tributary meets a channel), and not on the flow-dividing junctions that are the defining feature of deltas. Jasek (1995) investigated the theoretical effect of islands (a

type of multi-channel environment) on ice jam thickness. Several researchers have investigated the hydraulics of spring breakup in cold region deltas in Canada, such as the Mackenzie delta (e.g. Beltaos et al., 2012, Blackburn et al., 2015), the Slave River delta (Zhang et al. 2017), and the Peace-Athabasca delta (e.g. Beltaos, 2007 and 2017b). These studies focused on steady-state conditions or did not consider channel junctions in their analysis. Kolerski and Shen (2015) simulated a historical ice jam in the multi-channel St. Clair River Flats using the 2D DynaRICE numerical model. This model partitioned water flow and ice movements between the delta channels, but few observations of ice movements were available to verify the accuracy of this simulation. Various 1D and 2D modelling approaches have been recently applied to the Hay River delta (i.e. Brayall and Hicks, 2012; De Coste et al., 2017; Oveisy and She, 2017). These efforts were focused on flood forecasting and matching measured top of ice profiles, and did not investigate the ice processes that occurred at the channel junctions. Advances in our understanding of how ice moves through delta junctions have been hampered by a lack of field measurements of these difficult-to-observe processes.

The Hay River delta is an ideal field laboratory for studying ice jam processes in a multi-channel network. The delta consists of a single main channel junction where processes at the junction can be observed in isolation. Here, river ice processes can be observed "full-scale" and without making the assumptions inherent in physical or numerical modelling. Further, the river is a well-known site for studying river ice processes because of its frequently occurring dynamic breakups and a history of major flooding at the Town of Hay River (THR) and the K'atl'odeeche First Nation. In fact, 11 "significant" floods have been recorded in the delta since 1914 (Kovachis, 2011), making

work here important for the safety of the riverside communities.

The aim of this research was to determine, both qualitatively and quantitatively, the basic dynamic river ice processes that occur at a simple delta channel junction when an ice jam is forming or consolidating there. To do so, dynamic water and ice movements were observed over three breakup seasons in the Hay River delta. The six events documented in this paper elucidate the ice jam processes that may occur at dividing channel junctions. An understanding of these basic processes is important for flood forecasting in channel networks in general, and in particular, is directly and immediately useful for the flood watch committee of the THR. Knowledge of these basic processes is also important in the development and testing of numerical models that aim to simulate and predict ice movement in multi-channel networks.

4.3 Study Site and Methods

4.3.1 Site Description and Instrumentation

The Hay River flows north from British Columbia and Alberta to the delta at its mouth on Great Slave Lake (GSL) in Canada (Figure 4.1a and 4.1b). Detailed site descriptions can be found in Stanley and Gerard (1992), Kovachis (2011), and Nafziger et al. (2016). Figure 4.1d shows the bed profile of the study reach. The bed slope upstream of the study reach is ~0.02%; the reach from km 1034 to km 1093 is steeper (slope 0.1%, not including the falls) and contains two waterfalls: Alexandra Falls and Louise Falls. From km 1093 to GSL (~km 1114) the river slope flattens (~0.02 to 0.03%) and terminates in a multi-channel delta, where the two secondary channels, the East and West Channels, are joined at the main delta junction at km 1108.0 (Figure 4.1c). The

thalweg of the West Channel is higher than the East Channel; therefore, flow in the West Channel is close to zero during summer and winter low flows. At the main channel junction, the thalweg is located in the eastern part of the East Channel (Brayall and Hicks, 2012). An additional channel junction, which was not considered in this study, is located in the West Channel at km 1111.1.

During three spring breakups (2010, 2011, 2013), water levels and ice conditions were observed at several locations along the river and at time intervals ranging from 1 to 60 min (Figure 4.1, Table 4.1). This research also considered additional ice observations from the breakup of 2009. Water levels were measured with self-contained submersible pressure transducer and data loggers (Schlumberger Diver models 501 and 601, accuracy: 1.0 and 0.5 cm H_2O) with synchronized clocks, installed on the riverbed according to the method described by Nafziger et al. (2016). The elevations of the instruments were measured using a real-time kinematic global positioning system (RTK-GPS) referenced to local geodetic benchmarks using a site calibration (typical vertical accuracy < ~0.03 m). The same RTK-GPS system was used to measure profiles of the top of ice elevations of stabilized ice jams. Ice conditions were observed, when lighting conditions allowed, using time-lapse cameras (various models used) mounted on trees or poles on the riverbanks. Ice conditions were also monitored in person from the river banks and from aircraft, allowing for periodic documentation of ice conditions between camera observation stations. The THR also operated cantilever-mounted water level observation stations (accuracy ~0.1 m) and cameras at km 1032.0, 1067.5, and 1098.1.

Rating curves were available at two locations in the study reach. The Water Survey of Canada (WSC) operates a water level and flow gauge (#O7B001) at km 1095.3;

however, this site was often ice-covered or in the backwater of ice jams, rendering discharge estimates inaccurate. A rating curve was also available for the THR station at km 1032.0. This observation station was located ~2 km upstream of Alexandra Falls and was therefore normally unaffected by ice jams and was ice-free early in the breakup season. This rating curve was used to provide incoming discharge estimates for the lower reaches of the Hay River.

4.3.2 Analysis Methods

Ice movements were observed in the time-lapse photographs with emphasis on identifying when stationary ice began to move and when moving ice ceased moving. In this study, the term "moving front" is used to describe the advancing interface between stationary and moving ice during ice jam consolidation, whereas the term "stopping front" is used to describe the upstream retreating interface between stationary and moving ice as ice jam consolidation ceases (similar to the terminology adopted by Zufelt, 1990). Moving ice was identified when the ice cover changed completely over photographic intervals of 5 min or more. If the ice cover was observed to move slightly over an interval of 5 minutes (i.e. within the field of view of the photograph), this was considered "creeping consolidation" instead of movement. Where the speed of the creeping consolidation was quantified, the distance individual pieces of ice moved was calculated using the distance the camera was from the ice pieces and the measured angle of the field of view of the camera.

Water level features were also tracked as they moved through the delta. Examples of the typical features observed are shown in Figure 4.2, including the time of arrival of:

1. The leading edge of the "consolidation wave", the water wave that advanced downstream into the delta and was accompanied by the ice moving front.
2. The leading edge of the "rejection wave," caused by the stopping of the ice, which retreated upstream.
3. The water level peak that accompanied the ice stopping front, which retreated upstream. This is referred to as the "stopping front water level peak."
4. The leading edge and peak features of the "instigated wave," the water wave that advanced downstream through one of the secondary delta channels due to ice movements in the other secondary channel. In some cases, this instigated wave caused ice consolidation in the channel in which it travelled.
5. The leading edge and peak features of the "escaped wave", the portion of the consolidation wave or the instigated wave that advanced downstream but was not accompanied by ice movement. It advanced past the main channel junction or past the furthest downstream extent of consolidation (i.e. past the ice jam toe).

The celerities of the water level features were calculated from the time a specific feature took to travel between observation locations. The error in the calculated celerity comes from the uncertainty (average 1.5 min, maximum 34 min) in defining when the water level feature arrived at an observation station. This uncertainty was due to the length of the time interval between observations and to gradually changing water levels, which made the leading edges or peaks of the water level features indistinct. Where these uncertainties resulted in a large error in celerity (especially when the distance between stations was small), these celerities were not included in further analyses and are not included in Table 4.2. The celerities of the ice features (i.e the ice stopping front or

moving front) were not calculated because camera observations were taken at a coarser time interval than water level readings and the location of the stopping and moving fronts tended to be coincident with water level features that could be tracked more accurately.

The celerities of theoretical dynamic and diffusive waves were approximated using an open-water, steady-state analysis at the carrier discharge (i.e. the discharge unaffected by ice jam release waves). This approach was suggested by Beltaos and Burrell (2005) and was also used on upstream reaches of the Hay River by Nafziger et al. (2016). The carrier discharges were estimated using the rating curve at km 1032.0 and travel times to the delta, which were estimated from the travel times of observed ice runs in this reach. The diffusive wave celerity ($C_{diffusive}$) and dynamic wave celerity ($C_{dynamic}$) were calculated using Equations 4.1 and 4.2, respectively (after Henderson, 1966).

$$C_{diffusive} = \frac{5}{3} U_0 \tag{4.1}$$

$$C_{dynamic} = U_0 + \sqrt{g y_0} \tag{4.2}$$

Where U_0 and y_0 are the respective reach-averaged velocity and depth of the undisturbed open-water flow at the carrier discharge, and g is the gravitational acceleration. These celerities represent approximate values of the theoretical upper and lower bounds of wave celerity that may be observed in the field. They are therefore useful for assessing the relative importance of the dynamic versus diffusive wave components in the observed events. In order to calculate U_0 and y_0 in the delta channels, the incoming discharge was partitioned between the two channels using discharge partition curves developed by Brayall and Hicks (2012) for the Hay River delta.

4.4 Observed Events

4.4.1 General Event Descriptions

Six events from the three study years were analyzed. Each event covered a time period when moving ice was observed at the main delta junction because an ice jam was either forming or consolidating. The six events are described below. Events 2 and 6 are considered in further detail in subsequent sections because they illustrate each process that was observed in the other events.

- **Event 1 (morning of April 25, 2010)** A large ice jam (~28 km long) formed with toes in the delta at GSL (West Channel) and km 1111.6 (East Channel) and the head at km 1084 (Main Channel). This ice jam formed from ice runs that resulted from the release of an ice jam at km 1049; which was itself released when ice runs and water waves from the release of other ice jams upstream of Alexandra Falls reached that location. The initial ice movements in the delta and the stopping of the ice in the East Channel were not observed; but the stopping of the ice in the West Channel and subsequent movements in the East Channel were observed.
- **Event 2 (April 25, 2010 ~17:00)** The 28 km-long ice jam that formed in Event 1 consolidated to form a 15 km-long ice jam and caused minor flooding. The toe in the East Channel moved from km 1111.6 to GSL and the head moved from ~km 1084 to ~km 1099. Ice movement occurred only in the East Channel.
- **Event 3 (May 8, 2011 ~18:00)** An ice jam formed in the delta following the release of a 22 km-long ice jam located upstream of the THR (at km 1101.3 to km 1079), which occurred following a rain shower. The toes of the newly-formed

jam were at GSL (West Channel) and km 1111.2 (East Channel) and the head was between km 1103.3 and km 1106.1 (Main Channel). The ice first stopped moving in the East Channel and then later stopped in the West Channel.

- **Event 4 (May 11, 2013 ~19:00)** An ice jam formed in the Hay River delta following the release of a small ice jam at km 1095 and the arrival of ice runs from upstream. The ice first stopped moving in the East Channel, then movement alternated between the East and West Channels. The toes of this ice jam were located at km 1111.3 (West Channel) and km 1110.0 (East Channel) and the head was downstream of km 1103.3 (Main Channel). The mobilization and stopping of the ice cover from ~18:40 to ~19:30 were considered part of this event.
- **Event 5 (May 11, 2013 ~20:30)** The ice jam that formed during Event 4 consolidated by first moving in the West Channel, then movement alternated between the channels. During this consolidation, the ice jam toes did not move but the head moved downstream from ~km 1104 to downstream of km 1106.0 (Main Channel).
- **Event 6 (May 11, 2013 ~22:00)** The ice jam that formed in Event 4 consolidated further, with ice movements first in the West Channel, then in the East Channel. The toe of the ice jam in the East Channel moved from km 1110.0 to km 1110.2 and the toe in the West Channel remained at ~km 1111.3, while the head moved from downstream of km 1106 to ~km 1107 (Main Channel).

4.4.2 Event 2 (April 25, 2010 ~ 17:00)

Figure 4.3 shows the tracking of water level features and ice movements during Event 2. Uncertainty in the measurement of the time of arrival of the ice and water level

features are shown with vertical error bars. (Where the error bars are not visible, they are smaller than the data marker). In Figure 4.3, the shaded areas represent the ice conditions. In most cases, a change in ice conditions was almost coincident with a tracked water level feature. However, a water level record was not available at km 1106.1, but ice observations were. Therefore, the line separating moving ice and stationary ice at that location was not coincident with the interpolated path of the stopping front water level peak.

During Event 2, creeping consolidation was observed at stations closest to the head of the ice jam before the full-scale consolidation of the ice jam occurred (Figure 4.3). For example, at km 1103.3 individual pieces of ice moved approximately 2 m in 5 minutes (0.4 m/min). In the Main Channel, the moving front was coincident with the leading edge of a ~0.5 m amplitude water wave, starting at the upstream end of the ice jam. This wave moved at celerities of 5.1 to 7.5 m/s in the Main Channel, then at 3.6 m/s in the East Channel and 4.0 to 4.7 m/s in the West Channel. After this wave passed each observation location, the ice jam continued to consolidate and water levels continued to drop for a time. As the leading edge of the water wave moved downstream and through the main channel junction, the ice moved in the East Channel, and no ice movements were observed in the West Channel.

In the East Channel, as the leading edge of the water wave and the moving front reached the toe of the ice jam, the toe pushed downstream to GSL and stopped (Figure 4.3). The ice stopping front retreated upstream from this new toe location, as did a rejection wave. The leading edge of the rejection wave retreated at celerities of 2.3 to 4.4 m/s in the East Channel, and 1.8 to 4.2 m/s in the Main Channel. The stopping front

water level peak retreated upstream at celerities of 1.2 to 3.4 m/s in the East Channel and 0.8 to 1.3 m/s in the Main Channel. Both the rejection wave and the stopping front water level peak moved fastest in the reach closest to the toe of the ice jam. When the rejection wave reached the main delta junction, it raised water levels and caused an instigated wave to advance down the West Channel (Figure 4.3). The leading edge of the instigated wave propagated from the leading edge of the rejection wave and the peak of the instigated wave propagated from the stopping front water level peak. Since the peak of the instigated wave in the West Channel was flat-topped, both the front and back of the peak of this wave are documented in Figure 4.3. The leading edge of the instigated wave advanced at celerities of 1.3 to 2.4 m/s in the West Channel. The front of the peak advanced at 1.1 m/s while the back of the peak advanced at 0.6 to 0.7 m/s.

Figure 4.4 shows the propagation of the advancing consolidation wave and the retreating rejection wave as they were observed passing different observation stations in the delta. Figure 4.4a shows the downstream propagation of the consolidation wave, which advanced through the main delta junction at point "A" in Figure 4.3. As the consolidation wave advanced from km 1103.3 to km 1108.0, the amplitude of the wave increased from ~0.40 m to ~0.55 m. The amplitude of this wave continued to increase as it travelled into the East Channel, where consolidation was happening with the travel of the wave. However, in the West Channel (where no consolidation was occurring), the amplitude of the wave attenuated from ~0.55 m to ~0.2 m from km 1108.0 to km 1110.2. The leading edge of this wave advanced at similar celerities down the two channels, shown by the similar arrival time at km 1110.1 in the East Channel and km 1110.2 in the West Channel. The origin of the secondary peak observed at km 1110.1 and km 1108.0

was not observed. However, because this peak retreated upstream, it could be the result of a temporary stopping of the ice jam movement.

Figure 4.4b shows the retreat of the rejection wave (solid line) caused by the stopping of the ice in the East and Main Channels and the downstream propagation of the resulting instigated wave in the West Channel. These waves propagated through the main delta junction at point "B" in Figure 4.3. As the rejection wave retreated upstream, the time between the leading edge and the peak increased. The changes in water level at km 1110.1 in the West Channel are due to the propagation of the low and high water levels from the junction down the West Channel.

4.4.3 Event 6 (May 11, 2013 ~22:00)

Figure 4.5 shows the tracking of water level features and ice movements during Event 6. During this event, the stopping of ice in the West Channel caused the consolidation and toe movement of the ice jam in the East Channel. At the beginning of this event, the ice jam that was in place in the delta began to consolidate, accompanied by the leading edge of a small (~ 0.2 m amplitude) wave. As this wave advanced downstream through the main delta junction (at a celerity of 2.8 m/s), the ice jam consolidated in the West Channel and no ice movement was observed in the East Channel. Then as the ice stopped in the West Channel, the stopping front and associated water level peak retreated upstream to the junction, increasing water levels there. The ice in the East Channel then started to consolidate, and a small instigated wave advanced down the East Channel (at a celerity of 4.0 m/s). This consolidation wave caused the toe of the ice jam in the East Channel to move downstream by 0.2 km. The escaped

instigated wave continued to propagate downstream in the East Channel past the new toe of the jam and under the intact ice, but had a small amplitude (0.06 to 0.1 m) and celerities of 4.0 to 6.0 m/s. The stopping front and associated water level peak then retreated upstream in the East Channel and then in the Main Channel (at celerities of 3.8 to 5.8 m/s).

4.5 Analysis and Discussion

4.5.1 Junction Geometry

Figure 4.6 shows the observed patterns of ice movement through the main delta junction. The path that moving ice took through the junction could be seen from the air, even after the ice had stopped moving. This was because the ice had different colours and/or textures (see Figure 4.6a) depending on how recently it moved and where the ice originated from upstream. For example, ice that originated from above Alexandra Falls tended to consist of smaller pieces due to its travel over the falls. Figure 4.6b shows the situation when ice moved freely in both channels (i.e. during an ice run or during ice jam formation); in this case, there was a small stagnation area only at the apex of the junction. When ice moved in only in the East Channel (Figure 4.6c), the ice moved first across the entire junction. Then, when water levels dropped, the ice in only the eastern part of the junction moved. When the ice moved in only in the West Channel, the path the moving ice took through the junction depended on the water and ice levels. At higher ice and water levels (increasing from Figure 4.6d to 4.6f), the shear plane between the moving and stationary ice was located more to the east and moving ice covered more of the junction area.

4.5.2 Ice Movement

Figure 4.7 shows observations of alternating ice movements between the East and West Channels in 2013. Local river watchers have long observed this behaviour; but until this study, it was unexplained and unpredictable. The documented advancing and retreating waves in the delta demonstrate that the ice and water movements in the respective secondary channels affect each other (e.g. Figures 4.3 and 4.5). Figure 4.8 shows a conceptual explanation of this relationship. When the ice stopped in the initial channel the water levels increased at the junction, resulting in an 'instigated wave' that advanced down the opposite channel. This instigated wave likely increased the discharge and the water surface slope of the second channel, thus increasing the drag on the underside of the ice and the downslope component of ice weight in the accumulation. This wave also lifted and separated the ice floes, weakening the accumulation and making it more susceptible to consolidation. By this time, the ice in the initial channel had sufficiently thickened to withstand the forces resulting from the momentum of the moving ice. At this time the ice in both channels was stationary, while the ice continued to move upstream of the junction. Then the ice started moving in the second channel, due to the momentum of the upstream ice imparting a force on the wave-weakened accumulation. This behaviour indicates that the prediction of ice jam consolidation in channel networks requires consideration of unsteady ice jam dynamics, unlike in the single channel case where a steady flow approximation of the peak discharge may be reasonable (e.g. She et al., 2008).

4.5.3 Water Level Feature Celerities

The observed water level features were tracked for all six events and the celerities of these features are summarized in Table 4.2 and on Figures 4.3 and 4.5 for Events 2 and 6, respectively. The stopping front water level peaks moved upstream with celerities ranging from 1.2 to 8.1 m/s and tended to have lower celerities when travelling through open water than through channels with an ice jam. Event 2 (Figure 4.3) was the only event where detailed tracking for both the stopping front water level peak and the leading edge of the rejection wave were available. In this case, the leading edge of the rejection wave retreated upstream with a greater celerity than did the stopping front water level peak in the same reaches. The leading edge of waves that advanced downstream ranged in celerity from 2.8 to 7.5 m/s, moving faster through channel sections with intact or somewhat deteriorated ice than through ice-jam-covered sections of the channel.

The celerities of the downstream advancing features (i.e. the features of the consolidating, instigated and escaped waves) were compared to the theoretical open water $C_{diffusive}$ and $C_{dynamic}$ and were expressed as a fraction of $C_{dynamic}$ (Table 4.2). The carrier discharges used when determining the wave celerities are also included in Table 4.2. These features were grouped into six different types for convenience in discussing trends in the data. Type A features were the leading edges of the consolidation waves. Their celerities ranged from 0.6 to 1.5 times $C_{dynamic}$ and were highest when travelling through intact-ice-covered sections of the main channel. Type B features were the leading edge of the escaped wave that advanced downstream of the main channel junction in the West Channel while the East Channel consolidated in Event 2. Type B features travelled with celerities of 0.7 to 0.8 of $C_{dynamic}$. Type C features were the leading edges of escaped waves that advanced down a channel after ice had stopped further upstream. They

travelled with celerities of 0.4 to 1.0 of $C_{dynamic}$, with celerities closer to $C_{dynamic}$ when travelling through sections of the channels covered with intact ice. Type D features were the peak features of these escaped waves or instigated waves that were not accompanied by ice movements, and they travelled with celerities from 0.1 to 0.6 of $C_{dynamic}$. Type E features were the leading edges of instigated waves that caused consolidation in the channel through which they advanced, and travelled at celerities of 0.7 to 0.9 of $C_{dynamic}$. If the leading edge of the instigated wave did not cause consolidation, it moved at a slower celerity (0.2 to 0.4 of $C_{dynamic}$) and were denoted as Type F features in Table 4.2. Overall, the leading edges of waves were more dynamic than the peaks and waves were more dynamic if they were accompanied by ice movements or if they travelled through intact ice. The leading edges of instigated waves were no less dynamic than waves that originated upstream if they were accompanied by ice movements.

4.5.4 Origin of Consolidation Waves

The origin of the wave that accompanied the consolidation of the ice jam in Event 2 could not be determined with certainty. Figure 4.9 shows the water level hydrographs at three locations in the study reach, spanning the time period from before Event 1 to after Event 2. The consolidation wave was observed at km 1103.3 (Figure 4.9c), km 1098.1 (Figure 4.9b), and km 1095.3 (not shown, because the WSC gauge record is incomplete), which were all located within the consolidating ice jam. However, the wave was not observed upstream of the ice jam at km 1067.5 (Figure 4.9a). There were no additional ice jam or ice runs between km 1067.5 and the upstream end of the ice jam, as confirmed during a reconnaissance flight, and there were no significant tributaries in the same reach. Therefore, the wave may have come from within the ice jam itself. The wave origin may

be related to the creeping consolidation observed in the upstream section of the ice jam (see Figure 4.3).

The creeping behaviour of an ice jam may be expected. Ice jams are often considered as granular materials, which are known to display creep behaviour under constant loading. For example, McDowell (2003) noted that the creep behaviour of a granular material is consistent with the behaviour caused by both the sliding of granular particles past each other and the crushing of the particles. Healy and Hicks (2006) observed creeping consolidation during their physical model studies of ice jams made from simulated polyethylene ice. For a meltable material like ice, an additional cause of creep could be the melting of ice particles. Melting and crushing may be more prominent at the upstream end of an ice jam where heat from water flowing underneath is absorbed and used to warm, weaken, and ultimately melt the ice pieces. This melting process may be enhanced on the Hay River, where the north-flowing river brings with it higher water temperatures and high sediment loads (and thus reduced albedo and enhanced shortwave radiation absorption) from the open stretches upstream of the delta. Indeed, longer periods of creeping consolidation were observed at the more upstream sections of the ice jam in Event 2 (Figure 4.3).

As the ice jam slowly shortens because of creeping consolidation, water is released from storage and could result in a wave being formed. The water is released from the melting ice and from the backwater zone of the ice jam, which shortens as the ice jam shortens. This could result in a water wave, as postulated for a similar situation by Beltaos (2017a). If this occurred in Event 2, the implication is that the ice jam caused its own consolidation and release. This possible mechanism should be studied further

because it has implications for breakup and freeze-up ice jams and the flooding they cause.

The consolidation in Event 2 caused minor flooding, yet the wave that caused the consolidation was of small amplitude (~0.5 m). This is smaller than the waves which were thought to cause flooding and were investigated by De Coste et al. (2017). The discharges of these waves would result in an open-water amplitude of ~1.1 m at km 1095.3. The steepness of the wave may be a reason why this wave had the effect it did, was because of the steepness of the wave. For example, Figure 4.10 shows how the water level slope measured across different reaches along the ice jam changed with the passing of the consolidation wave. As the wave front passed an observation station the water surface slope increased, an effect that was most pronounced at the toe of the jam (Reach H, km 1110.4 to km 1111.4, Figure 4.10b). The slope increased most at the toe because of the amplification of the wave in this area of the ice jam (see Figure 4.4). The increased water surface slope served to increase the velocity and to weaken the ice accumulation by lifting and separating it. Further, all the ice movement during Event 2 was in the East Channel (Figure 4.3). Therefore, the majority of the force from the momentum of the ice accumulation upstream of the main channel junction was exerted on the ice jam in the East Channel. If both channels had moved, the momentum would have been partitioned between the two channels. This may have resulted in a thinner ice jam in the East Channel and in less toe movement and flooding. These two mechanisms may explain how so small a wave was able to cause the flooding it did.

4.6 Summary and Conclusions

This study examined six events over three breakup seasons where ice movement occurred at the main delta junction of the Hay River at Hay River, NWT. Ice movements due to ice jam formation and consolidation, as well as the accompanying water level features, were tracked through the channels of the delta. This work qualitatively and quantitatively described how ice and water moved through the main delta junction and described the causes and underlying mechanisms of ice jam movement at dividing junctions.

During all six events, ice movements first occurred at the upstream end of the ice jam and the moving front moved downstream at the leading edge of a small-amplitude water wave. Ice stopping always occurred from downstream to upstream and was accompanied by a rejection wave. This behaviour resulted in ice movement that alternated between the East and West Channels. A conceptual model was presented that explained how the unsteady flow conditions and ice dynamics at the junction may have caused this alternating pattern. Therefore, the capability to simulate unsteady ice jam dynamics may be important for any numerical model used to simulate breakup processes in multi-channel delta environments. Finally, the consolidation of one observed ice jam may have resulted from a wave that originated from the melting and creeping consolidation of the ice jam itself.

4.7 Acknowledgements

This research was funded through grants from the Natural Sciences and Engineering Research Council of Canada; financial and logistical support was also provided by Indigenous and Northern Affairs Canada (INAC). All of this support is

gratefully acknowledged. The authors would also like to thank the Town of Hay River (THR) for their in-kind and logistical support of this study. Special thanks to Ross Potter (THR), as well as to Shawne Kokelj and Meg McCluskie (INAC) for their logistical and technical support in the field. The authors would also like to thank Janelle Banack, Michael Brayall, Stefan Emmer, Christopher Krath, Joshua Maxwell, David Watson, Nadia Kovachis Watson, and Liming Zhao for their assistance in the field.

4.8 References

Beltaos S. 2007. The role of waves in ice jam flooding of the Peace-Athabasca Delta. Hydrological Processes, 21(19):2548-59.

Beltaos S. 2017a . Frequency of ice jam flooding of the Peace-Athabasca delta. Canadian Journal of Civil Engineering, in press.

Beltaos, S. 2017b. Hydrodynamics of storage release during river ice breakup. Cold Regions Science and Technology, 139:36-50.

Beltaos, S., Carter, T., Rowsell, R., 2012. Measurements and analysis of ice breakup and jamming characteristics in the Mackenzie Delta, Canada. Cold Regions Science and Technology, 82:110-123.

Beltaos, S., Burrell, B.C. 2005. Field measurements of ice-jam-release surges. Canadian Journal of Civil Engineering, 32(4):699-711.

Blackburn, J., She, Y., Hicks, F., Nafziger, J. 2015. Ice effects on flow distributions in the Mackenzie Delta. CGU HS Committee on River Ice Processes and the

Environment 18th Workshop on the Hydraulics of Ice Covered Rivers. Quebec City, Canada. August 18-20

Brayall, M., Hicks, F.E. 2012. Applicability of 2-D modeling for forecasting ice jam flood levels in the Hay River Delta, Canada. Canadian Journal of Civil Engineering, 39(6):701-12.

De Coste, M., She, Y., Blackburn, J. 2017. Incorporating the effects of upstream ice jam releases in the prediction of flood levels in the Hay River delta, Canada. Canadian Journal of Civil Engineering, 44(8):643-51.

Emmerton, C.A., Lesack, L.F.W., Marsh, P. 2007. Lake abundance, potential water storage, and habitat distribution in the Mackenzie River Delta, western Canadian Arctic. Water Resources Research, 43.

Ettema, R., Muste, M. 2001. Laboratory observations of ice jams in channel confluences. Journal of Cold Regions Engineering, 15(1):34-58.

Healy, D., Hicks, F.E. 2006. Experimental study of ice jam formation dynamics. Journal of Cold Regions Engineering, 20(4):117-39.

Henderson, F. 1966. Open Channel Flow. Macmillan Publishing Co., Inc., New York.

Jasek, M. 1995. Ice jam simulations in rivers with islands. CGU HS Committee on River Ice Processes and the Environment 8th Workshop on the Hydraulics of Ice Covered Rivers. Kamloops, Canada.

Kolerski, T., Shen, H.T. 2015. Possible effects of the 1984 St. Clair River ice jam on bed

changes. Canadian Journal of Civil Engineering, 42(9):696-703.

Kovachis, N. 2011. Patterns of river breakup timing and sequencing, Hay River, NWT. Master's Thesis. University of Alberta, Edmonton, Canada.

McDowell, G.R. Micromechanics of creep of granular materials. Géotechnique, 53(10):915-6.

Nafziger J., She, Y., Hicks, F. 2016. Celerities of waves and ice runs from ice jam releases. Cold Regions Science and Technology, 123:71-80.

Oveisy, A., She, Y. 2017. Modelling Ice Jam Formation in the Hay River Delta during 2009 Breakup. CGU HS Committee on River Ice Processes and the Environment 19th Workshop on the Hydraulics of Ice Covered Rivers. Whitehorse, Canada. July 9-12.

Stanley, S.J., Gerard, R. 1992. Ice jam flood forecasting: Hay River, NWT. Canadian Journal of Civil Engineering, 19(2):212-23.

She, Y. Hicks, F., Steffler, P., Healy, D. 2008. Effects of unsteadiness and ice motion on river ice jam profiles. Proceedings of the 19th IAHR International Symposium on Ice. Vancouver, Canada. July 6-11.

Zhang, F., Mosaffa, M., Chu, T., Lindenschmidt, K.E. 2017. Using remote sensing data to parameterize ice jam modeling for a northern inland delta. Water, 9(5),306.

Zufelt, J.E. 1990. Experimental Observations of Shoving and Thickening: Comparison to Equilibrium Thickness Theory. 10th Proceedings of the 10th IAHR International

Symposium on Ice. Espoo, Finland.

Table 4.1. Observation locations and data intervals on the Hay River

Observation Location river station, landmark	**Water Level Measurements** year, observation interval (min)			**Ice Condition Observations** year, observation interval (min)		
	2010	2011	2013	2010	2011	2013
Main Channel						
km 1032.0 upstream of Alexandra Falls (THR)	5	5	5	5	15	15
km 1034.3 at Alexandra Falls	-	-	-	-	5	1
km 1036.6 at Louise Falls	-	-	-	-	5	-
km 1048.2 at Town of Enterprise	-	-	-	-	-	5
km 1067.5 at Paradise Road (THR)	1	1	-	5	15	15
km 1095.3 at WSC gauge #07B001	15	15	15	15	-	5
km 1098.1 at Pine Point Bridge (THR)	1	1	-	15	15	15
km 1103.3 at Chamber of Commerce Park	1	2	1	5	-	5
km 1106.1 downtown near courthouse	-	1	1	5	5	5
km 1107.3 at Riverview Drive	-	-	-	-	-	60
km 1108.0 at the channel junction	1	1	1	5	-	1

"THR" denotes stations operated by the Town of Hay River

Table 4.1 is continued on the next page.

Table 4.1. *continued.* Observation locations and data intervals on the Hay River

Observation Location river station, landmark	**Water Level Measurements** year, observation interval (min)			**Ice Condition Observations** year, observation interval (min)		
	2010	2011	2013	2010	2011	2013
East Channel						
km 1108.6 at Riverside Cemetary	1	2	1	-	-	5
km 1109.4 near road to airport	-	2	1	-	-	60
km 1110.1 to 1110.4 south of NTCL yard *	1	-	-	-	-	5
km 1111.4 at NTCL yard	1	1	-	5	5	5
km 1112.4 at public dock	-	-	-	5	-	-
km 1112.9 at float plane dock	-	-	1	-	-	5
km 1113.6 at ice road	-	2	1	-	-	-
West Channel						
km 1108.5 at West Channel bridge	-	-	1	5	-	5
km 1110.2 to 1110.4 at air beacon *	1	1	1	-	-	5
km 1111.8 at north end of runway	1	-	-	-	-	60
km 1112.0 near end of channel	-	2	1	-	-	60

* range in station is due to slightly different instrument placement in different years

Table 4.2 Celerities of observed water level features in the Hay River Delta.

Event	Feature Tracked	Channel	Travel Direction	Ice Move?	Q_c, m^3/s	Ice Condition	X_1, km	X_2, km	$C_{feat.}$, m/s (error range)	$C_{diff.}$ m/s	$C_{dyn.}$ m/s	$C_{feat.} \div C_{dyn.}$	Gr.
1	stopping front WL peak	West	up	-	74	ice jam	1112.0	1110.2	1.6	-	-	-	-
	stopping front WL peak	East	up	-	296	ice jam	1110.1	1108.6	5.0	-	-	-	-
	stopping front WL peak	Main	up	-	370	ice jam	1108.0	1103.3	4.6 (3.6-6.5)	-	-	-	-

Q_c is the carrier discharge in the measured channel

"up" and "down" refer to upstream and downstream travel directions, respectively

X_1 and X_2 are the river stations at the endpoints of the reach over which the discharge was measured

$C_{feat.}$ is the celerity of the WL feature

$C_{diff.}$ is the celerity of the theoretical diffusive wave

$C_{dyn.}$ is the celerity of the theoretical dynamic wave

Gr. is the group referred to in the text.

Table 4.2 is continued on the following pages.

Table 4.2 *continued.* Celerities of observed water level features in the Hay River Delta.

Event	Feature Tracked	Channel	Travel Direction	Ice Move?	Q_c, m^3/s	Ice Condition	X_1, km	X_2, km	$C_{feat.}$, m/s (error range)	$C_{diff.}$ m/s	$C_{dyn.}$ m/s	$C_{feat.} \div C_{dyn.}$	Gr.
2	leading edge of consolidation wave	Main	down	Y	425	ice jam	1098.1	1103.3	5.1 (4.8-5.4)	2.1	6.5	0.8	A
	leading edge of consolidation wave	Main	down	Y	425	ice jam	1103.3	1108.0	7.5 (6.5-8.7)	1.9	5.8	1.3	A
	leading edge of consolidation wave	East	down	Y	340	ice jam, toe	1108.6	1110.1	3.6 (3.1-4.2)	1.0	6.3	0.6	A
	leading edge of escaped wave	West	down	N	85	ice jam	1108.0	1110.2	4.7 (4.2-5.4)	0.6	6.1	0.8	B
	leading edge of escaped wave	West	down	N	85	ice jam	1110.2	1112.0	4.0	0.6	6.1	0.7	B

Table 4.2 is continued on the following pages.

Table 4.2 *continued.* Celerities of observed water level features in the Hay River Delta.

Event	Feature Tracked	Channel	Travel Direction	Ice Move?	Q_c, m^3/s	Ice Condition	X_1, km	X_2, km	$C_{feat.}$, m/s (error range)	$C_{diff.}$ m/s	$C_{dyn.}$ m/s	$C_{feat.} \div C_{dyn.}$	Gr.
2	stopping front WL peak	East	up	-	340	ice jam	1111.4	1110.1	3.4 (3.1-3.6)	-	-	-	-
	stopping front WL peak	East	up	-	340	ice jam	1110.1	1108.6	1.2	-	-	-	-
	stopping front WL peak	Main	up	-	425	ice jam	1108.0	1103.3	1.3 (1.2-1.4)	-	-	-	-
	stopping front WL peak	Main	up	-	425	ice jam, open water	1103.3	1098.1	0.8 (0.7-1.0)	-	-	-	-
	leading edge of rejection wave	East	up	-	340	moving ice jam	1111.4	1110.1	4.4 (3.6-5.5)	-	-	-	-
	leading edge of rejection wave	East	up	-	340	moving ice jam	1110.1	1108.6	2.3 (2.1-2.5)	-	-	-	-
	leading edge of rejection wave	Main	up	-	425	moving ice jam	1108.0	1103.3	4.2 (4.1-4.4)	-	-	-	-

Table 4.2 is continued on the following pages.

Table 4.2 *continued.* Celerities of observed water level features in the Hay River Delta.

Event	Feature Tracked	Channel	Travel Direction	Ice Move?	Q_c, m^3/s	Ice Condition	X_1, km	X_2, km	$C_{feat.}$, m/s (error range)	$C_{diff.}$ m/s	$C_{dyn.}$ m/s	$C_{feat.} \div C_{dyn.}$	Gr.
2	leading edge of rejection wave	Main	up	-	425	moving ice jam	1103.3	1098.1	1.8 (1.5-2.2)	-	-	-	-
	front of peak of instigated wave	West	down	N	85	ice jam	1108.0	1110.2	1.1 (1.0-1.2)	0.6	6.1	0.2	D
	back of peak of instigated wave	West	down	N	85	ice jam	1108.0	1110.2	0.6	0.6	6.1	0.1	D
	front of peak of instigated wave	West	down	N	85	ice jam	1110.2	1112.0	1.1	0.6	6.1	0.2	D
	back of peak of instigated wave	West	down	N	85	ice jam	1110.2	1112.0	0.7	0.6	6.1	0.1	D
	leading edge of instigated wave	West	down	N	85	ice jam	1108.0	1110.2	2.4 (1.8-3.4)	0.6	6.1	0.4	F
	leading edge of instigated wave	West	down	N	85	ice jam	1110.2	1112.0	1.3 (1.0-1.8)	0.6	6.1	0.2	F

Table 4.2 is continued on the following pages.

Table 4.2 *continued.* Celerities of observed water level features in the Hay River Delta.

Event	Feature Tracked	Channel	Travel Direction	Ice Move?	Q_c, m^3/s	Ice Condition	X_1, km	X_2, km	$C_{feat.}$, m/s (error range)	$C_{diff.}$ m/s	$C_{dyn.}$ m/s	$C_{feat.} \div C_{dyn.}$	Gr.
3	leading edge of consolidation wave	Main	down	Y	280	deteriorated ice	1095.3	1098.1	3.4 (2.2-7.7)	1.7	6.0	0.6	A
	leading edge of consolidation wave	Main	down	Y	280	intact/ deteriorated ice	1098.1	1103.3	7.2	1.8	5.7	1.3	A
	leading edge of consolidation wave	Main	down	Y	280	intact/ deteriorated ice	1103.3	1106.1	6.5	1.6	5.2	1.3	A
	leading edge of consolidation wave	Main	down	Y	280	intact/ deteriorated ice	1106.1	1108.0	7.2 (5.4-10.8)	1.5	4.8	1.5	A

Table 4.2 is continued on the following pages.

Table 4.2 *continued.* Celerities of observed water level features in the Hay River Delta.

Event	Feature Tracked	Channel	Travel Direction	Ice Move?	Q_c, m^3/s	Ice Condition	X_1, km	X_2, km	$C_{feat.}$, m/s (error range)	$C_{diff.}$ m/s	$C_{dyn.}$ m/s	$C_{feat.} \div C_{dyn.}$	Gr.
3	leading edge of consolidation wave	West	down	Y	56	intact/ deteriorated ice	1108.0	1110.3	4.7 (3.8-6.3)	0.5	5.4	0.9	A
	leading edge of consolidation wave	West	down	Y	56	intact/ deteriorated ice	1110.3	1111.8	3.9 (3.2-5.1)	0.5	5.4	0.7	A
	leading edge of escaped wave	East	down	N	224	ice jam	1110.3	1111.4	2.6 (1.7-6.1)	0.3	6.5	0.4	C
	leading edge of escaped wave	East	down	N	224	intact ice	1111.4	1113.6	5.2 (4.6-6.1)	0.4	6.8	0.8	C
	stopping front WL peak	West	up	-	56	ice jam	1111.8	1110.3	2.1	-	-	-	-
	stopping front WL peak	West	up	-	56	ice jam	1110.3	1108.0	7.6	-	-	-	-

Table 4.2 is continued on the following pages.

Table 4.2 *continued.* Celerities of observed water level features in the Hay River Delta.

Event	Feature Tracked	Channel	Travel Direction	Ice Move?	Q_c, m^3/s	Ice Condition	X_1, km	X_2, km	$C_{feat.}$, m/s (error range)	$C_{diff.}$ m/s	$C_{dyn.}$ m/s	$C_{feat.} \div C_{dyn.}$	Gr.
3	stopping front WL peak	Main	up	-	280	ice jam	1108.0	1106.1	8.1	-	-	-	-
	stopping front WL peak	Main	up	-	280	ice jam, open water	1106.1	1103.3	5.7	-	-	-	-
4	stopping front WL peak	West	up	-	15	ice jam	1110.4	1108.5	3.9 (3.4-4.4)	-	-	-	-
	leading edge of escaped wave	East	down	N	60	ice jam	1108.6	1109.4	4.0	0.3	4.7	0.9	C
	stopping front WL peak	Main	up	-	75	ice jam	1108.0	1106.1	3.4	-	-	-	-
	stopping front WL peak	Main	up	-	75	ice jam, open water	1106.1	1103.3	4.4	-	-	-	-

Table 4.2 is continued on the following pages.

Table 4.2 *continued.* Celerities of observed water level features in the Hay River Delta.

Event	Feature Tracked	Channel	Travel Direction	Ice Move?	Q_c, m^3/s	Ice Condition	X_1, km	X_2, km	$C_{feat.}$, m/s (error range)	$C_{diff.}$ m/s	$C_{dyn.}$ m/s	$C_{feat.} \div C_{dyn.}$	Gr.
5	stopping front WL peak	Main	up	-	75	ice jam, open water	1108.0	1106.1	5.4 (4.9-5.8)	-	-	-	-
	stopping front WL peak	Main	up	-	75	open water	1106.1	1103.3	4.6 (4.0-5.4)	-	-	-	-
	leading edge of consolidation wave	West	down	Y	15	ice jam	1108.5	1110.4	4.1 (3.6-4.7)	0.2	4.7	0.9	A
	leading edge of escaped wave	West	down	N	15	ice jam	1110.4	1111.9	2.2 (2.1-2.3)	0.2	4.7	0.5	C
	leading edge of escaped wave	East	down	N	60	ice jam, intact ice	1108.6	1109.4	4.7	0.3	4.7	1.0	C

Table 4.2 is continued on the following page.

Table 4.2 *continued.* Celerities of observed water level features in the Hay River Delta.

Event	Feature Tracked	Channel	Travel Direction	Ice Move?	Q_c, m^3/s	Ice Condition	X_1, km	X_2, km	$C_{feat.}$, m/s (error range)	$C_{diff.}$ m/s	$C_{dyn.}$ m/s	$C_{feat.} \div C_{dyn.}$	Gr.
6	leading edge of consolidation wave	West	down	Y	15	ice jam	1108.5	1110.4	2.8 (2.7-2.9)	0.2	4.7	0.6	A
	leading edge of instigated wave	East	down	Y	60	ice jam	1108.6	1109.4	4.0	0.3	4.7	0.9	E
	leading edge of escaped wave	East	down	N	60	ice jam, intact ice	1109.4	1112.9	4.0	0.1	6.0	0.7	E
	leading edge of escaped wave	East	down	N	60	intact ice	1112.9	1113.6	6.0	0.1	6.3	1.0	C
	peak of escaped wave	East	down	N	60	intact ice	1112.9	1113.6	4.0	0.1	6.3	0.6	D
	stopping front WL peak	East	up	-	60	ice jam	1109.4	1108.6	4.0	-	-	-	-
	stopping front WL peak	Main	up	-	75	ice jam, open water	1108.0	1106.1	5.8	-	-	-	-
	stopping front WL peak	Main	up	-	75	open water	1106.1	1103.3	3.8	-	-	-	-

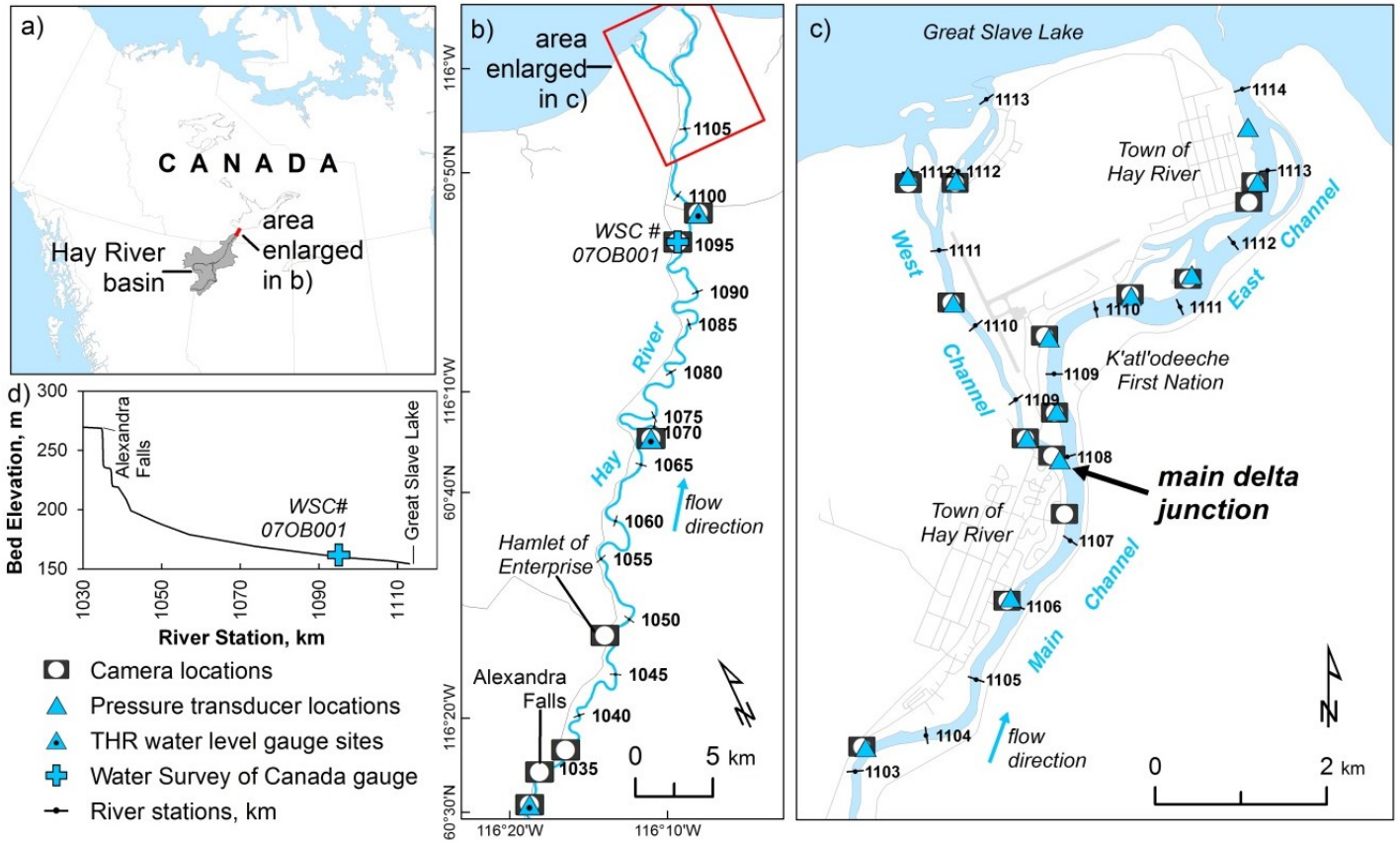

Figure 4.1. Study location in a) the Hay River basin, including observation sites located b) upstream of the Hay River delta and c) in the Hay River delta; and d) bed profile of the study reach. THR = Town of Hay River

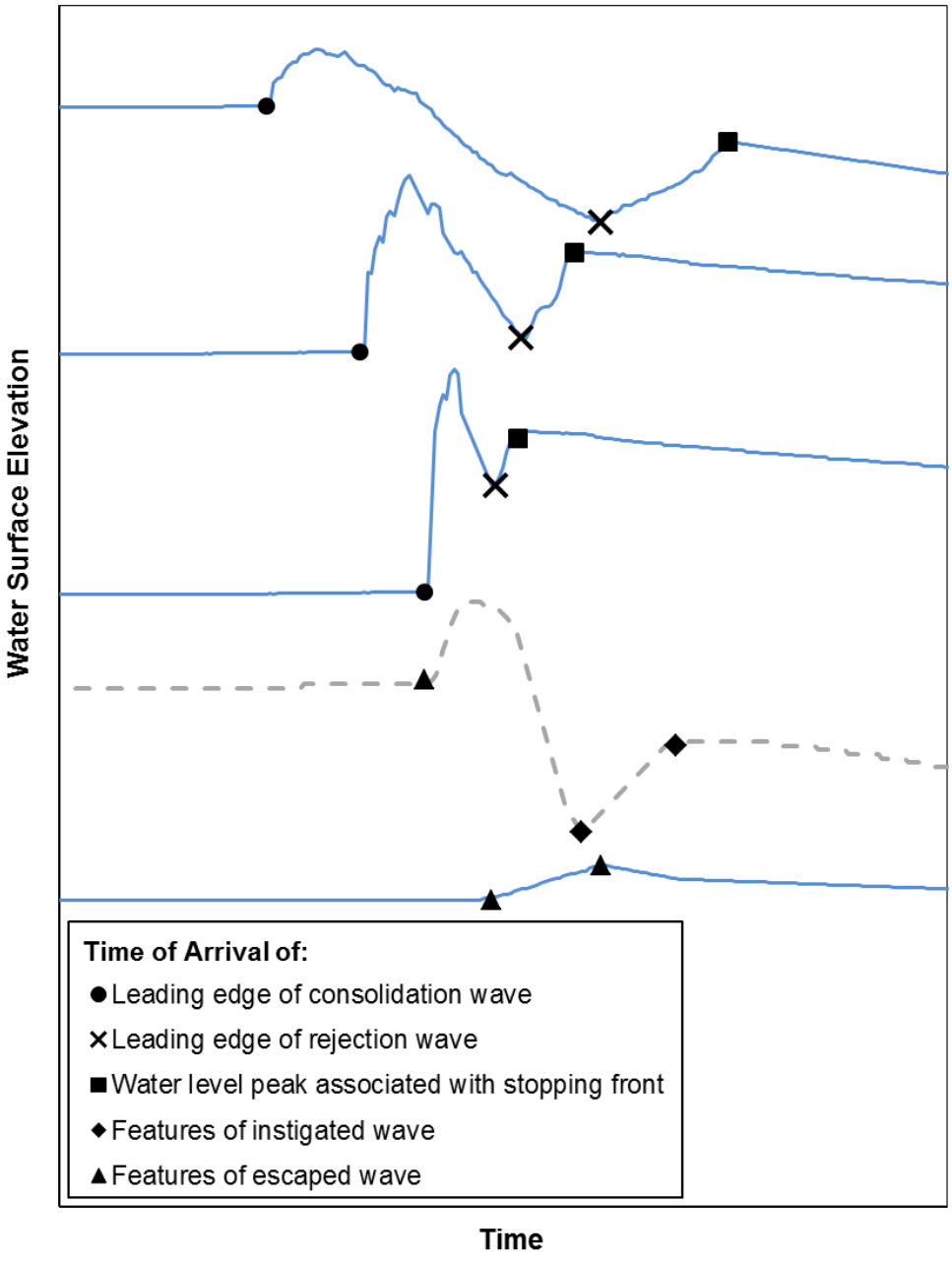

Figure 4.2. Definition of tracked features for all events, each line represents the observed water level at several different observation stations. The grey, dotted line represents water level observations in the opposite delta channel from where the initial consolidations took place.

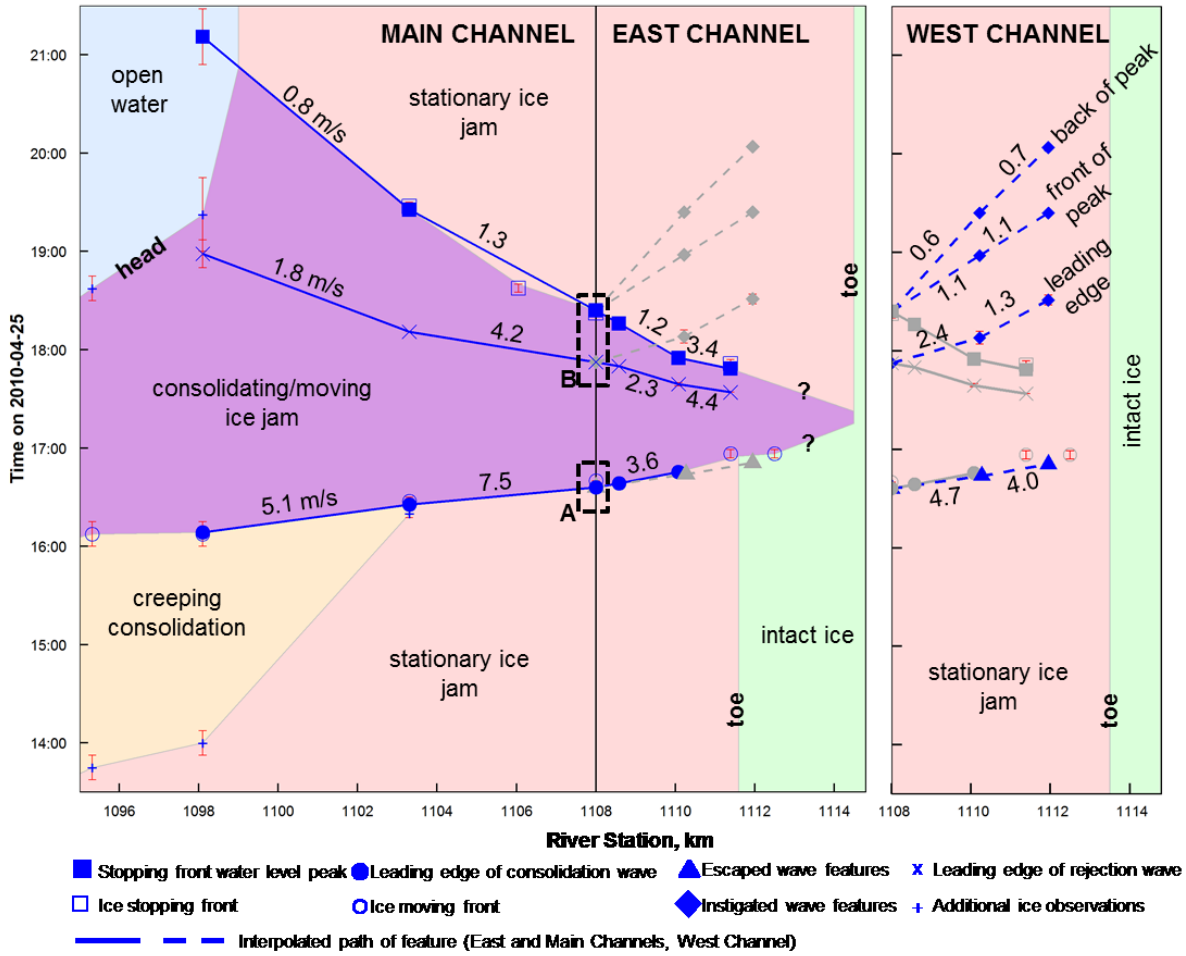

Figure 4.3. Water level and ice features tracked through time and space during ice jam consolidation Event 2. Left panel shows ice conditions and feature celerities in the Main and East Channels, right panel shows the same in the West Channel. Grey lines show water level features tracked in the opposite delta channel.

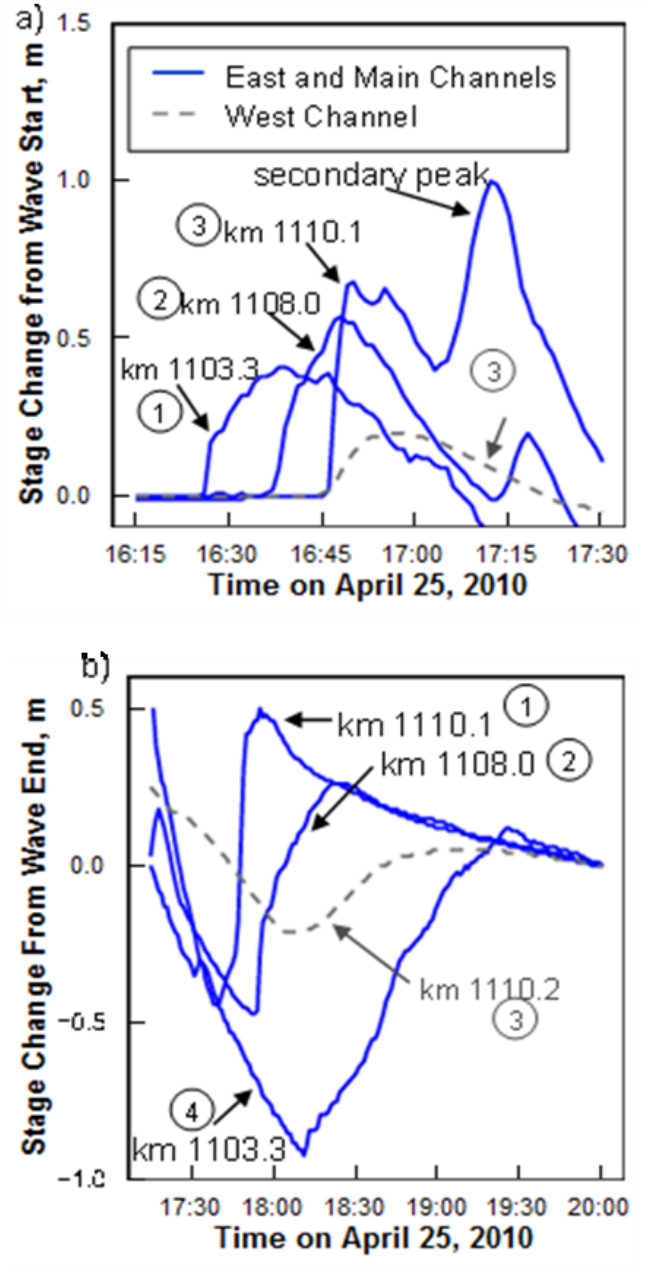

Figure 4.4. Propagation of a) the consolidation wave in the East and Main Channels and associated escaped waves in the West Channel; and b) the rejection wave in East and Main Channels and associated instigated wave in West Channel during ice jam consolidation Event 2. The circled numbers indicated the order of propagation of the waves.

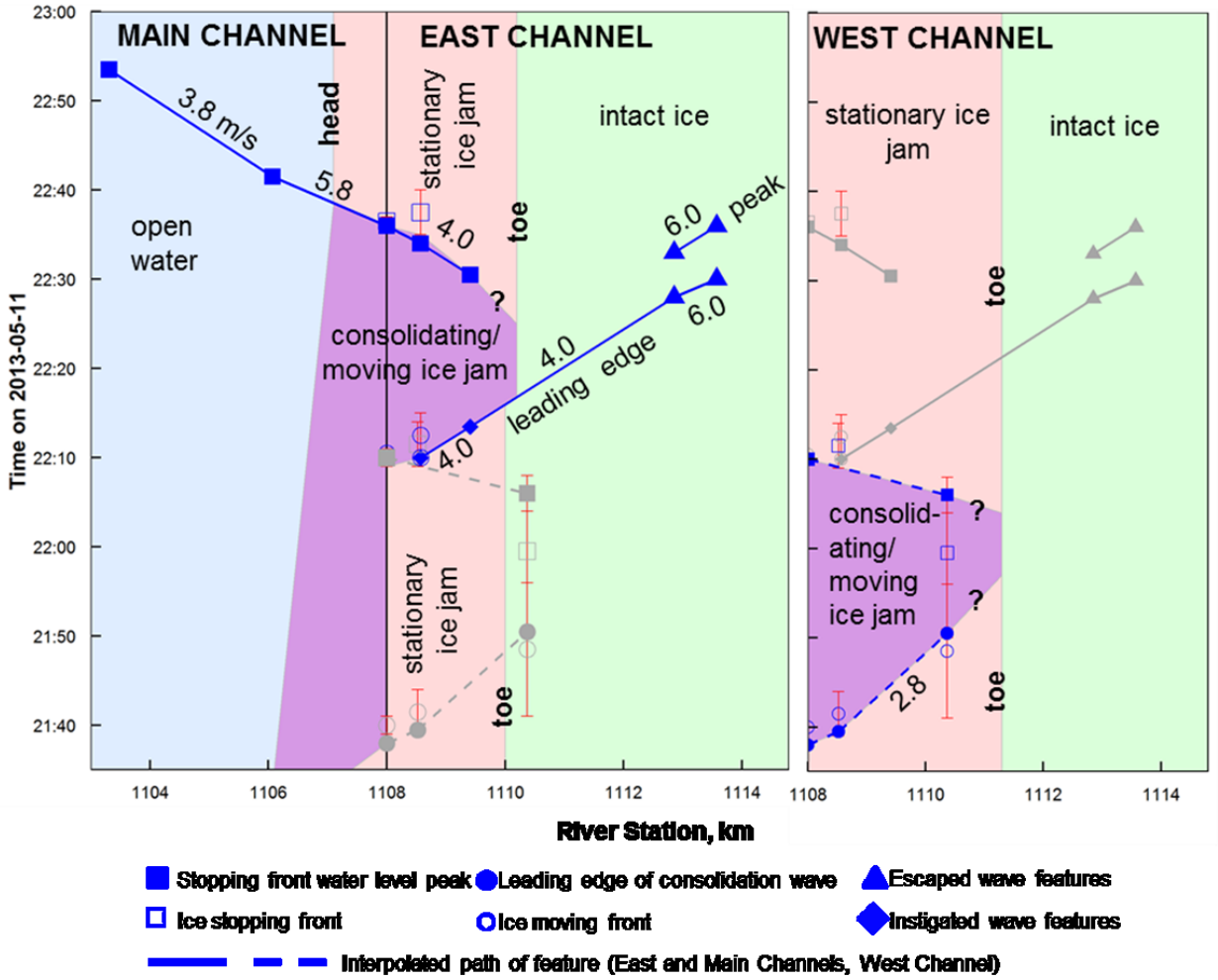

Figure 4.5. Water level and ice features tracked through time and space during ice jam consolidation Event 6. Left panel shows ice conditions and feature celerities in the Main and East Channels, right panel shows the same in the West Channel. Grey lines show water level features tracked in the opposite delta channel.

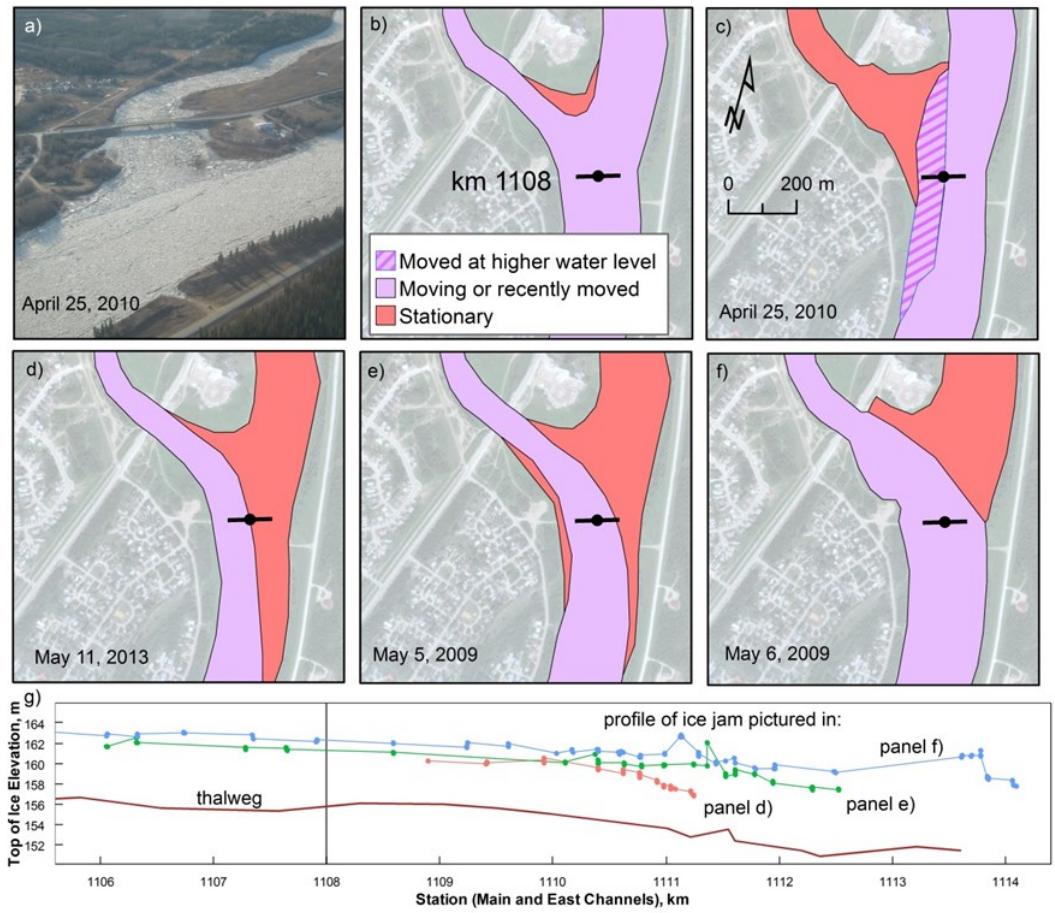

Figure 4.6. Ice jam geometry at the main delta junction a) as seen from the air, b) during ice run before ice jam formation, c) typical ice movement geometry during ice movement in the East Channel, d) to f) different ice jam geometry during ice movement in the West Channel for different ice levels in the East Channel as shown in g).

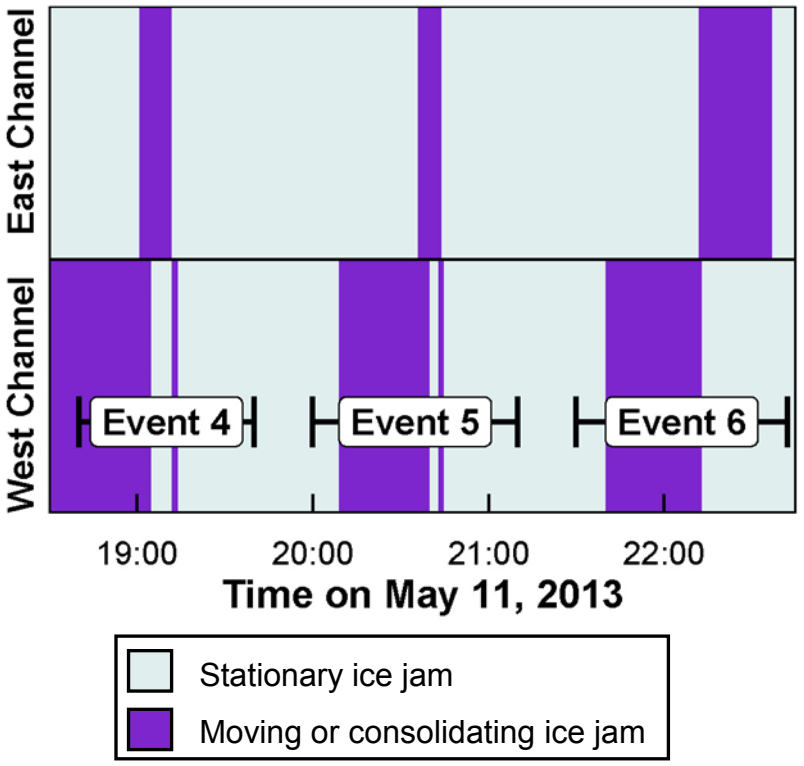

Figure 4.7. Ice moments alternating between the East and West Channels at the main delta junction during ice jam consolidation Events 4, 5, and 6.

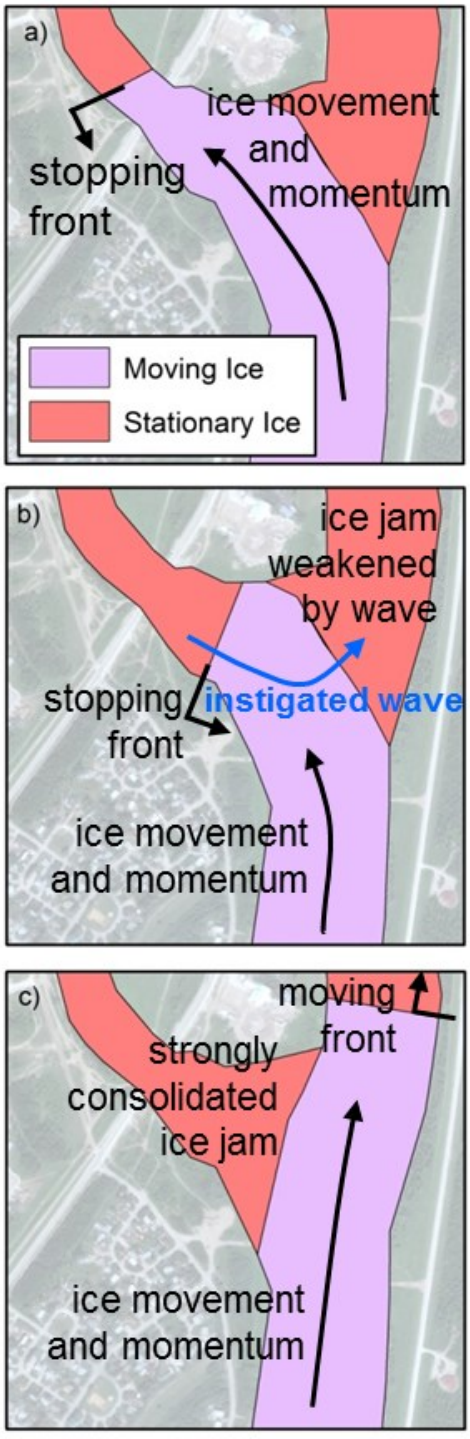

Figure 4.8. Conceptual ice jam processes at a dividing junction during ice jam stopping.

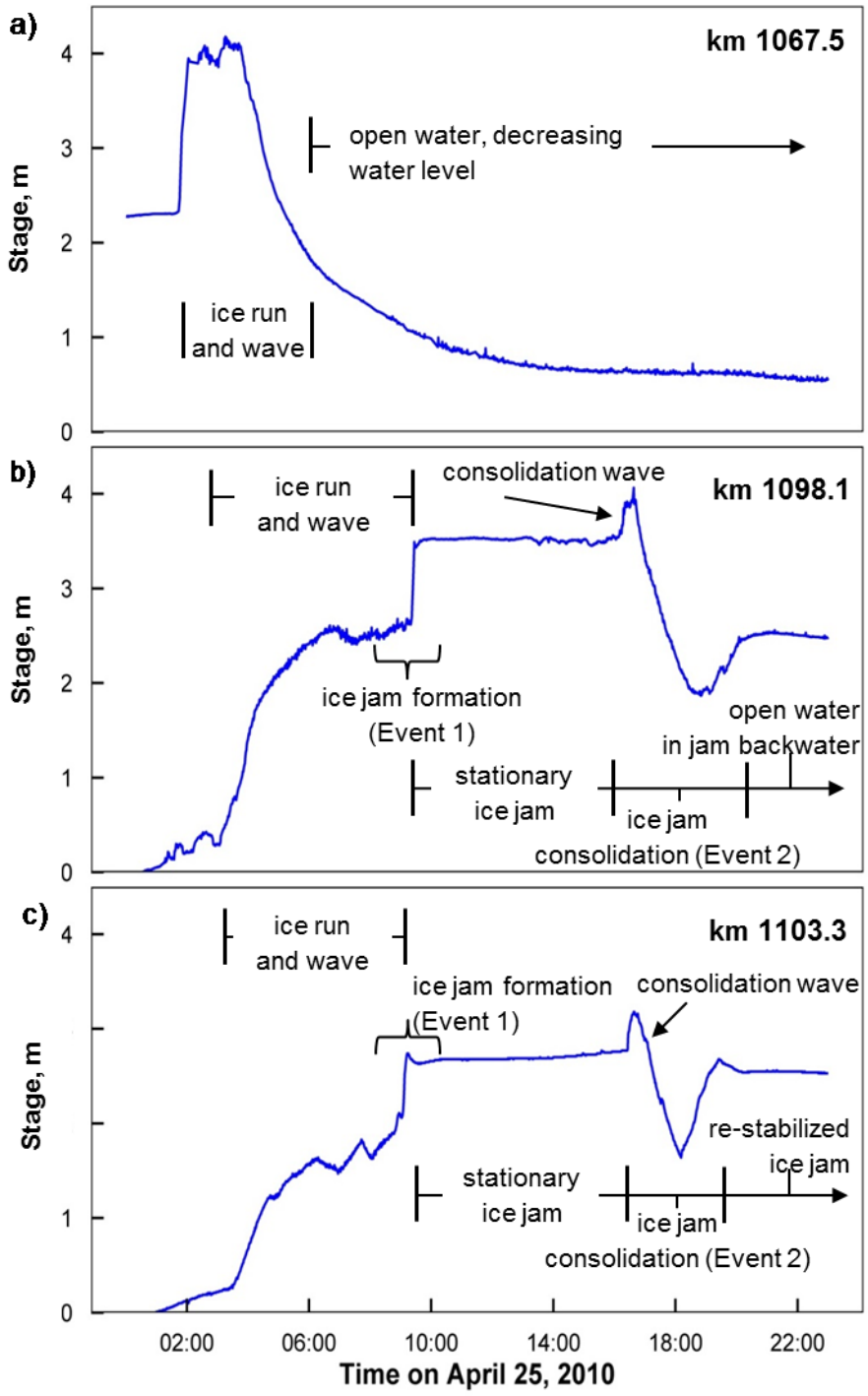

Figure 4.9. Water levels and ice conditions during the jam consolidation Event 2, at various observation stations, showing no upstream source for consolidation wave.

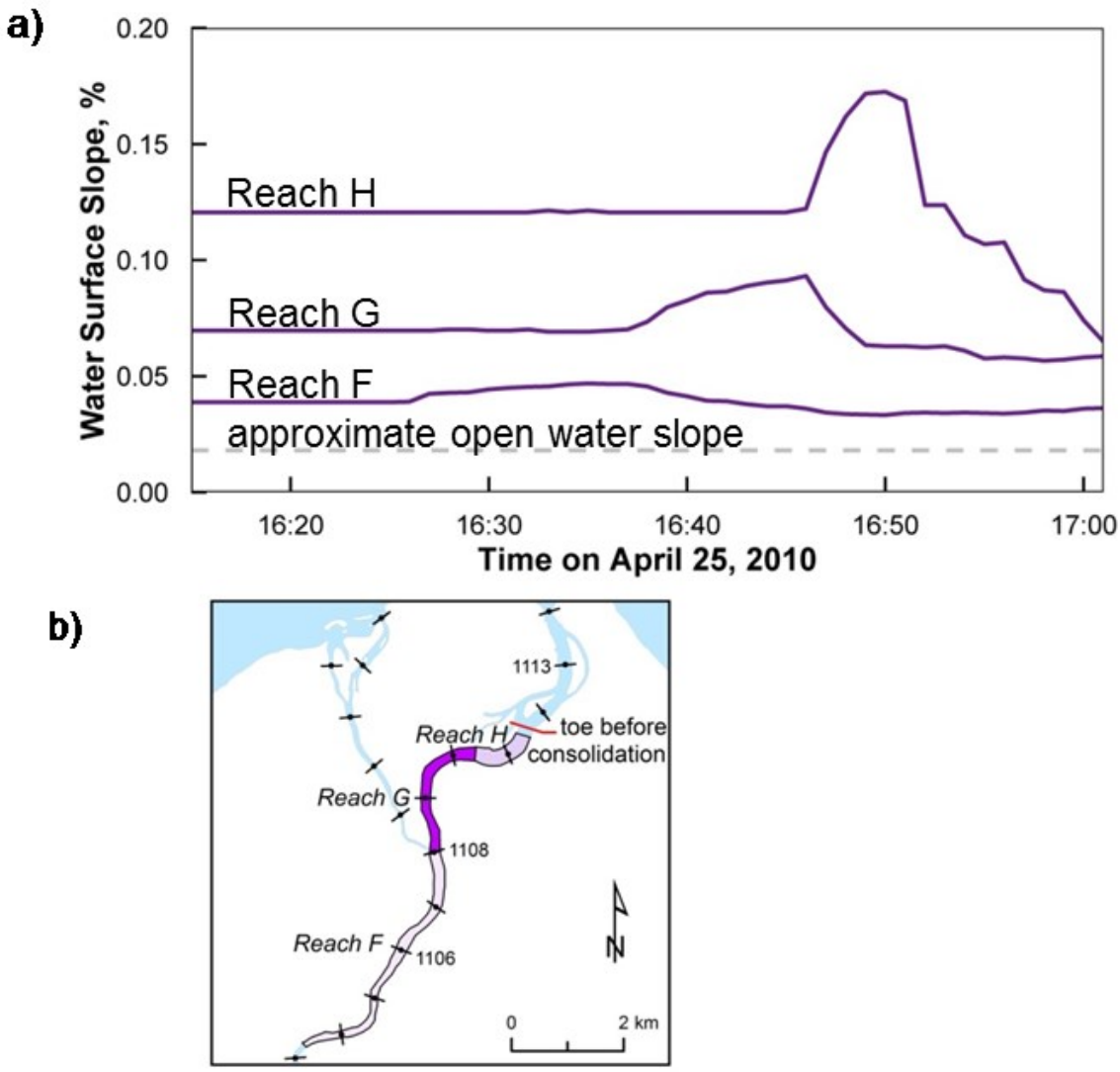

Figure 4.10. a) Variation in water surface slope over three reaches during ice jam consolidation Event 2. The reaches over which the slopes were measured are shown in b).

Chapter 5. Conclusions and Recommendations

5.1 General Conclusions

This research project improved our understanding of unsteady river ice processes using full-scale field experiments in situations where a dearth of detailed observations has hampered scientific progress. This dearth of data existed because these processes are short-lived and therefore logistically challenging to measure. However, understanding these processes is important in order to develop conceptual models of these processes and the predictive numerical models that are based on them. In this thesis, three different unsteady river ice processes were investigated, including:

1) anchor ice processes in small headwater streams (Chapter 2),
2) ice jam release processes in single-channel river reaches (Chapter 3), and
3) ice jam evolution processes in multi-channel river systems (Chapter 4).

In each case, these processes were observed over multiple years and multiple examples of each were analyzed. As a result, this thesis presents a more complete picture of each process than had previously existed in the published record and provides several original contributions, which are summarized in the following subsections.

5.1.1 Anchor Ice Processes

In Chapter 2 of this thesis, a large number of anchor ice formation and release events (161 events) were observed and analyzed. This work confirms that for these streams, thermal processes are an important control on anchor ice release. It was demonstrated

that a linear heat transfer approach was useful for predicting anchor ice release in 93 % to 98 % of cases, depending on the method used. This approach is particularly important because it used easily-measured (and often publicly-available) meteorological data. This chapter contains the first-ever assessment of the effect that hydropower flow regulation has on the anchor ice regime of small streams. A conceptual model of the anchor ice and surface regime in these environments was presented. Finally, this chapter presents several fundamental observations of anchor ice, such as: ice accumulation morphology, event duration, effect on water level, modes of incorporation into seasonal ice cover, modes of release, and growth rates. Taken together, this chapter represents one of the most complete pictures of anchor ice processes ever compiled.

5.1.2 Ice Jam Release Waves and Ice Runs

Chapter 3 of this thesis presents detailed analyses of the water waves and ice runs that originate from ice jam releases. It presents the first-ever series of simultaneous water wave and ice run observations and demonstrated how these two phases separated as they advanced downstream. Prior research had assumed that the peak water level and the peak ice concentration tended to travel together; this research shows that this is not necessarily the case. In fact, the ice run may travel entirely in front of, entirely behind, or travel with the peak water level. These observations were taken over a channel length much longer than can be practically accommodated by laboratory physical models and therefore provide important validation data for predictive numerical models. Water waves are invisible to aerial observers, and this research shows that they should not be assumed to be coincident with the ice runs that can be easily observed from aircraft. This has implications for breakup flood forecasters, because both phases of ice jam releases are

important when predicting ice jam floods in real time.

5.1.3 Ice Jam Processes in Multi-Channel Environments

Chapter 4 of this thesis presents detailed observations and analysis of unsteady ice and water movements in a simple multi-channel network. Prior to this thesis, no such observations existed in the river ice literature. This work qualitatively and quantitatively described how ice and water moved through the main delta junction and revealed the causes and underlying mechanisms of ice jam movement at dividing junctions. Rejection waves were documented, as were waves that were instigated by ice movements in the opposite delta channel. The resulting pattern of alternating channel ice movements had been observed in the Hay River delta in the past but remained unexplained until this research. These observations allowed for the development of a new conceptual model that shows how the momentum of the ice cover and the unsteady flow conditions are particularly important in multichannel environments. This new understanding of ice jams in multi-channel environments is directly applicable to the flood watch operations of the Town of Hay River and for the testing and development of numerical models of these processes.

In addition, Chapter 4 presents a new possible mode of release of ice jams. Historically, ice jams were thought to release under the influence of waves originating from upstream of the ice jam, and weakened the ice cover and/or dislodged downstream geometric constraints. In Chapter 4, the water wave that caused the release of one ice jam may have originated from within the ice jam itself caused by the water released from storage by melting and creeping consolidation.

5.2 Recommendations for Future Research

There are several avenues of future work that would continue to expand our knowledge of the fundamental river ice processes presented in this thesis. Some of these are presented in the following subsections.

5.2.1 Anchor Ice

This research focused on anchor ice at locations where anchor ice was expected or known to occur. Future research should continue to parse out why anchor ice accumulates at some locations and not at others. Parameters such as turbulent intensity, vertical and horizontal velocity, and bed shear stress, may be important variables to measure or calculate.

This research was successful at applying a general, linear heat transfer approach for predicting anchor ice release. This approach may be further refined by investigating other effects that thermal processes have on the ice-pebble bond. First, how hyporheic flow (e.g. under-gravel flow) and anchor ice processes affect each other should be investigated. Second, how heat from shortwave radiation is absorbed or conducted by the substrate and how that affects ice adherence should be investigated.

The next step in anchor ice research should be to test existing numerical formulations of anchor ice growth and release using these observed events to determine how well they can be simulated. This will provide insight on how these models should be modified or improved.

5.2.2 Ice Jam Release Waves and Ice Runs

This research was successful in determining how water waves and ice runs propagate from an ice jam release. In Chapter 3, the propagation celerity of the ice run was hypothesized to be affected by friction from the banks and by slowing water velocities in the accompanying water wave. Future research should aim to separate the effects of these two processes. The water surface velocity and the vertical velocity distribution in ice jam release waves and how they are affected by the presence of ice has not been well documented. Yet, the water surface velocity has an important impact on ice transport. A physical laboratory model could be used to investigate this for distances close to an ice jam release, but field-based analogues may be necessary to capture velocities in waves that have attenuated over long distances.

5.2.3 Ice Jam Processes in Multi-Channel Environments

The research in Chapter 4 was successful in developing new conceptual models for how ice and water move in multi-channel systems. The next step in this research should be to test existing numerical models of ice jam dynamics to see whether they can simulate the processes that were observed in this study. This would provide insight on how these models need to be modified or improved.

Chapter 4 presents a new mode of ice jam release, whereby a wave was generated from within the ice jam. Existing ice dynamic models should be employed to determine whether such a wave can be simulated. This may be done by removing ice volume from the model and adding it to the water volume. This highlights the need for developing and testing numerical models that can accurately simulate ice melt processes.

References

Andrishak, R. and Hicks, F. 2008. Simulating the effects of climate change on the ice regime of the Peace River. Canadian Journal of Civil Engineering, 35(5):461-472.

Ashton, G.D. (Ed.), 1986. River and Lake Ice Engineering. Water Resources Publications, Littleton, Co. USA.

Beltaos, S. 2003. Discussion of “Ice jam release surges, ice runs, and breaking fronts: field measurements, physical descriptions, and research needs". Canadian Journal of Civil Engineering, 30(5):949-950.

Beltaos, S. 2007. The role of waves in ice jam flooding of the Peace-Athabasca Delta. Hydrological Processes, 21(19):2548-59.

Beltaos, S. 2013. Hydrodynamic characteristics and effects of river waves caused by ice jam releases. Cold Regions Science and Technology, 85:42-55.

Beltaos, S. 2014. Hydrodynamic properties of ice-jam release waves in the Mackenzie Delta, Canada. Cold Regions Science and Technology, 103: 91-106.

Beltaos, S. 2017a. Hydrodynamics of storage release during river ice breakup. Cold Regions Science and Technology, 139:36-50.

Beltaos, S. 2017b . Frequency of ice jam flooding of the Peace-Athabasca delta. Canadian Journal of Civil Engineering, in press.

Beltaos, S., Burrell, B. Ismail, S. 1994. Ice and sedimentation processes in the Saint John River, Canada. Proceedings of the 12th IAHR Symposium on Ice, Trondheim, Norway, pp. 11-21.

Beltaos, S., Burrell, B.C. 2005. Field measurements of ice-jam-release surges. Canadian Journal of Civil Engineering, 32(4):699-711.

Beltaos, S., Carter, T., Rowsell, R., 2012. Measurements and analysis of ice breakup and jamming characteristics in the Mackenzie Delta, Canada. Cold Regions Science and Technology, 82:110-123.

Bisaillon, J.F. Bergeron, N.E. 2009. Modeling anchor ice presence–absence in gravel bed rivers. Cold Regions Science and Technology, 55(2):195-201.

Blackburn, J., Hicks, F. 2003. Suitability of dynamic modeling for flood forecasting during ice jam release surge events. ASCE Journal of Cold Regions Engineering, 17(1): 18-36.

Blackburn, J., She, Y., Hicks, F., Nafziger, J. 2015. Ice effects on flow distributions in the Mackenzie Delta. CGU HS Committee on River Ice Processes and the Environment 18th Workshop on the Hydraulics of Ice Covered Rivers. Quebec City, Canada. August 18-20

Brayall, M., Hicks, F.E. 2012. Applicability of 2-D modeling for forecasting ice jam flood levels in the Hay River Delta, Canada. Canadian Journal of Civil Engineering, 39(6):701-12.

Brown, R.S. 1999. Fall and early winter movements of cutthroat trout, Oncorhynchus clarki, in relation to water temperature and ice conditions in Dutch Creek, Alberta. Environmental Biology of Fishes, 55(4):359-368.

De Coste, M., She, Y., Blackburn, J. 2017. Incorporating the effects of upstream ice jam releases in the prediction of flood levels in the Hay River delta, Canada. Canadian Journal of Civil Engineering, 44(8):643-51.

Doering, J.C., 2002. Closure to "Laboratory study of anchor ice growth" by JC Doering, LE Bekeris, MP Morris, KE Dow, and WC Girling. ASCE Journal of Cold Regions Engineering, 16(2):99-100.

Doering, J.C., Bekeris, L.E., Morris, M.P., Dow, K.E. and Girling, W.C. 2001. Laboratory study of anchor ice growth. ASCE Journal of Cold Regions Engineering,15(1):60-66.

Dubé, M., Turcotte, B., Morse, B. 2015. Steep channel freezeup processes: understanding complexity with statistical and physical models. Canadian Journal of Civil Engineering, 42(9):622-633.

Emmerton, C.A., Lesack, L.F.W., Marsh, P. 2007. Lake abundance, potential water storage, and habitat distribution in the Mackenzie River Delta, western Canadian Arctic. Water Resources Research, 43.

Ettema, R., Muste, M. 2001. Laboratory observations of ice jams in channel confluences. ASCE Journal of Cold Regions Engineering, 15(1):34-58.

Ettema, R., Muste, M. and Kruger, A. 1999. Ice Jams in River Confluences. CRREL Report 99-6, US Army Corps of Engineers, New Hampshire, USA.

Gebre, S., Alfredsen, K., Lia, L., Stickler, M., Tesaker, E. 2013. Review of ice effects on hydropower systems. ASCE Journal of Cold Regions Engineering. 27(4):196-222.

Girling, W.C. and Groeneveld, J. 1999. Anchor ice formation below limestone generating station. CGU HS Committee on River Ice Processes and the Environment 10th Workshop on River Ice, Winnipeg, Manitoba.

Healy, D., Hicks, F., 2007. Experimental study of ice jam thickening under dynamic flow conditions. ASCE Journal of Cold Regions Engineering 21 (3), 72–91.

Henderson, F. 1966. Open Channel Flow. Macmillan Publishing Co., Inc., New York.

Hicks, F., Cui, W., Andres, D. 1997. Modelling thermal breakup on the Mackenzie River at the outlet of Great Slave Lake, NWT. Canadian Journal of Civil Engineering, 24(4):570-85.

Hicks, F., Steffler, P., & Gerard, R. 1992. Finite element modeling of surge propagation and an application to the Hay River, NWT. Canadian Journal of Civil Engineering, 19(3): 454-462.

Hothorn, T., Hornik, K., van de Wiel, M.A., Zeileis, A. 2006. A lego system for conditional inference. The American Statistician, 60(3):257-263.

Hutchison, T.K., and Hicks, F.E. 2007. Observations of ice jam release waves on the Athabasca River near Fort McMurray, Alberta. Canadian Journal of Civil

Engineering, 34(4): 473-484.

Jasek, M. 1995. Ice jam simulations in rivers with islands. CGU HS Committee on River Ice Processes and the Environment 8th Workshop on the Hydraulics of Ice Covered Rivers. Kamloops, Canada.

Jasek, M. 2003. Ice jam release surges, ice runs, and breaking fronts: field measurements, physical descriptions, and research needs. Canadian Journal of Civil Engineering, 30(1): 113-127.

Jasek, M., Beltaos, S. 2008. Chapter 8. Ice-jam release: javes, ice runs and breaking fronts. In River Ice Breakup, Beltaos S (ed.). Water Resources Publications: Highlands Ranch, CO.

Jasek, M., Shen, H.T., Pan, J. and Paslawski, K. 2015. Anchor ice waves and their impact on winter ice cover stability. CGU HS Committee on River Ice Processes and the Environment 18th Workshop on River Ice, Québec City, Québec.

Kalke, H., Schneck, C., McFarlane, V., Loewen, M., Jasek, M. 2016. Rafting of sediment by anchor ice releases. In Proceedings of the 23rd International Symposium on Ice, International Association of Hydraulic Engineering and Research, Ann Arbor, Michigan.

Kalke, H., McFarlane, V., Schneck, C., Loewen, M. 2017. The transport of sediments by released anchor ice. Cold Regions Science and Technology, 143:70-80.

Kempema, E.W. and Ettema, R. 2011. Anchor ice rafting: observations from the Laramie

River. River Research and Applications, 27(9):1126-1135.

Kerr, D.J., Shen, H.T. and Daly, S.F. 1997. Anchor ice formation and growth on gravel channel bed. CGU HS Committee on River Ice Processes and the Environment 9th Workshop on River Ice, CGU-HS Committee of River Ice Processes and the Environment, Fredericton, NB, September 24-26.

Kerr, D.J., Shen, H.T., Daly, S.F. 2002. Evolution and hydraulic resistance of anchor ice on gravel bed. Cold Regions Science and Technology, 35(2):101-114.

Khan, A., Steffler, P., Gerard, R. 2000. Dam-break surges with floating debris. Journal of Hydraulic Engineering, 126(5): 375-379.

Kolerski, T., Shen, H.T. 2015. Possible effects of the 1984 St. Clair River ice jam on bed changes. Canadian Journal of Civil Engineering, 42(9):696-703.

Kovachis, N. 2011. Patterns of river breakup timing and sequencing, Hay River, NWT. Master's Thesis. University of Alberta, Edmonton, Canada.

Kowalczyk, T. and Hicks, F. 2003. Observations of dynamic ice jam release on the Athabasca River at Fort McMurray, AB. CGU HS Committee on River Ice Processes and the Environment 12th Workshop on River Ice. Edmonton, June19-20.

Lind, L. and Nilsson, C. 2015. Vegetation patterns in small boreal streams relate to ice and winter floods. Journal of Ecology, 103(2):431-440.

Liu, L., Shen, H. T. 2004. Dynamics of ice jam release surges. In Proceedings of the 17th

IAHR Symposium on Ice. June 21-25, 2004. St. Petersburg, Russia.

Malenchak, J. 2011. Numerical Modelling of River Ice Processes on the Lower Nelson River. Ph.D. Thesis. Department of Civil Engineering. University of Manitoba, Winnipeg, Manitoba, Canada.

Malenchak, J., Doering, J. and Shen, H.T. 2011. Modeling of anchor ice and aufeis formation at Sundance Rapids. CGU HS Committee on River Ice Processes and the Environment 16th Workshop on River Ice. Winnipeg, Manitoba.

Martin, M.D., Brown, R.S., Barton, D.R. and Power, G. 2001. Abundance of stream invertebrates in winter: seasonal changes and effects of river ice. Canadian Field Naturalist, 115(1):68-74.

McDowell, G.R. Micromechanics of creep of granular materials. Géotechnique, 53(10):915-6.

Nafziger J., She, Y., Hicks, F. 2016. Celerities of waves and ice runs from ice jam releases. Cold Regions Science and Technology, 123:71-80.

Nafziger, J., Hicks, F., Thoms, P., McFarlane, V., Banack, J., Cunjak, R.A. 2013. Measuring supercooling prevalence on small regulated and unregulated streams in New Brunswick and Newfoundland, Canada. CGU-HS Committee of River Ice Processes and the Environment 17th Workshop on River Ice, Edmonton, Alberta.

Oveisy, A., She, Y. 2017. Modelling Ice Jam Formation in the Hay River Delta during 2009 Breakup. CGU HS Committee on River Ice Processes and the Environment

19th Workshop on the Hydraulics of Ice Covered Rivers. Whitehorse, Canada. July 9-12.

Qu, Y.X. and Doering, J., 2007. Laboratory study of anchor ice evolution around rocks and on gravel beds. Canadian Journal of Civil Engineering, 34(1):46-55.

R Core Team. 2014. R: A language and environment for statistical computing. R Foundation for Statistical Computing, Vienna, Austria. URL: http://www.R-project.org.

Roussel, J.M., Cunjak, R.A., Newbury, R., Caissie, D. and Haro, A. 2004. Movements and habitat use by PIT-tagged Atlantic salmon parr in early winter: the influence of anchor ice. Freshwater Biology, 49(8):1026-1035.

She, Y., Hicks, F. 2006. Modeling ice jam release waves with consideration for ice effects. Cold Regions Science and Technology, 45(3): 137-147.

She, Y. Hicks, F., Steffler, P., Healy, D. 2008. Effects of unsteadiness and ice motion on river ice jam profiles. Proceedings of the 19th IAHR International Symposium on Ice. Vancouver, Canada. July 6-11.

She, Y., Andrishak, R., Hicks, F., Morse, B., Stander, E., Krath, C., Keller, D., Abarca, N., Nolin, S., Nzokou Tanekou, F., Mahabir, C. 2009a. Athabasca River ice jam formation and release events in 2006 and 2007. Cold Regions Science and Technology, 55(2): 249-261.

She, Y., Hicks, F., Steffler, P., and Healy, D. 2009b. Constitutive model for internal

resistance of moving ice accumulations and Eulerian implementation for river ice jam formation. Cold Regions Science and Technology, 55(3): 286-294.

Shen, H.T. 2005. CRISSP1D Programmer's Manual. CEATI Report No. T012700-0401. Department of Civil and Environmental Engineering, Clarkson University, Potsdam, New York.

Stanley, S.J., Gerard, R. 1992. Ice jam flood forecasting: Hay River, NWT. Canadian Journal of Civil Engineering, 19(2):212-23.

Stickler, M. and Alfredsen, K.T. 2009. Anchor ice formation in streams: a field study. Hydrological Processes, 23(16):2307-2315.

Stickler, M., Alfredsen, K.T., Linnansaari, T., Fjeldstad, H.P. 2010. The influence of dynamic ice formation on hydraulic heterogeneity in steep streams. River Research and Applications, 26(9):1187-1197.

Stickler, M., Alfredsen, K.T., Linnansaari, T., Fjeldstad, H.P. 2010. The influence of dynamic ice formation on hydraulic heterogeneity in steep streams. River Research and Applications, 26(9):1187-1197.

Terroux, A.C.D, Sherstone, D.A., Kent, T.D., Anderson, J.C., Bigras, S.C., Kriwoken, L.A. 1981. Ice regime of the lower Mackenzie River and the Mackenzie delta. National Hydrology Research Institute Report, Environment Canada.

Tesaker, E. 1994. Ice formation in steep rivers. Proceedings of the 12th International Symposium on Ice, International Association of Hydraulic Engineering and

Research, Trondheim, Norway.

Tesaker, E. 1996. Interaction between ice and water flow in rapids. Proceedings of the 13th International Symposium on Ice, International Association of Hydraulic Engineering and Research, Beijing, China.

Tremblay, P., Lacey, R.J., Leconte, R. 2013. The impact of grain orientation and pebble surface roughness on the bond strength of simulated anchor ice. Cold Regions Science and Technology, 96:36-44.

Tremblay, P., Leconte, R., Lacey, R.J., Bergeron, N. 2014. Multi-day anchor ice cycles and bedload transport in a gravel-bed stream. Journal of Hydrology, 519:364-375.

Tsang, G., 1982. Frazil and Anchor Ice: a Monograph. Natural Resources Council Subcommittee on Hydraulics of Ice Covered Rivers, Ontario, Ottawa, Canada.

Turcotte, B. and Morse, B. 2011. Ice processes in a steep river basin. Cold Regions Science and Technology, 67(3):146-156.

Turcotte, B., Morse, B. and Anctil, F. 2014. Cryologic continuum of a steep watershed. Hydrological Processes, 28(3):809-822.

Turcotte, B., Morse, B., Dubé, M., Anctil, F. 2013. Quantifying steep channel freezeup processes. Cold Regions Science and Technology, 94:21-36.

Watson, D. 2011. Observation and modeling of ice jam release events on the Hay River, NWT. M.Sc. thesis, University of Alberta.

Watson, D., Hicks, F. and Andrishak, R. 2009. Analysis of Observed 2008 Ice Jam

Release Events on the Hay River, NWT. CGU HS Committee on River Ice Processes and the Environment 15th Workshop on River Ice, St. John's, NL.

Wong, J., Beltaos, S., Krishnappan, B. 1985. Laboratory tests on surges created by ice jam releases. Canadian Journal of Civil Engineering, 12(4): 930-933.

Zhang, F., Mosaffa, M., Chu, T., Lindenschmidt, K.E. 2017. Using remote sensing data to parameterize ice jam modeling for a northern inland delta. Water, 9(5),306.

Zufelt, J.E. 1990. Experimental Observations of Shoving and Thickening: Comparison to Equilibrium Thickness Theory. Proceedings of the 10th IAHR International Symposium on Ice. Espoo, Finland.

Zufelt, J.E., Ettema, R. 2000. Fully coupled model of ice -jam dynamics. ASCE Journal of Cold Regions Engineering, 14(1):24-41.